Electronic Supporting Information

Kinetics and DFT studies on the Water Oxidation by Ce^{4+} Catalyzed by $[Ru(terpy)(bpy)(OH_2)]^{2+}$

Ayano Kimoto,[1,2] Kosei Yamauchi,[1] Masaki Yoshida,[1,2] Shigeyuki Masaoka,[*1,2,3] and Ken Sakai[*1,4]

[1]*Department of Chemistry, Faculty of Science, Kyushu University, Hakozaki 6-10-1, Higashi-ku, Fukuoka 812-8581, Japan.*

[2] *Institute for Molecular Science, Higashiyama 5-1, Myodaiji, Okazaki 444-8787, Japan.*

[3]*PRESTO, Japan Science and Technology Agency (JST), Honcho 4-1-8, Kawaguchi, Saitama, 332-0012, Japan.*

[4]*International Research Center for Molecular Systems (IRCMS), Kyushu University*

masaoka@ims.ac.jp, ksakai@chem.kyushu-univ.jp

Contents:

Experimental Details

Materials.

$Ce^{IV}(NH_4)_2(NO_3)_6$ was purchased from Wako Pure Chemical Industries, Ltd. $[Ru(terpy)(bpy)(OH_2)](PF_6)_2$ was prepared as previously described.[1]

Measurements.

Stopped-flow experiments were performed using a UNISOKU USP-SFM-S20 with a mixing ratio of 1:1 by volume, and the time-course of spectral changes were monitored on a Shimadzu MultiSpec-1500 spectrophotometer, equipped with a 1024 element photodiode array detector, which allows rapid scanning with a minimum interval of 0.1 sec (see Figures 1 and S5). The global kinetic analysis was carried out using the singular value decomposition (SVD) method in SPECFIT[2], where the spectra in the range of 400-800 nm were used. The spectra below 400 nm were excluded from analysis because of the strong absorption of $Ce(NH_4)_2(NO_3)_6$. The amount of O_2 evolved was monitored using a YSI model 5300 oxygen meter at 20 °C under Ar atmosphere, as described elsewhere.[3]

DFT calculations.

Calculations were carried out using the DFT method implemented in the Gaussian 03 suite program.[4] The structures were fully optimized using the B3LYP method which uses hybrid Becke's three-parameter exchange functional of Lee, Yang, and Parr with the correlation energy functional.[5,6] All the calculations, except for Figure S15b, Tables S4h-k and S5h-k, were performed using the standard double-ζ type LanL2DZ basis set[7] implemented in Gaussian 03, without adding any extra polarization or diffuse function. The LanL2DZ basis set also uses relativistic effective core potentials (RECP) for the Ru atom to account for the scalar relativistic effects of the inner 28 core electrons ($[Ar]3d^{10}$) for Ru. Moreover, based on the suggestion from one of the reviewers for this paper, calculations using a higher level of basis set were also carried out using the LACVP** basis set, which uses the LanL2DZ basis set for Ru and the 6-31G** basis set[8] for H, C, N and O (the results are given in Figure S15b and Tables S4h-k and S5h-k). Structures of model compounds in aqueous media were computed using the polarizable continuum model (PCM).[9] All the stationary points were characterized by their harmonic vibrational frequencies as minima. The exited states were calculated by the TD-DFT[10] method within the Tamm-Dancoff approximation as implemented in Gaussian 03, where the hybrid B3LYP functional along with the basis sets described above were employed. At least 300 excited states were computed in each calculation. To obtain the simulated spectrum of each species, transition energies and oscillator strengths have been interpolated by a Gaussian convolution with a common σ value of 0.2 eV.

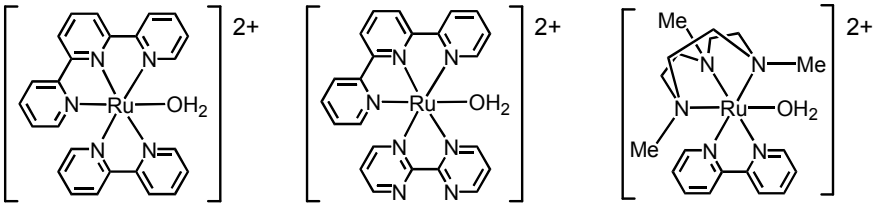

Scheme S1. Structures of mononuclear aquaruthenium catalysts

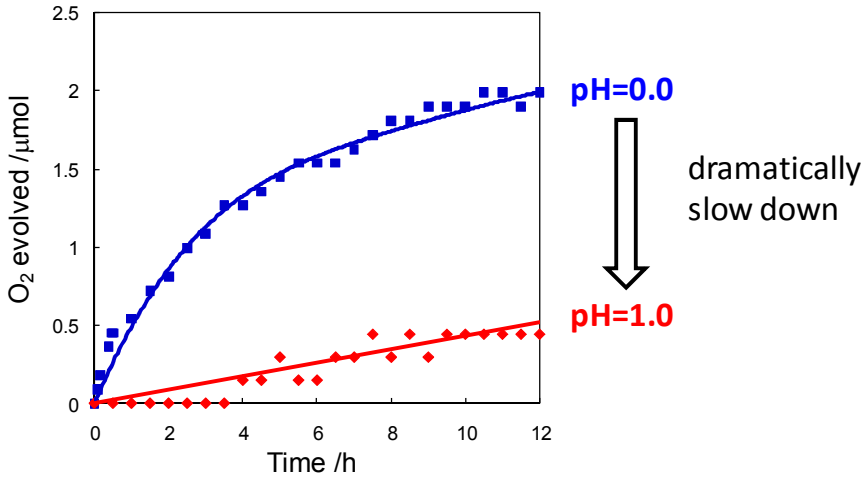

Figure S1. Oxygen evolution from an aqueous 0.1 or 1.0 M $HClO_4$ solution (2.0 mL, pH =1.0 or 0.0) containing $Ce^{IV}(NH_4)_2(NO_3)_6$ (5.0 mM) in the presence of $[Ru^{II}(terpy)(bpy)(OH_2)](PF_6)_2$ (0.05 mM) as a catalyst. Each measurement was initiated by adding the catalyst in a 1:1 mixture of an aqueous $HClO_4$ solution and acetonitrile (100 μL) to a solution of the oxidant (10 mM) dissolved in an aqueous $HClO_4$ solution (2.0 mL, pH =1.0 or 0.0) at 20 °C under Ar atmosphere. The total volume of acetonitrile was 0.25% in this condition.

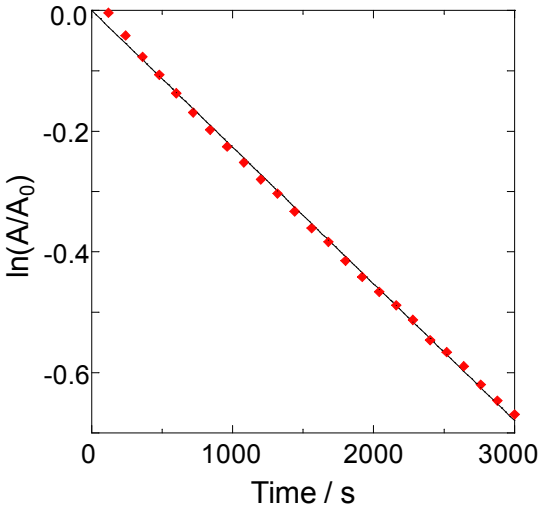

Figure S2. The results of least-squares fitting experiments, showing that the decay profile of Ce^{4+} shows a good fit to a single exponential function, where red squares correspond to the experimentally observed data points (absorbance at 360 nm, recorded every 2 minutes) and a black line denotes a calculated line according to the following equation:

$$\text{Abs.} = A\exp(-kt)$$

where the parameters are determined as $k = 2.2 \times 10^{-4}$ s^{-1} and $A = 0.13$. The catalysis was initiated by mixing a solution of the $[Ru^{II}(terpy)(bpy)(OH_2)](PF_6)_2$ (0.1 mM) and a solution of the $Ce^{IV}(NH_4)_2(NO_3)_6$ (4.0 mM) at 20 °C in 0.1 M $HClO_4$ (pH= 1.0).

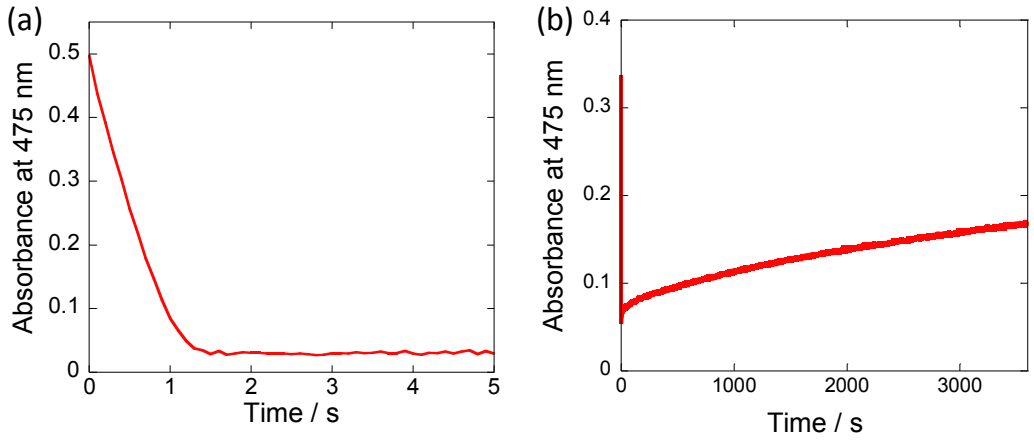

Figure S3. The time course of absorbance change at 475 nm after mixing an aqueous 0.1 M $HClO_4$ solution (pH= 1.0) containing $[Ru^{II}(terpy)(bpy)(OH_2)](PF_6)_2$ (0.05 mM) and 10 equiv. of Ce^{4+} (0.5 mM). The catalysis was initiated by mixing a solution of the catalyst (0.1 mM) and a solution of the oxidant (1.0 mM) at 20 °C under air. a) 0.0 – 5.0 sec (recorded every 0.1 sec). b) 0.0 – 3580 sec (recorded every 1.0 sec).

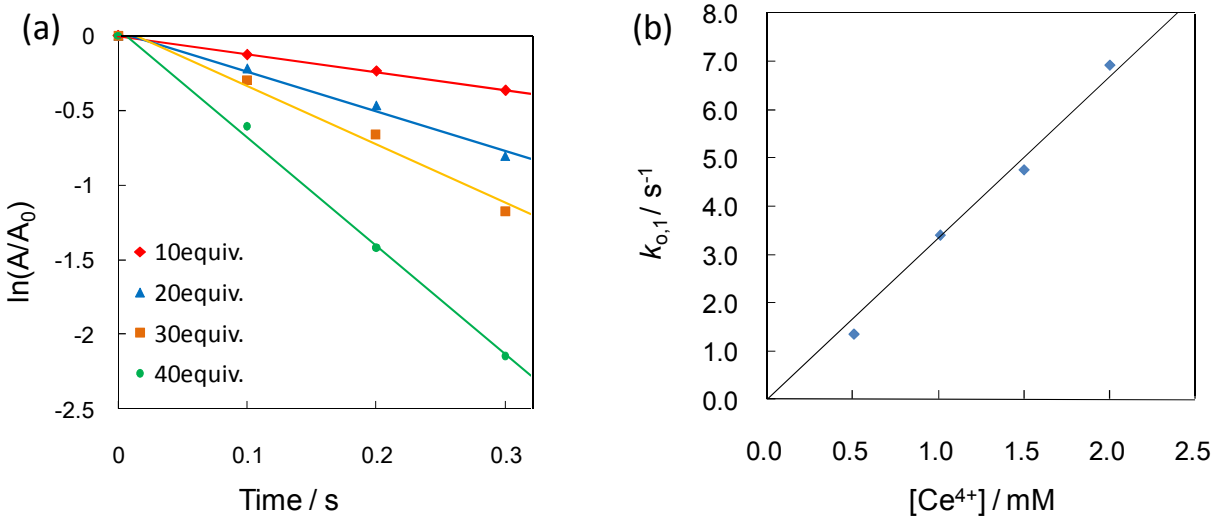

Figure S4. (a) Logarithmic plot of absorbance changes at 475 nm after mixing an aqueous 0.1 M $HClO_4$ solution (pH =1.0) containing $[Ru^{II}(terpy)(bpy)(OH_2)](PF_6)_2$ (0.1 mM) and an excess of Ce^{4+} at 20 °C under air, showing that the band at 475 nm decays as a single exponential function. (b) Plot of the observed pseudo-first-order rate constant ($k_{o,1}$) as a function of the Ce^{4+} concentration ($[Ce^{4+}]$). As the $k_{o,1}$ value linearly increases with $[Ce^{4+}]$, the rate law for the initial rapid process can be defined as $v_1 = k_{o,1}[Ru^{II}–OH_2] = k_1[Ce^{4+}][Ru^{II}–OH_2]$, where the rate constant was determined as $k_1 = 3.3 \times 10^3$ $M^{-1}s^{-1}$.

Global Kinetic Analysis in SPECFIT.

The analysis in SPECFIT has been carried out to resolve the independent spectral components given during the course of successive oxidation steps in the reaction of $[Ru^{II}(terpy)(bpy)(OH_2)]^{2+}$ and $Ce^{IV}(NH_4)_2(NO_3)_6$ at pH = 1.0. With this aim, we focus on one condition for the analysis in SPECFIT; 1 equiv. of $[Ru^{II}(terpy)(bpy)(OH_2)]^{2+}$ was mixed with 10 equiv. of $Ce^{IV}(NH_4)_2(NO_3)_6$ by the stopped-flow technique (the conditions are same to those in Figure S3). Since the overall reaction involves an initial very rapid process together with relatively slow subsequent processes (see Figure S3), it was not possible to record an *appropriate* spectral data set in a single run. In other words, repeated scanning of spectral changes up to 3600 sec with a recording interval of 0.1 sec affords a data set consisting of 36000 spectra, which cannot be handled within the available programs. Therefore, at least two data sets, which were separately recorded with different time intervals, had to be collected under the same experimental setup and combined into a single data set so that the data set can be reasonably handled in SPECFIT. One measurement mode adopted a time range of 0-300 sec with a data collection interval of 0.1 sec while the other adopted a time range of 0-3580 sec with a time interval of 1 sec. When the two data sets were combined into a single data set, the absorbance data recorded for the earlier time domain were scaled and/or shifted to fit the overlapping data near the connecting time region. In the present case, the range of 139-179 sec was adopted to fit the two data sets and the data were actually connected at 159 sec, corresponding to the midpoint of the overlapping region. The scaling and baseline correction factors were estimated by the least-squares calculations to minimize the shift of overlapping absorbance data at each sampling time in the range of 139-179 sec. Since simple connection of the two data sets affords a new data set made up of 1591 spectra from the earlier scan and 3341 spectra from the later scan, the total number of spectra had to be decreased to 959 spectra in order to enable the more realistic treatment of the data in SPECFIT. The partial elimination of the spectral data was carried out using the individually developed algorithm in a private program (SPECFITV7), developed by KS using the Delphi5 package.

Figure S5 shows the original data set employed to extract the spectral data in the time domain of 0-159 sec (all the 1591 spectra are overlayed in this figure) and those in the time domain of 159-3518 sec (data were actually collected every 1 sec but only those every 60 sec are shown here for clarity). Out of these spectral data, 459 and 499 spectra were extracted from the earlier and later data sets, respectively, and were combined into a single data set. The validity of our method used in connecting the two data sets could be reasonably evaluated during the course of the analysis in SPECFIT, as detailed below.

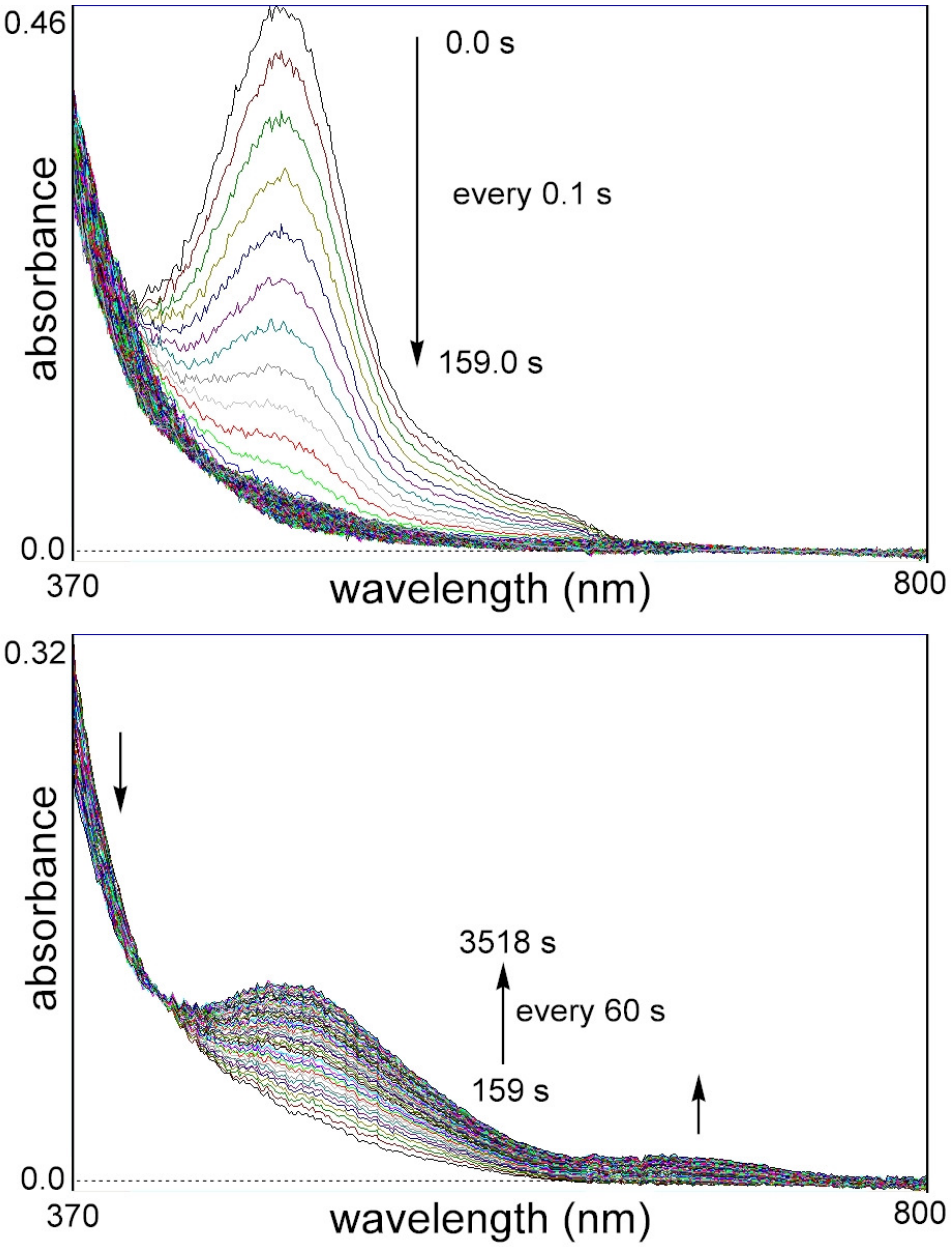

Figure S5. The time-course of spectral changes after the 1:1 mixing of $[Ru^{II}(terpy)(bpy)(OH_2)](PF_6)_2$ (0.10 mM) and $Ce^{IV}(NH_4)_2(NO_3)_6$ (1.0 mM; 10 equiv. with respect to the catalyst), in 0.1 M $HClO_4$ at 20 °C in air. (a) A time range of 0.0 – 159.0 sec with a data collection interval of 0.1 s. (b) A time range of 159.0 – 3518 sec with a data collection interval of 60 sec (data collection was actually carried out with an interval of 1 sec).

SPECFIT uses the Singular Value Decomposition (SVD) method at the initial treatment of the data set. The set of original data scans (**Y**) is accurately represented in a matrix form according to the SVD as **Y** = **U** x **S** x **V**. **U** and **V** are sets of orthogonal evolutionary and spectral eigenvectors, respectively. **S** is a set of singular factors. The SVD may be considered as one of the preferred methods of least-squares reduction from spectroscopic data. All the spectral fitting procedures in SPECFIT employs the factorized data set resulting from the SVD. Therefore, the data set employed in the actual kinetic analysis is considered as a noise-filtered spectral data set. In other words, the original data set imported into the SVD analysis is archived and is not used in the kinetic analysis in SPECFIT.

The SVD analysis in SPECFIT returns a list of predictions revealing how many eigenvectors may be correlated with useful data and which eigenvectors are likely to correspond to the irrelevant components, such as noise data arising from the measurement apparatus. For the present data set, the Factor Analysis (Principal Component Analysis) using the SVD returned 6 vectors as follows:

Table S1. List of Eigenvectors reported by the Factor Analysis in SPECFIT

#	Eigenvalue	Squaresum	Residual	Prediction
1	8.684E+02	4.932E+01	1.146E-02	Data Vector
2	4.510E+01	4.218E+00	3.351E-03	Data Vector
3	3.608E+00	6.106E-01	1.275E-03	Data Vector
4	2.332E-01	3.774E-01	1.002E-03	Data Vector
5	7.409E-02	3.033E-01	8.984E-04	Possibly Data
6	8.295E-03	2.950E-01	8.861E-04	Probably Noise

The results clearly indicated that there are at least 5 colored components involved during the course of this reaction. Note that here we use (as SPECFIT uses) the term ‘colored’ to denote that a certain chemical species has absorption detectable within the wavelength range adopted in the analysis, even if we work along with the UV region, which is not actually colored (it derives from the term ‘colorimetry’ in analytical chemistry). Although it is not straightforward to judge whether the fifth and sixth vectors are indeed attributable to those predicted in this table, a visual inspection of Vectors (**V**; Figure S6) as well as the scaled vector product of **U** x **S** (Figure S7) allowed us to give a clearer aspect for it. Figure S6 shows the normalized vectors of these eigenvectors, corresponding to those listed in the above table; all the vectors are normalized to fit the same window in Figure S6, and therefore the comparison of the intensities does not make sense. It can be considered that the lines with a lower noise level, such as components **1** and **2**, in Figure S6 possess larger eigenvalues, consistent with the numerical reports in the above table. On the other hand, lines with larger noise in Figure S6 are those which have to be magnified to fit the window due to the smaller eigenvalues. As shown in Figure S6, one may realize that the last component **6** has no remarkable

feature as a function of wavelength; it can be considered as a flat, zero component whose noise level becomes larger as the monitoring wavelength decreases.

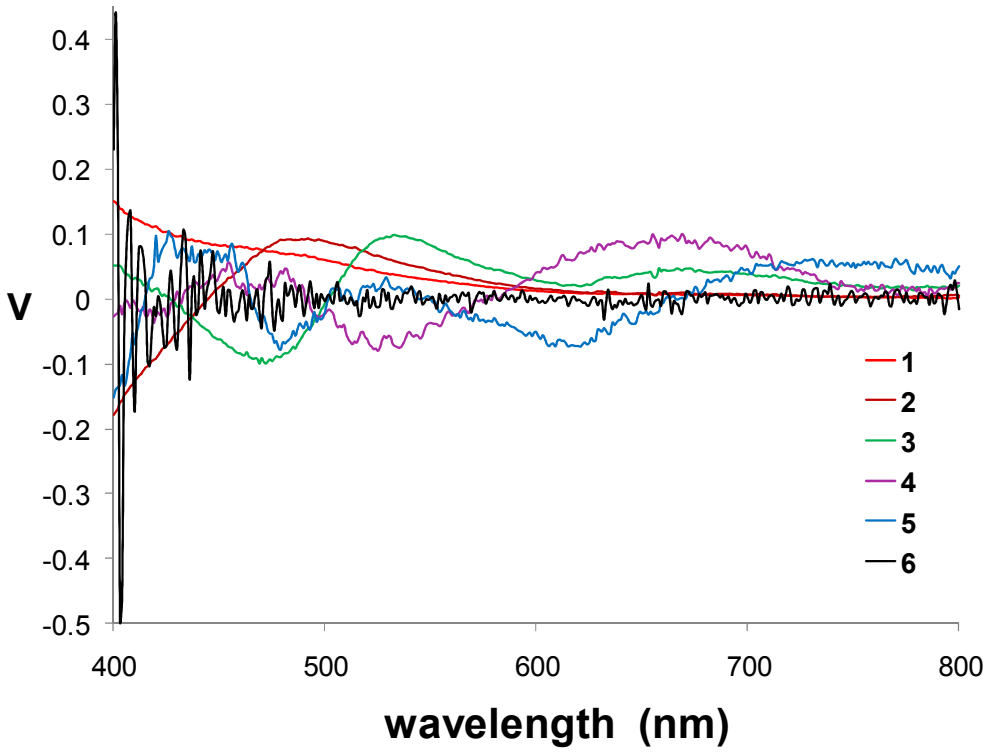

Figure S6. The normalized spectral eigenvectors as a function of wavelength. The lines with a lower noise level, such as components **1** and **2**, possess larger eigenvalues, while the component **6** has no remarkable feature.

On the other hand, the scaled vector product of **U** x **S** further provides a good evidence to judge that the sixth component (**6**) is actually attributable to a noise component. Figure S7 adopts three different magnification levels to clearly see the features of all the **U** x **S** components. As a result, Figure S7c (the black solid line) clearly shows that the last component **6** lacks any feature ascribable to a reaction profile. To the contrary, all other **U** x **S** features for **1**-**5** involve time dependent features during the reaction. Thus, it is reasonable to set up a kinetic model involving five eigenvectors, which are correlated with *at least* five colored species. It must be noted here that there is a case where the number of effective eigenvectors is smaller than the actual colored (observable) chemical species in a system. The most important example is a second-order reaction **A** + **B** → **C** + **D**, for which only two eigenvectors can be given in the SVD in spite of the involvement of 4 colored species. In such a case, a known spectrum of either **A** or **B** together with that of either **C** or **D** should be used to stabilize the interaction of the spectra of **A** and **B** or that of **C** and **D**. In other words, the use of known spectra for either **A** or **B** together with that for either **C** or **D** is the only way to resolve the behaviors of all the 4 colored species.

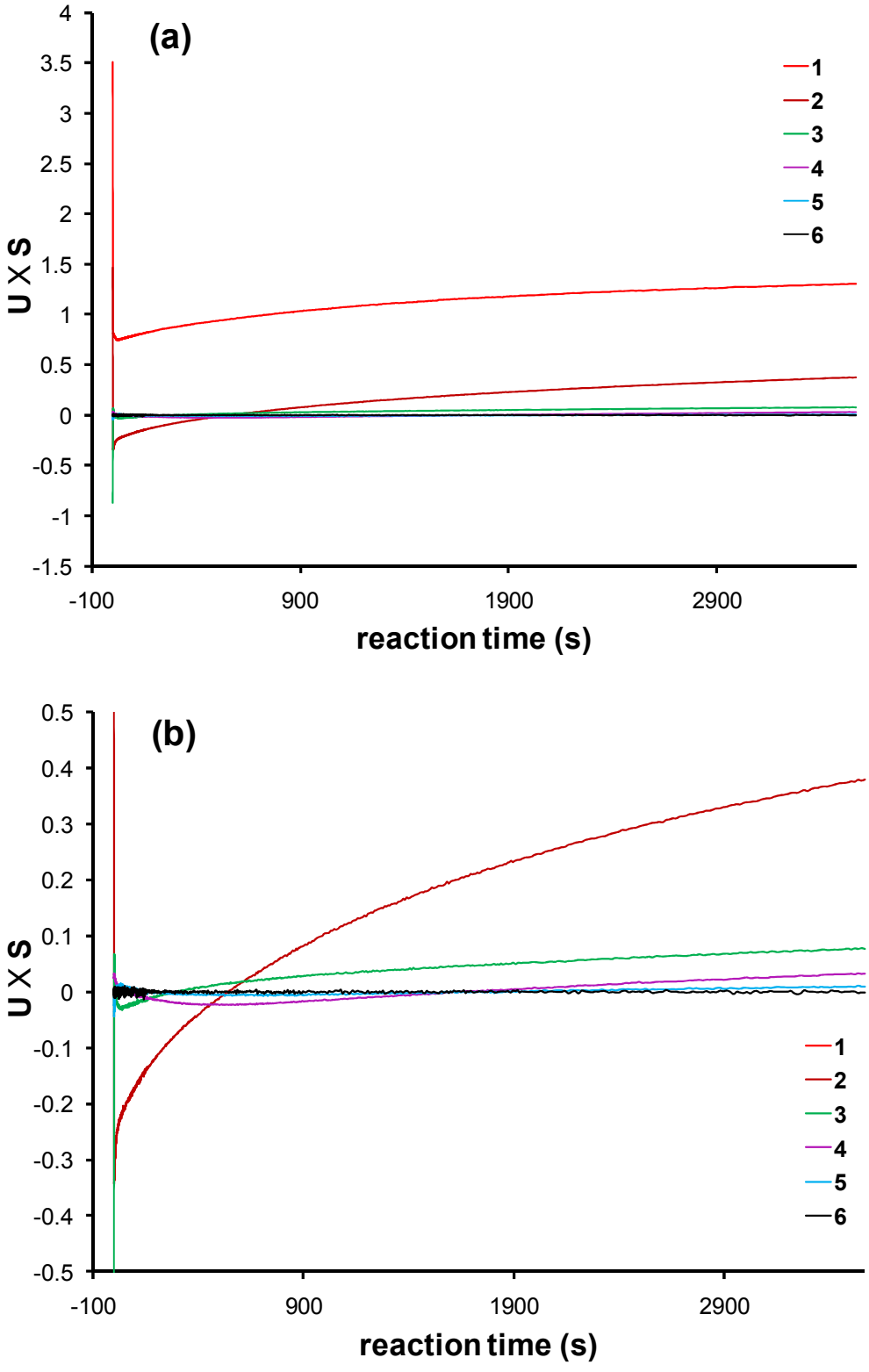

Figure S7. The scaled concentration eigenvectors as a function of the reaction time. Figures (b) and (c) are enlarged illustrations of (a) to clearly show the time dependent features of the eigenvectors. The line for component **6** lacks any feature ascribable to a reaction profile, while those for **1**-**5** involve time dependent features during the reaction.

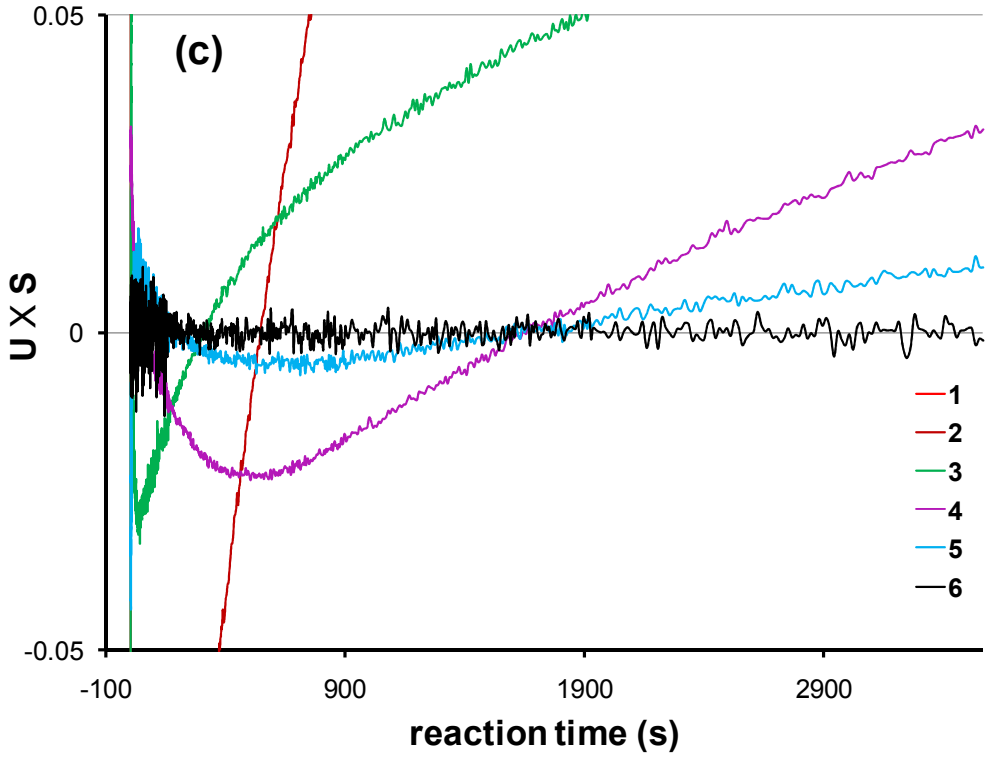

Figure S7 (continued).

As is known from the literatures,[11] the Ce^{4+} species has absorptivity at the higher-energy edge of the visible region, while the Ce^{3+} species generated during the reaction can be considered to have no absorptivity (these were also confirmed in our experiments). Thus, the Ce^{4+} and Ce^{3+} species are considered as colored and non-colored species, respectively. With these in mind, if the initial reaction step is considered as Ru^{II}-OH_2 + Ce^{4+} → Ru^{III}-OH_2 + Ce^{3+}, this is the case where two eigenvectors involve 3 colored species. Consequently, the 5 eigenvectors realized in the SVD analysis implies that at least 6 colored species including Ce^{4+} are involved in the observed successive reaction steps.

In the SVD-based spectral analysis in SPECFIT, the reliability of the final spectral features predicted is usually reinforced by adopting known spectra in the calculations. Usually, only one known spectrum may be required to solve the remaining spectral components. However, the uses of additional known spectra further improve the quality of the remaining predicted spectra. In the present case, the use of a known spectrum for the Ce^{4+} species was found to be inevitable to run the least-squares analysis to give a solution. The known spectrum of Ce^{4+} was separately determined under the identical experimental condition. Although the use of a known spectrum for the starting complex (i.e., $[Ru^{II}(terpy)(bpy)(OH_2)]^{2+}$) did not affect the results, this was also separately determined and was used in the calculations to ensure the reliability of the results given for the remainder. The known spectrum for this was determined by mixing the solution of the Ru complex with an aqueous 0.1 M $HClO_4$ solution free of Ce^{4+} under the same experimental setups.

The fundamental strategy for setting up the kinetic model for this system largely relies on the basic redox properties of $[Ru^{II}(terpy)(bpy)(OH_2)]^{2+}$, which was reported by Meyer et al. in the 1980s.[1] It is clear from this

report that this compound undergoes successive one-electron oxidation reactions at potentials lower than the redox potential for the $Ce^{4+/3+}$ couple (1.40 V vs. SCE at pH = 1.0).[12] At pH = 1.0, the Ru^{II}/Ru^{III} and Ru^{III}/Ru^{IV} couples were determined to appear at 0.81 and 1.00 V vs. SCE, respectively.[1] Moreover, the pKa values for $[Ru^{II}(terpy)(bpy)(OH_2)]^{2+}$ and $[Ru^{III}(terpy)(bpy)(OH_2)]^{3+}$ were reported to be 9.7 and 1.7, respectively.[1] The Ru^{II} species can be considered to be in the pure Ru^{II}-OH_2 form. Actually, the known spectrum obtained for this species (pH = 1) is quite consistent with the reported spectral feature, which was recorded at pH = 6.8.[1] On the other hand, the Ru^{III} species is considered as a 5:1 mixture of $[Ru^{III}(terpy)(bpy)(OH_2)]^{3+}$ and $[Ru^{III}(terpy)(bpy)(OH)]^{2+}$ ($Ka = 10^{-1.7} = 0.02 = [\text{hydroxo species}][H^+]/[\text{aqua species}]$, where $[H^+] = 0.1$ M). In other words, ca. 17% of the Ru^{III} species is the hydroxo form at pH = 1.0. However, these species cannot be resolved at a constant pH, and thereby a single spectral component corresponding to the sum of these species is only observable in the present spectral analysis. As a result, it is obvious from the literature that the initial two oxidation steps correspond to those for **A** + **B** → **C** + **D** and **C** + **B** → **E** + **D**, respectively. In addition, the spectral features of **A** and **E** are also available from the literature (as note below), which confirmed the validity of our assignment that the initial two steps correspond to these successive oxidation steps.

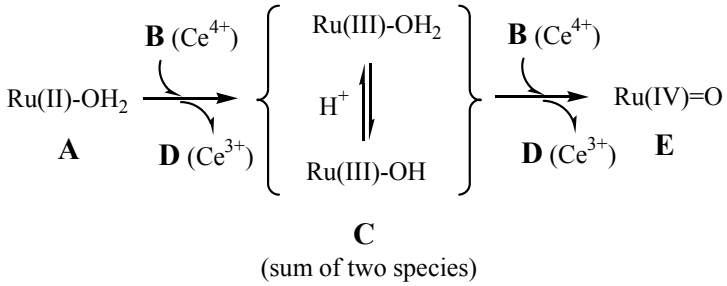

To regenerate the observed data, our initial approach was to suppose the following kinetic model, in which the final species **F** was supposed as the Ru^{V}=O species. This model indeed reproduced the observed data but some non-negligible systematic errors could not be eliminated. (see below)

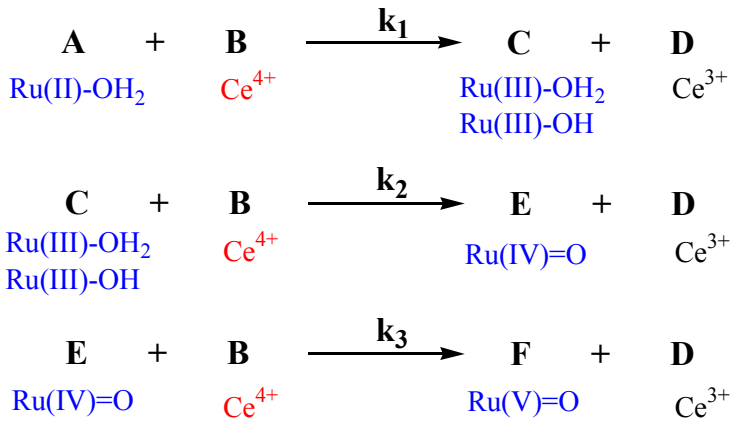

This indirectly indicated that the involvement of 6 colored species rather than 5 colored species in the above model (**A**, **B**, **C**, **E**, and **F**) is valid, consistent with the results of SVD analysis. We therefore pursued a possibility of having an additional step. During the course of these attempts, we finally realized that the

above 5-colored model fails to reproduce the event happening at around 200 sec after the mixing. This means that the final product remains unchanged but the formation of another intermediate should be taken into consideration. Mathematically, all the following models resulted in giving a good fit of the observed and calculated absorbance data at all the wavelengths.

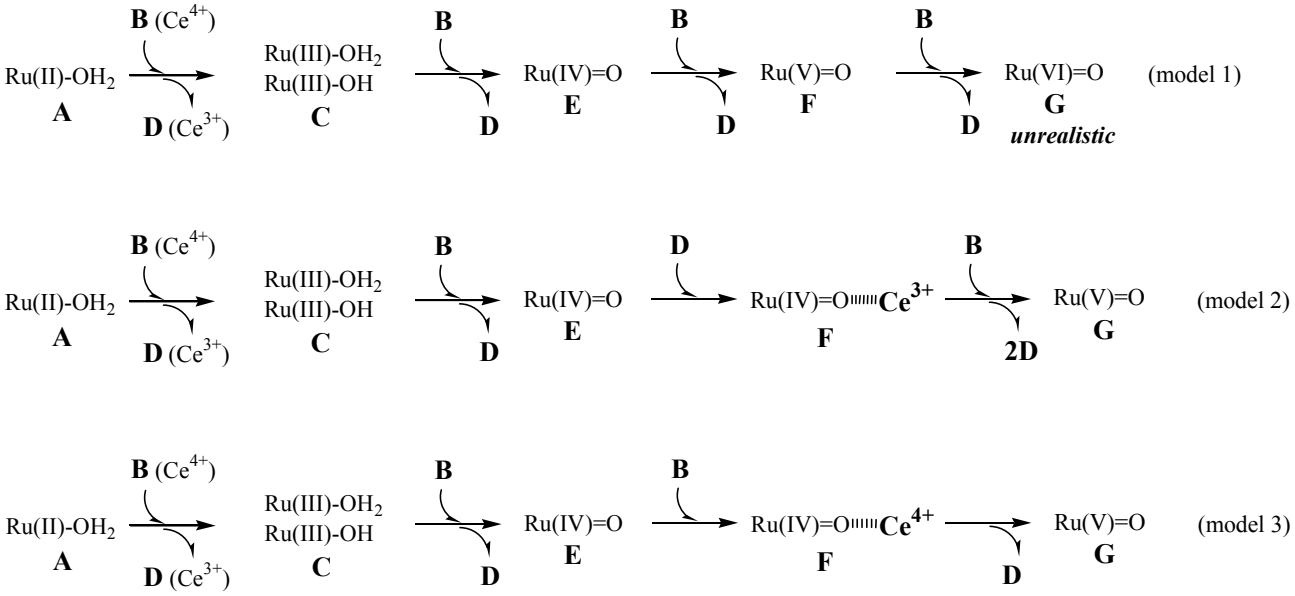

The first model (model 1) is clearly unrealistic and should be ruled out. In all the cases, the fourth Ru species **F** possesses absorption features which are not largely different from those of its precursor Ru^{IV}=O (**E**) except that the absorptivities are all higher in **F** in comparison with **E** (see Figure S8). It must be also noted that the absorptivity spectra obtained for **C**, **E**, and **G** are quite consistent with those resulted in the 5-colored model. In any model including the 5-colored model, the final product has been confirmed to have the same spectral feature, which has been most reasonably assigned as that of a Ru^{V}=O species based on its TD-DFT based spectral simulation. At the moment, the most likely interpretation for these observation is that simple outersphere electron transfer for the Ru^{II}/Ce^{IV} and Ru^{III}/Ce^{IV} couples are feasible, while that for the Ru^{IV}/Ce^{IV} couple is rather slow. Thereby, the oxidation of Ru^{IV}=O into Ru^{V}=O needs to proceeds via the formation of a certain intermediate to lower the activation barrier for the process. One rationale may be that the Ru^{IV}=O species forms an adduct with a certain coexisting species to lower the oxidation potential so that its oxidation becomes more feasible. In this context, the adduct formation of the Ru^{IV}=O species with Ce^{3+}, illustrated in model 2 (see above), is a candidate elucidating the observed behaviors. However, this is an unrealistic model again since the oxidation potential for the Ru^{IV}/Ru^{V} couple is not likely to be lowered by coordination of such a highly positive cationic species. Our tentative suggestion is that the reaction proceeds via the inner-sphere mechanism proposed in model 3 (i.e., eqs. 3 and 4 in the main text), because of the following reasons. It seems probable that the reaction rate for the outer-sphere electron transfer from Ru^{IV}=O to Ce^{4+} is slow but that for the inner-one becomes feasible so that inner-sphere route is adopted. If the inner-sphere electron transfer is still very slow, this kind of intermediate may become observable.

By tentatively adopting model 3 as the most plausible scheme, the least-squares analysis has been carried out to afford the following results. The kinetic model used is defined in the following menu.

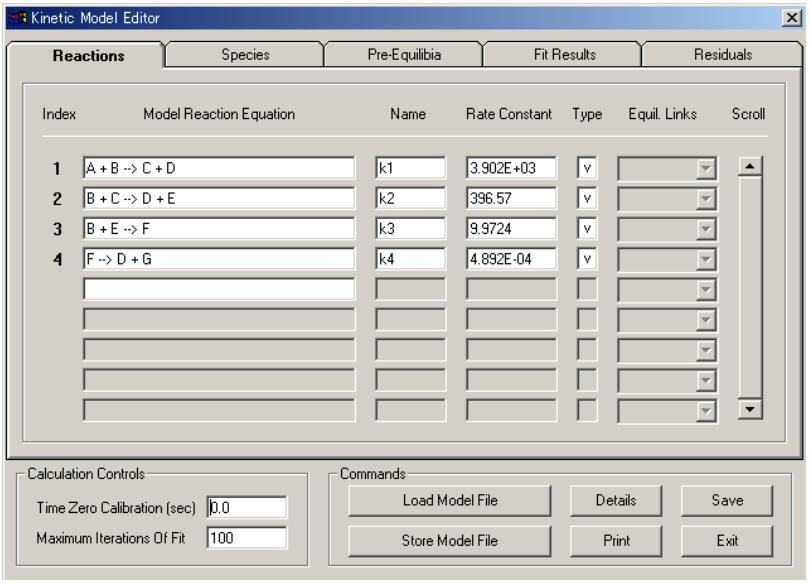

The flags 'v' (Type) in this menu denotes that the value is treated as a parameter to be refined in the least-squares calculations based on the Marquardt algorithm. Thus, all the four rate constants were refined. On the other hand, the initial concentrations of all the chemical species should be defined in the following menu, together with two additional definitions for each species. One is to define whether the species of interest has absorptivity within the wavelength region used to monitor the spectral changes. This is denoted as 'Colored' as follows. As shown in the menu, species **D** (Ce^{3+}) is treated as having no absorption.

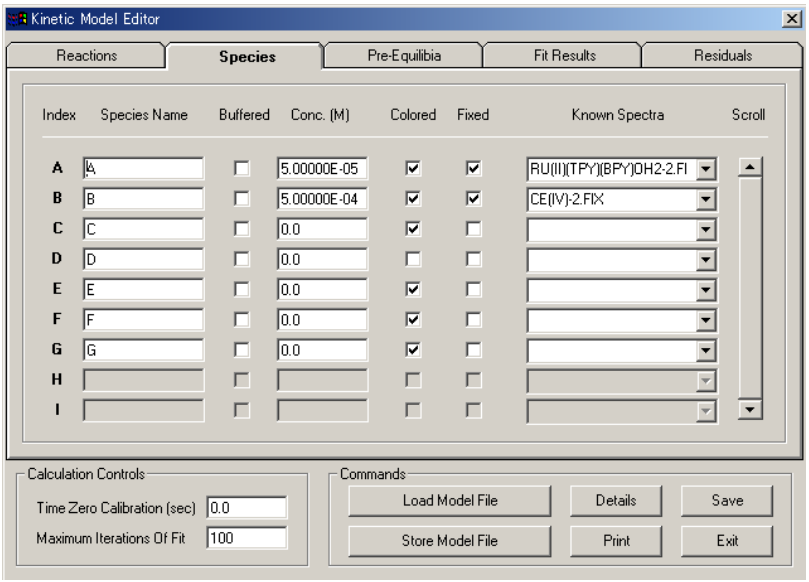

The other is to define whether the calculation uses molar absorptivity data for some species. In the present case, the molar absorptivity spectra of the starting complex (Ru^{II}-OH_2) and Ce^{4+} were separately determined under the same experimental conditions and were treated as known spectra as shown in this menu.

The least-squares calculations by adopting the above conditions returned acceptable level of convergence. Other details are shown in the Fit Results window illustrated below.

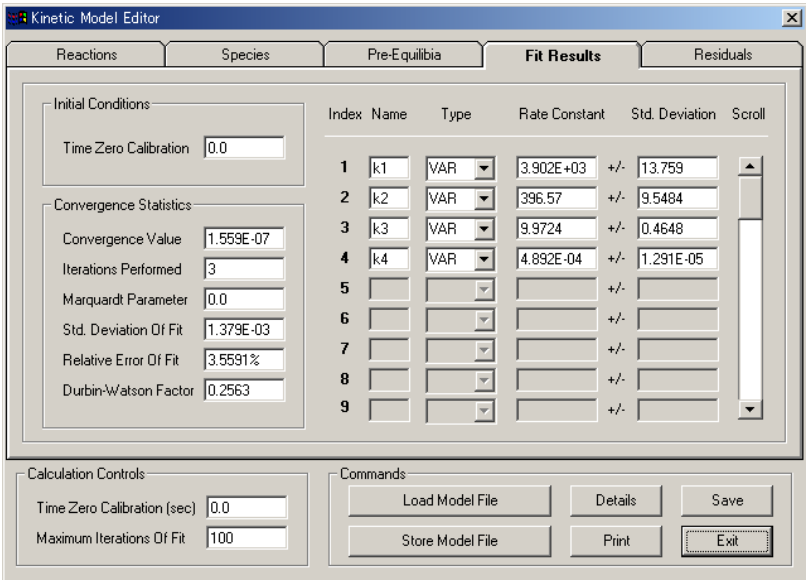

Figures S8 and S9 further demonstrate how the observed data are successfully regenerated. To show the validity of the finally adopted model, the results given for the 5-colored model are also depicted in Figures S8 and S9, in which systematic errors are clearly seen.

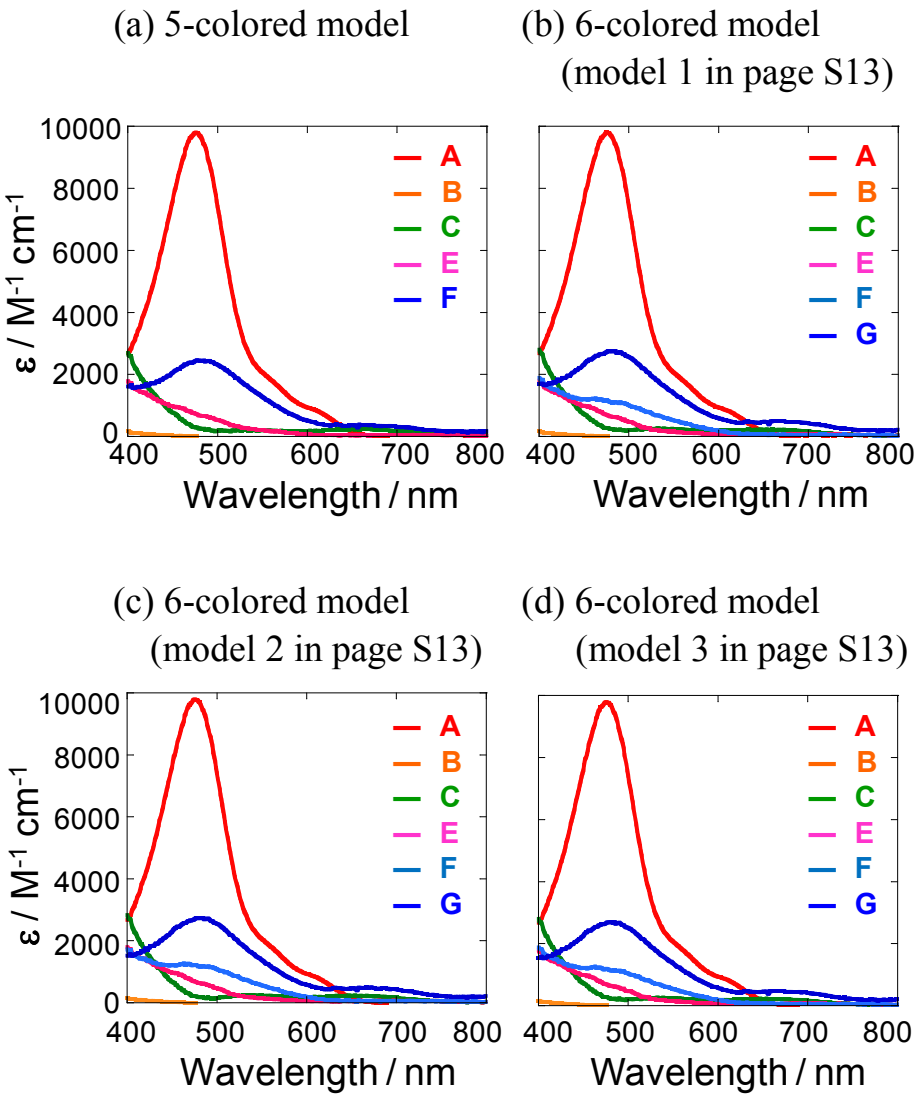

Figure S8. The spectral components extracted based on the 5-colored model (a) and the three 6-colored models illustrated in page S13 (b-d), determined from the data in Figure S5 by global kinetic analysis in SPECFIT.

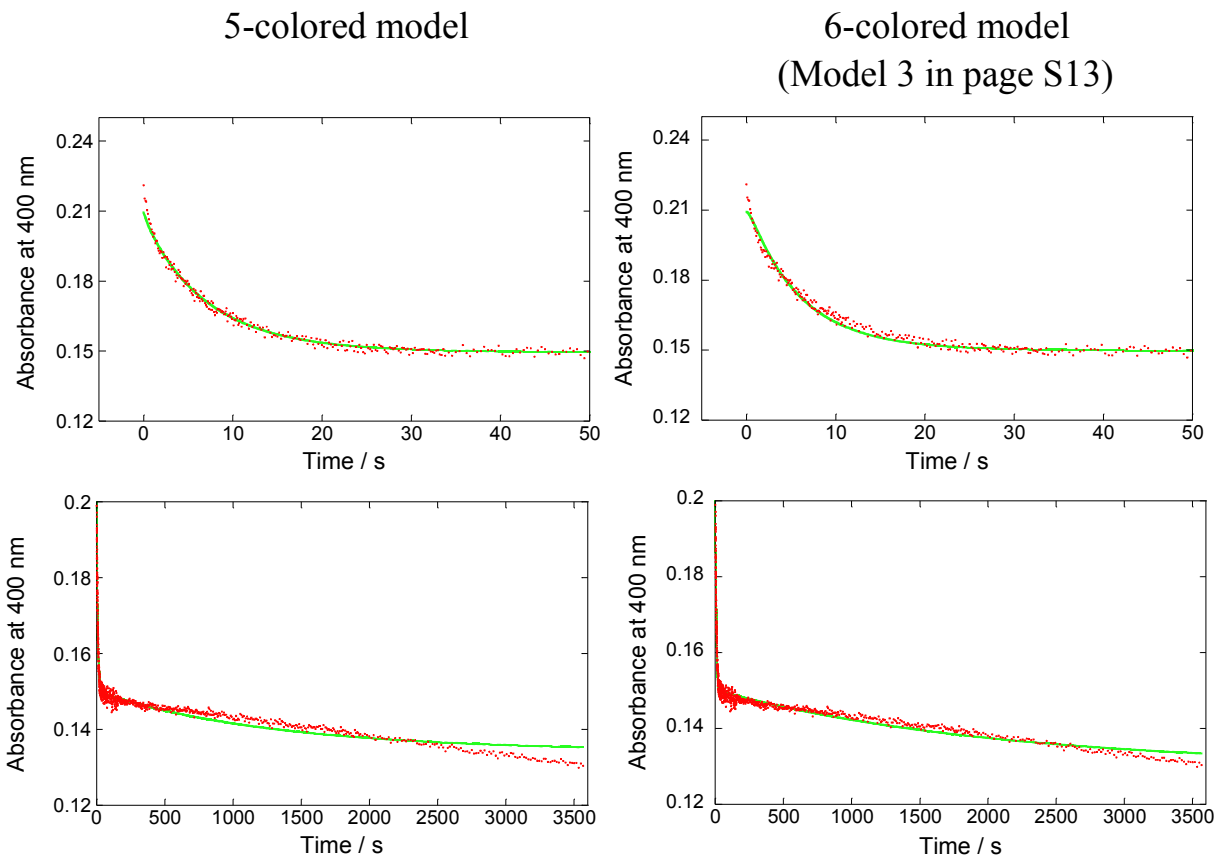

Figure S9. The comparative results of least-squares fitting experiments for the (left) 5-colored model and (right) 6-colored model, where model 3 in page S13 is adopted as the 6-colored model. This confirms that the use of the 6-colored model reproduces the experimental data better than that of the 5-colored model. The red dots correspond to the experimentally observed data points and the green lines denote calculated lines. The data sets for the 6-colored model are same to those used in Figure 2 in the main text.

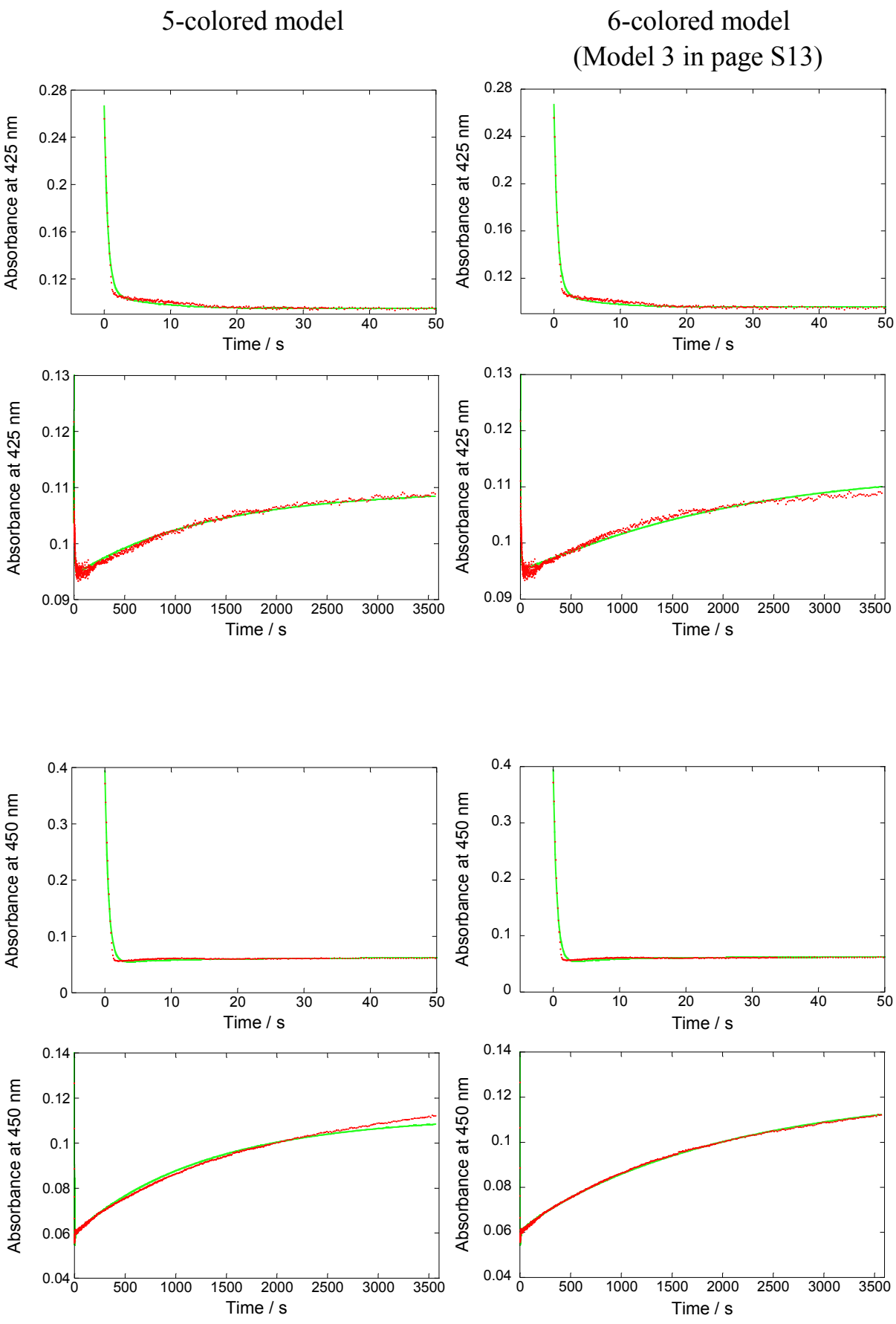

Figure S9 (continued).

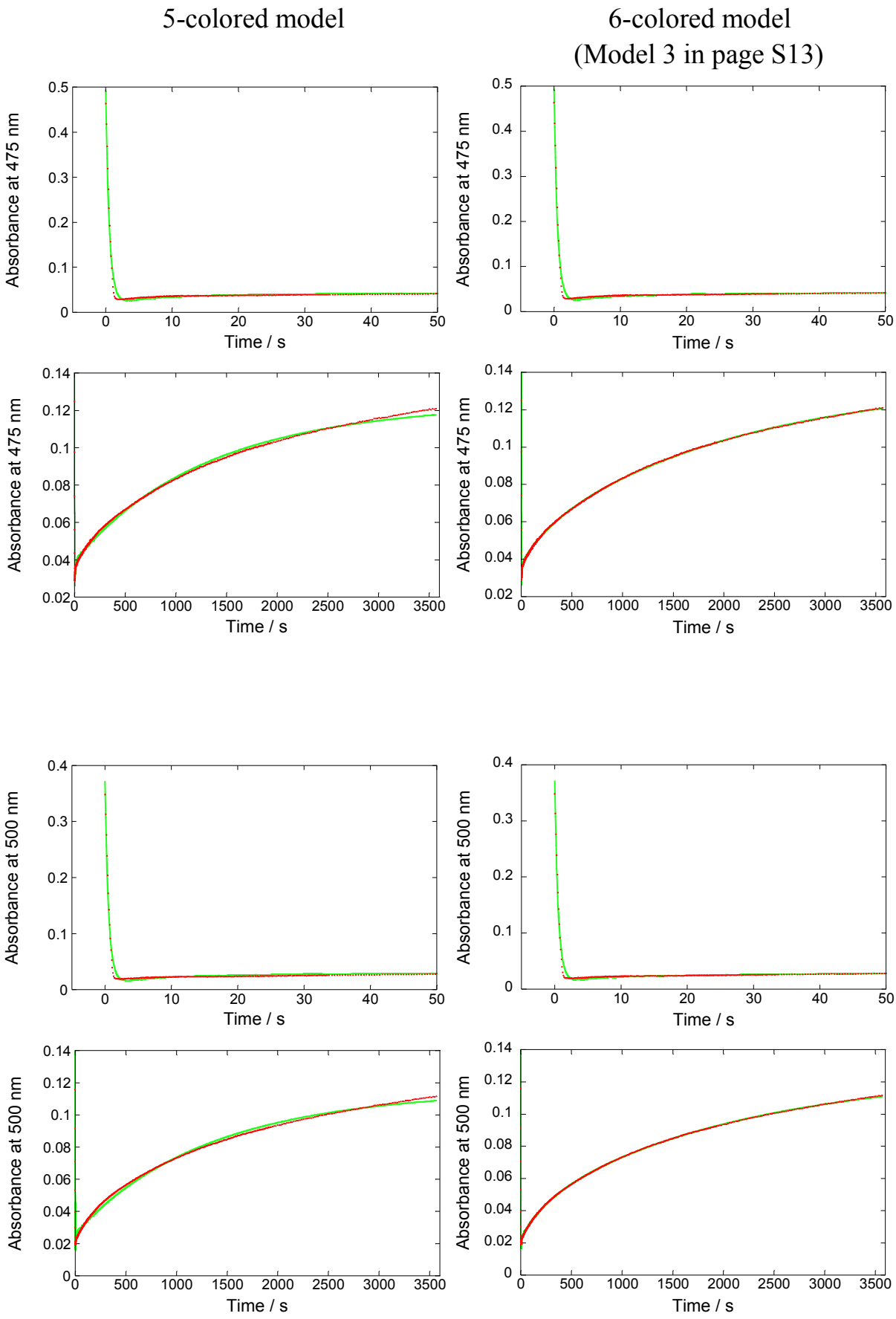

Figure S9 (continued).

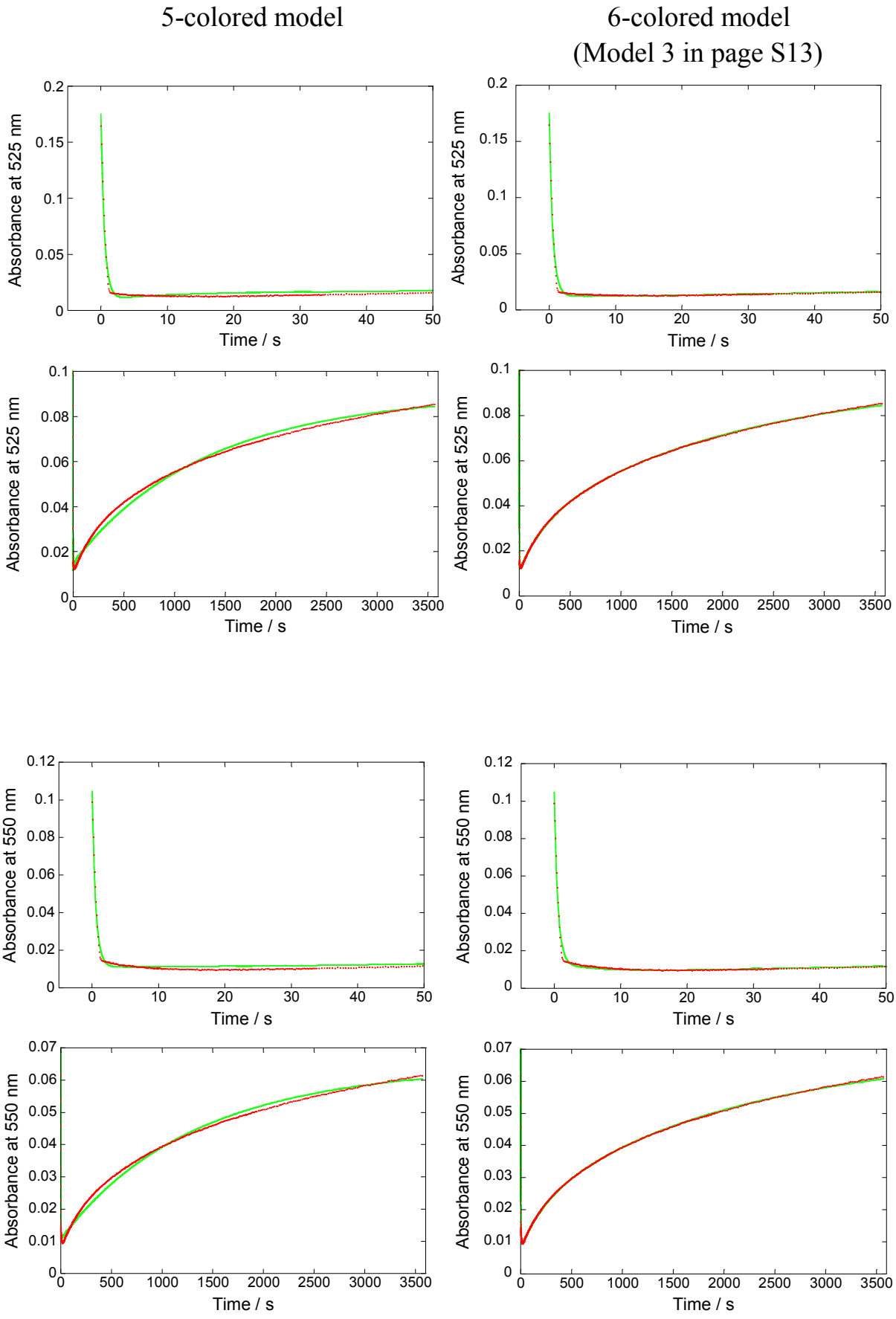

Figure S9 (continued).

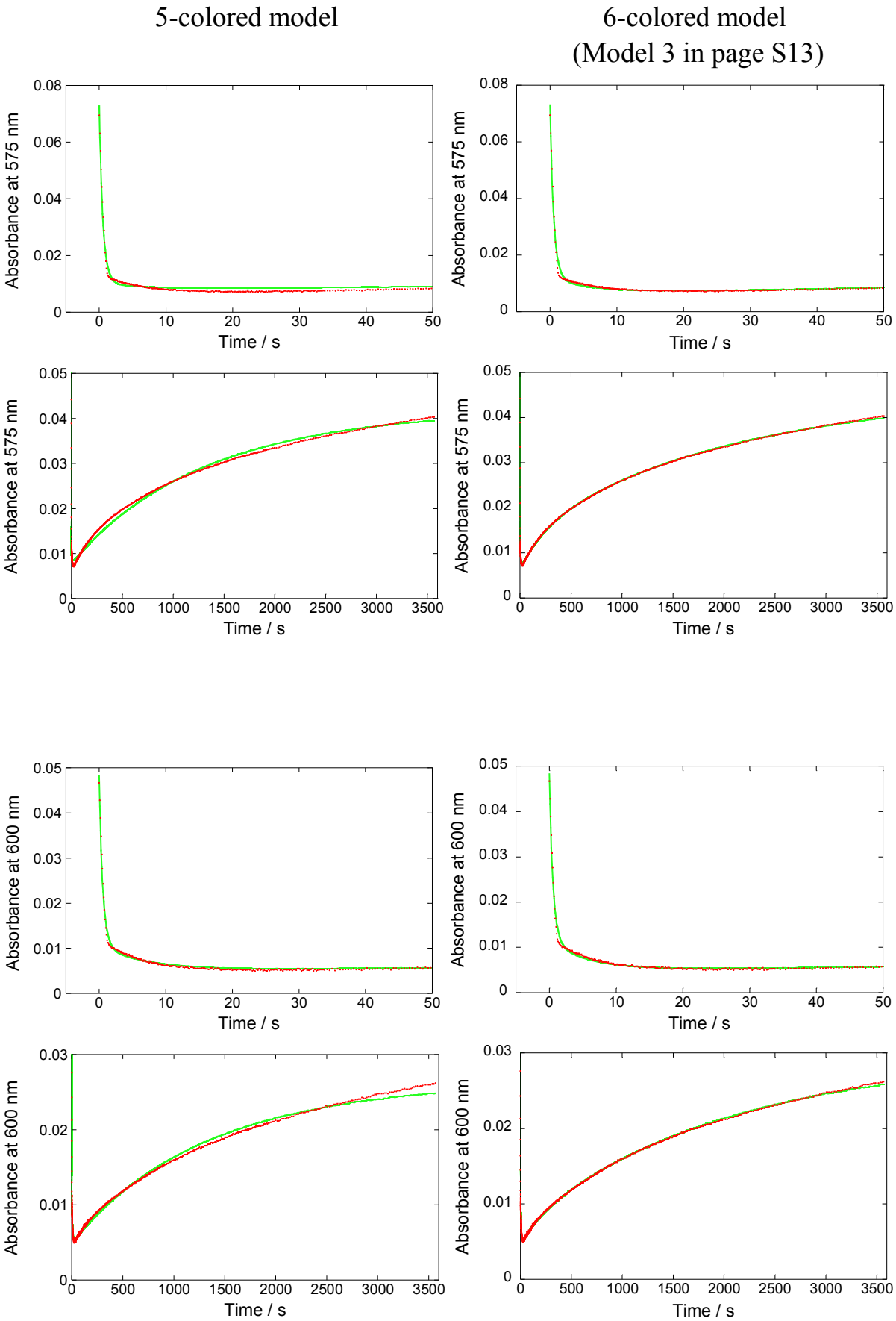

Figure S9 (continued).

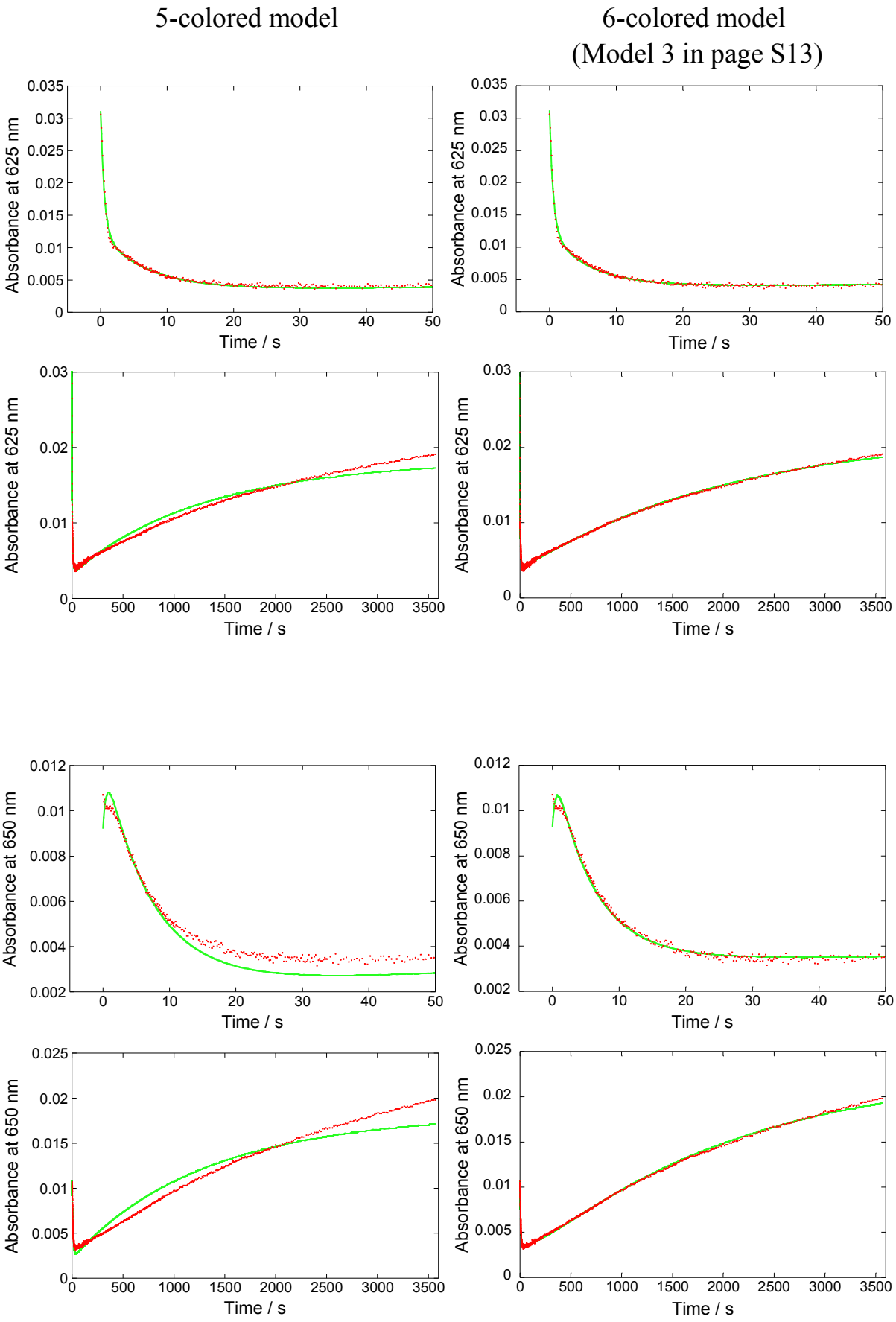

Figure S9 (continued).

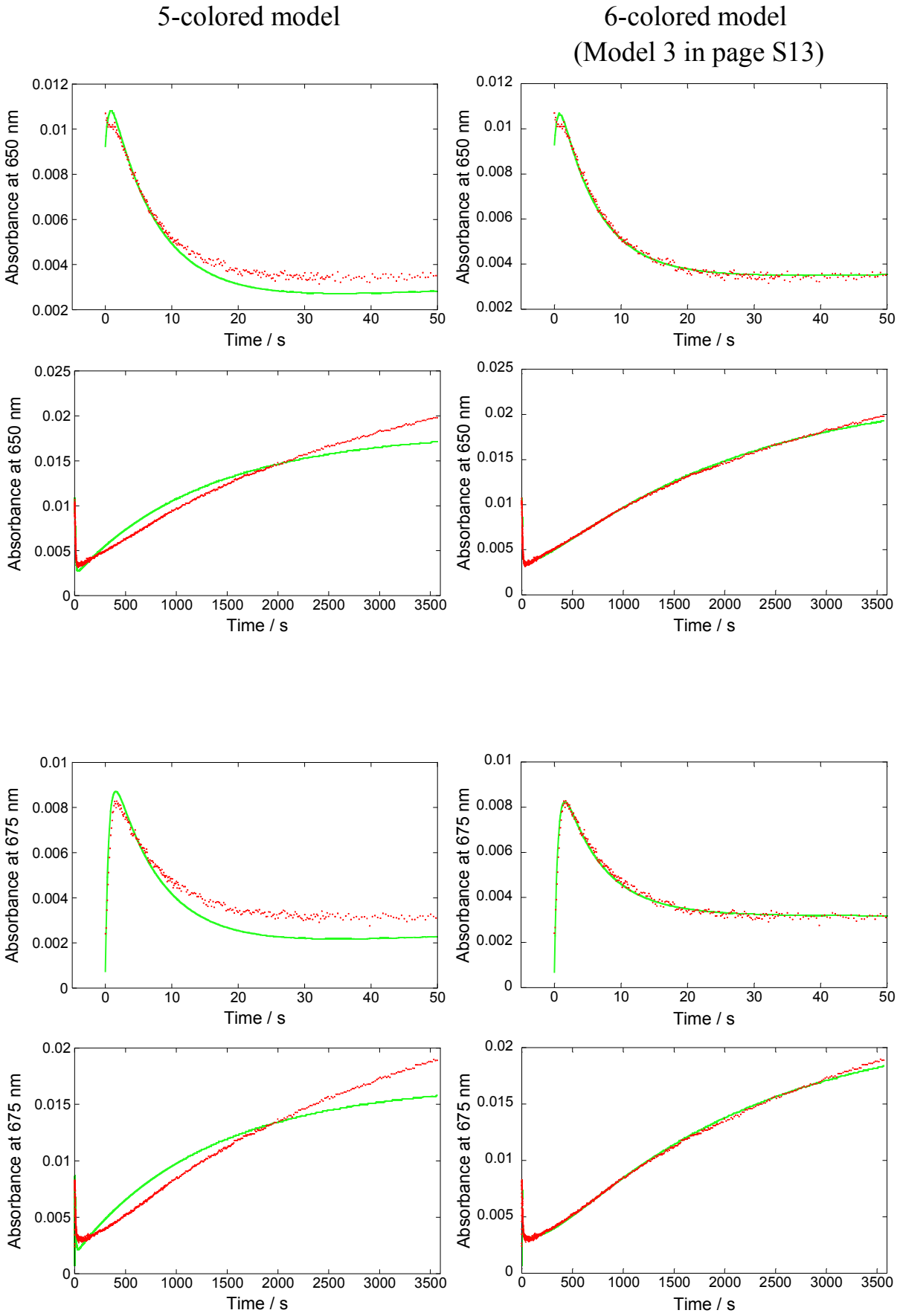

Figure S9 (continued).

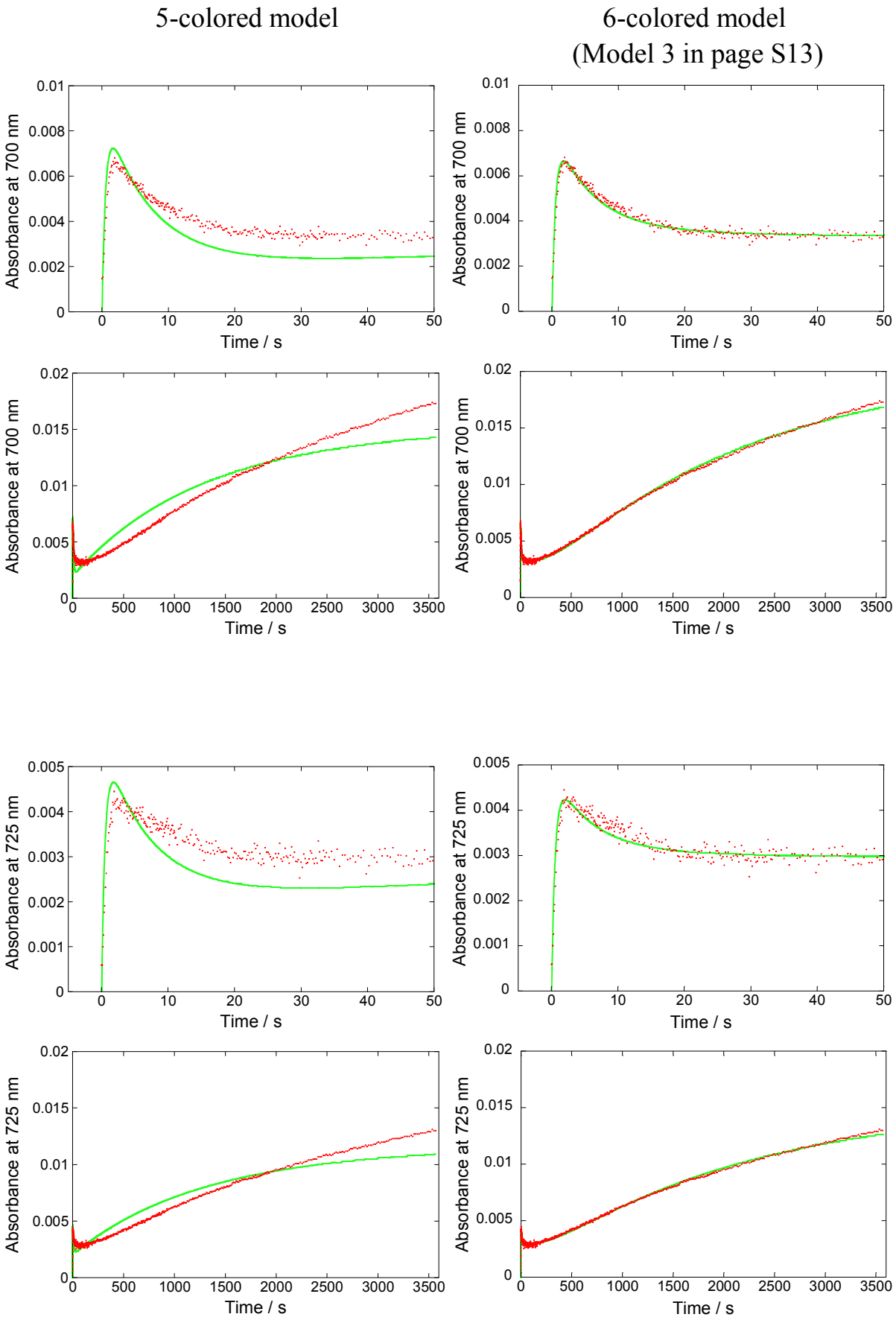

Figure S9 (continued).

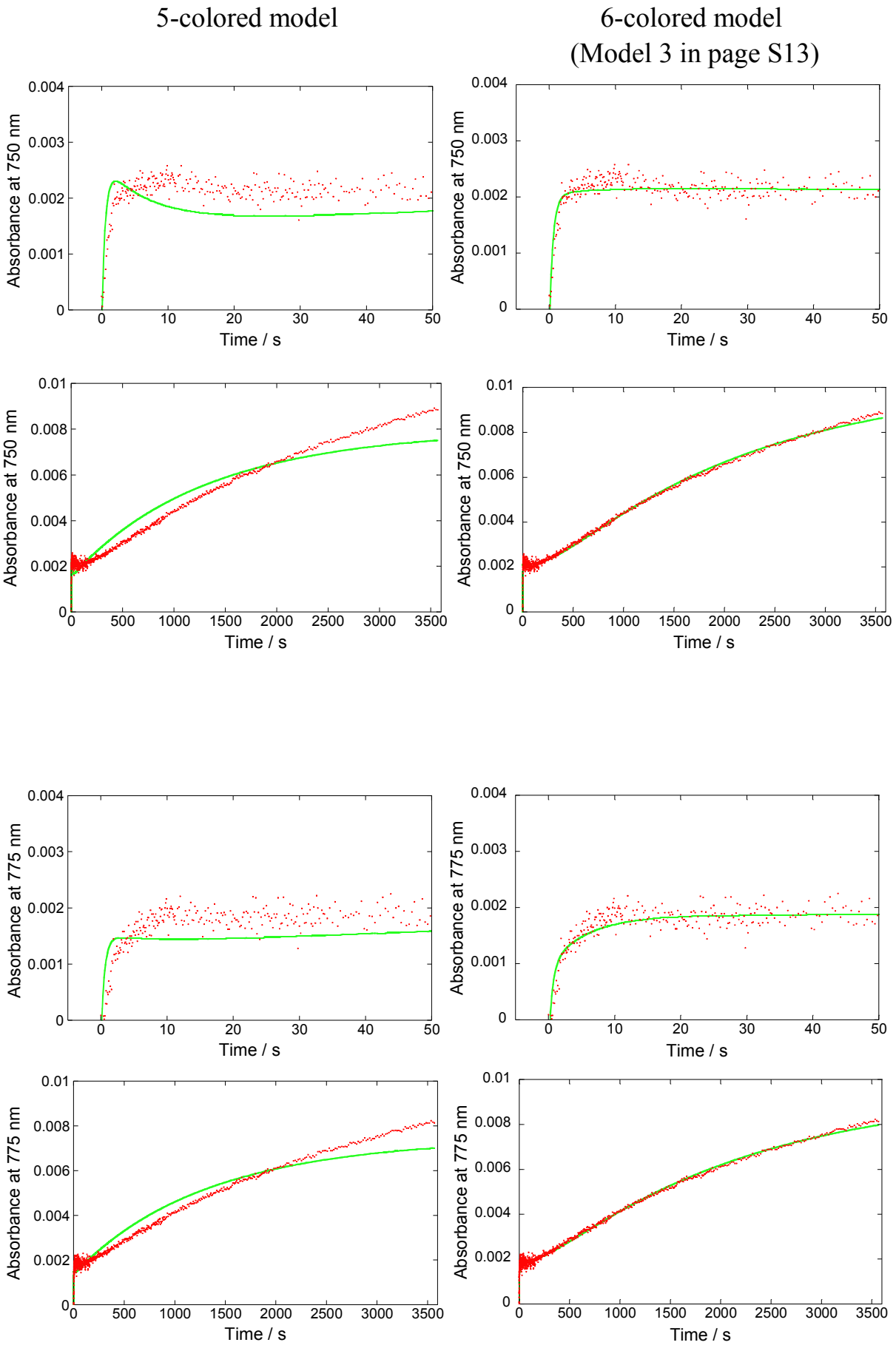

Figure S9 (continued).

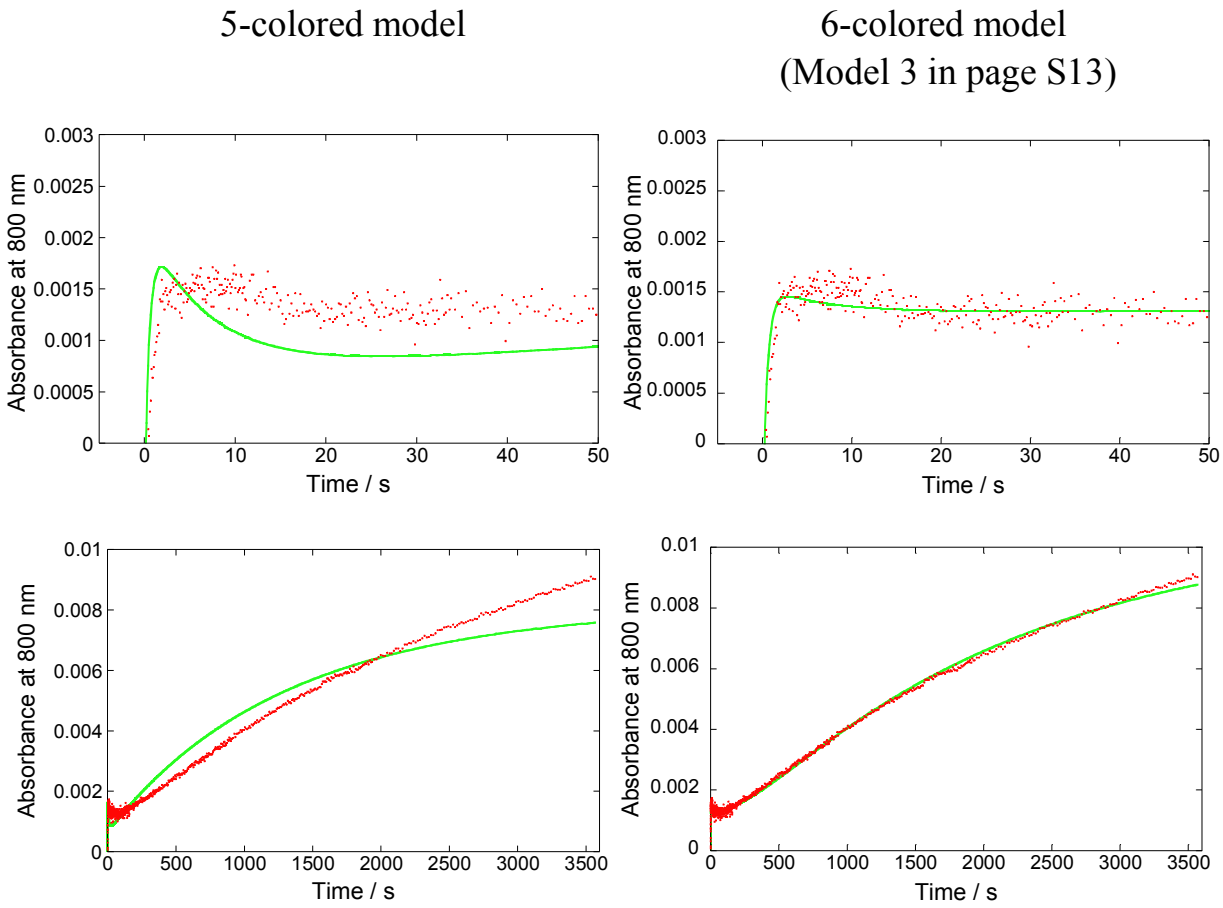

Figure S9 (continued).

Table S2. Rate constants, convergence values and relative errors for the 5- and 6-colored models illustrated in pages S12-S13, determined by global analysis in SPECFIT.

	model reactions	rate constants	standard deviation	convergence values	relative error of fit (%)
5-colored model	A+B → C+D C+B → E+D E+B → F+D	k_1 = 3900 $M^{-1}s^{-1}$ k_2 = 325.76 $M^{-1}s^{-1}$ k_3 = 1.9607 $M^{-1}s^{-1}$	±17.109 ±9.0689 ±0.01752	3.49×10^{-4}	4.2621
6-colored model (model 1)	A+B → C+D C+B → E+D E+B → F+D F+B → G+D	k_1 = 3901 $M^{-1}s^{-1}$ k_2 = 396.78 $M^{-1}s^{-1}$ k_3 = 10.531 $M^{-1}s^{-1}$ k_4 = 1.4011 $M^{-1}s^{-1}$	±13.752 ±9.5988 ±0.5089 ±0.03942	3.06×10^{-4}	3.536
6-colored model (model 2)	A+B → C+D C+B → E+D E+D → F F+B → G+2D	k_1 = 3626 $M^{-1}s^{-1}$ k_2 = 428.25 $M^{-1}s^{-1}$ k_3 = 40.415 $M^{-1}s^{-1}$ k_4 = 1.203 $M^{-1}s^{-1}$	±14.496 ±11.317 ±2.5816 ±0.04192	2.09×10^{-4}	4.0561
6-colored model (model 3)	A+B → C+D C+B → E+D E+B → F F → G+D	k_1 = 3902 $M^{-1}s^{-1}$ k_2 = 396.57 $M^{-1}s^{-1}$ k_3 = 9.9724 $M^{-1}s^{-1}$ k_4 = 4.892×10^{-4} s^{-1}	±13.759 ±9.5484 ±0.4648 $\pm1.291\times10^{-5}$	1.56×10^{-7}	3.5591

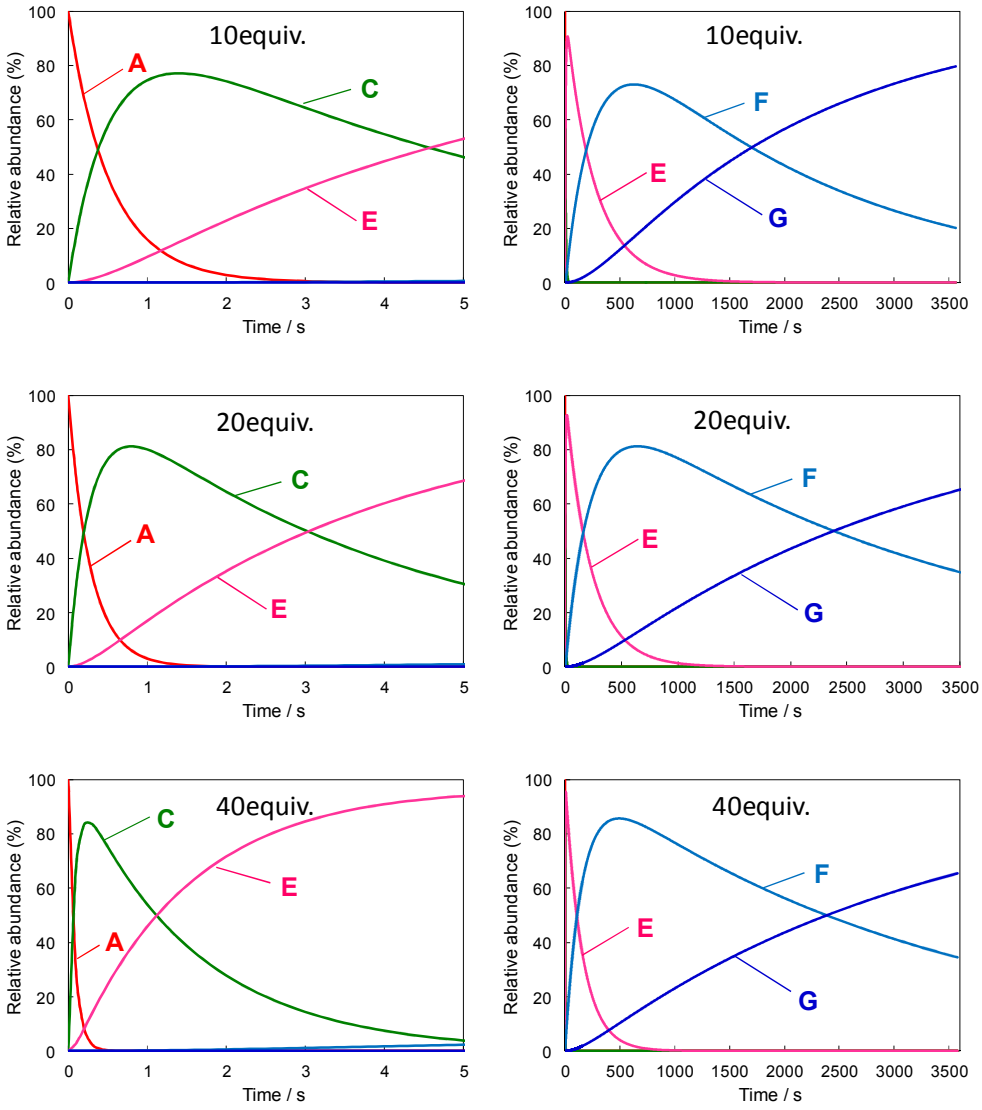

Figure S10. The relative abundances of **A** (red), **C** (green), **E** (pink), **F** (light blue), and **G** (blue) as a function of the reaction time. Where the rate constants were respectively determined as (a) $k_1 = 3.9 \times 10^3$ $M^{-1}s^{-1}$, $k_2 = 4.0 \times 10^2$ $M^{-1}s^{-1}$, $k_3 = 10.0$ $M^{-1}s^{-1}$ and $k_4 = 4.9 \times 10^{-4}$ $M^{-1}s^{-1}$, (b) $k_1 = 3.6 \times 10^3$ $M^{-1}s^{-1}$, $k_2 = 2.7 \times 10^2$ $M^{-1}s^{-1}$, $k_3 = 5.0$ $M^{-1}s^{-1}$ and $k_4 = 3.2 \times 10^{-4}$ $M^{-1}s^{-1}$ and (c) $k_1 = 6.3 \times 10^3$ $M^{-1}s^{-1}$, $k_2 = 3.5 \times 10^2$ $M^{-1}s^{-1}$, $k_3 = 3.5$ $M^{-1}s^{-1}$ and $k_4 = 3.1 \times 10^{-4}$ s^{-1}. The catalysis was initiated by mixing a solution of the catalyst (0.1mM) and a solution of the oxidant (1.0 mM for (a), 2.0 mM for (b), and 4.0 mM for (c)) in an aqueous 0.1 M $HClO_4$ solution (pH =1.0) at 20 °C under air. (left) 0.0 – 5.0 sec. (right) 0.0 – 3580 sec.

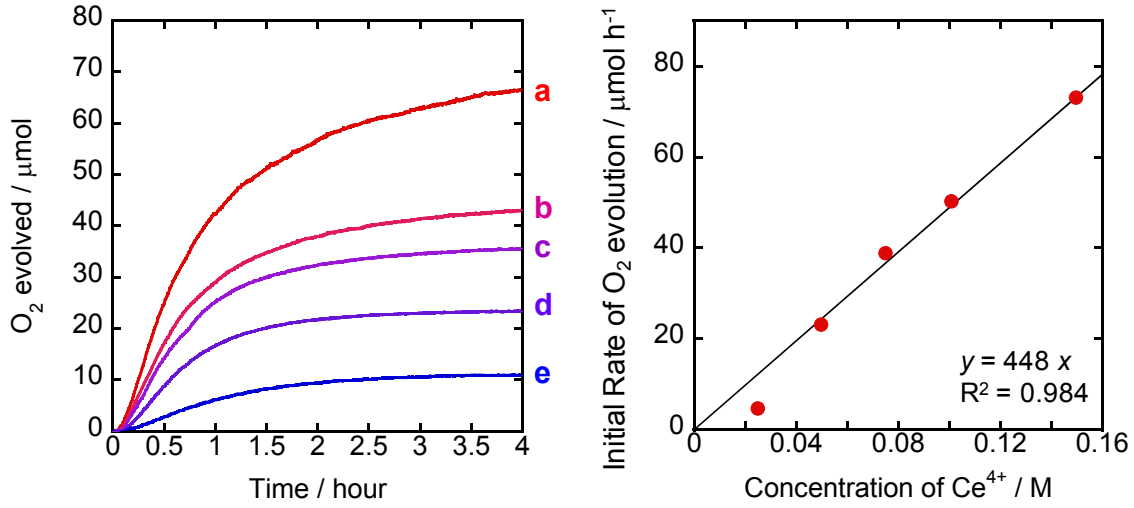

Figure S11. Oxygen evolution from an aqueous 1.0 M $HClO_4$ solution (2.0 mL) catalyzed by $[Ru(terpy)(bpy)(OH_2)](PF_6)_2$ (0.125 mM) with $Ce(NH_4)_2(NO_3)_6$ at various oxidant concentrations (left): (a) 0.150, (b) 0.101, (c) 0.0751, (d) 0.0498, (e) 0.0250 M. The initial gradients of the O_2 evolution curves were plotted as a function of the concentration of Ce^{4+} (right). The O_2 evolution was first order with respect to $[Ce^{4+}]$ (i.e., $v_{O2} = k_{obs}[Ce^{4+}]$), where $k_{obs} = 1.24 \times 10^{-7}$ s^{-1}. This linear correlation is consistent with our previous result, which revealed that the O_2 evolution curve shows a good fit to a single-exponential function.[3]

(a) $[Ru^{II}(terpy)(bpy)(OH_2)]^{2+}$

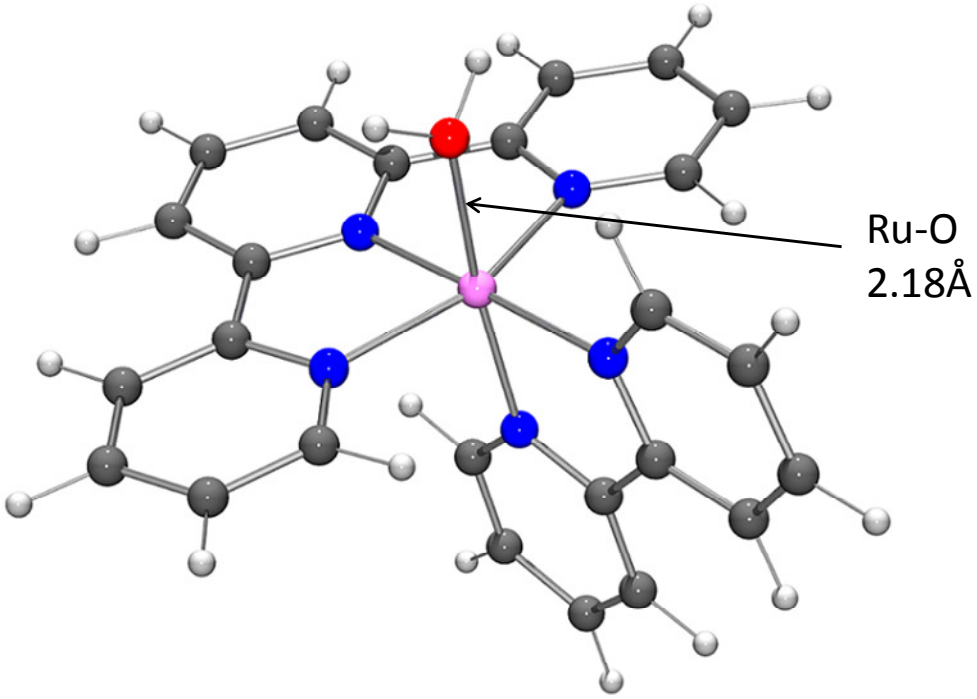

Figure S12. Structures of (a) $[Ru^{II}(terpy)(bpy)(OH_2)]^{2+}$ (singlet), (b) $[Ru^{III}(terpy)(bpy)(OH_2)]^{3+}$ (doublet), (c) $[Ru^{IV}(terpy)(bpy)(O)]^{2+}$ (triplet), (d) $[Ru^{V}(terpy)(bpy)(O)]^{3+}$ (doublet), (e) $[Ru^{III}(terpy)(bpy)(OOH)]^{2+}$ (doublet), (f) $[Ru^{IV}(terpy)(bpy)(OOH)]^{3+}$ (triplet), and (g) $[Ru^{III}(terpy)(bpy)(OO\bullet)]^{2+}$ (triplet), which were fully optimized at the (U)B3LYP level of DFT using the LanL2DZ basis set and the PCM method (solvation in water is taken into consideration). Coordinates are also supplied as Table S4.

Note:

The comparison of the O-O bond distances in the Ru-OOH and Ru-(OO•) units (Figures S12e-g) reveals that (i) Ru^{III}-OOH (Figure S12e) has a pure hydroperoxo character, (ii) Ru^{IV}-OOH (Figure S12f) only slightly bears a radical character at the OOH unit, and, importantly, (iii) Ru^{III}-(OO•) rather than Ru^{IV}-OO is a reasonable description for Figure S12g due to the fact that the O-O distance (1.36 Å) is substantially shorter than those of other compounds (1.48 Å and 1.14 Å) and much higher spin density is located over the two oxygen atoms (see also Table S4g).

(b) $[Ru^{III}(terpy)(bpy)(OH_2)]^{3+}$

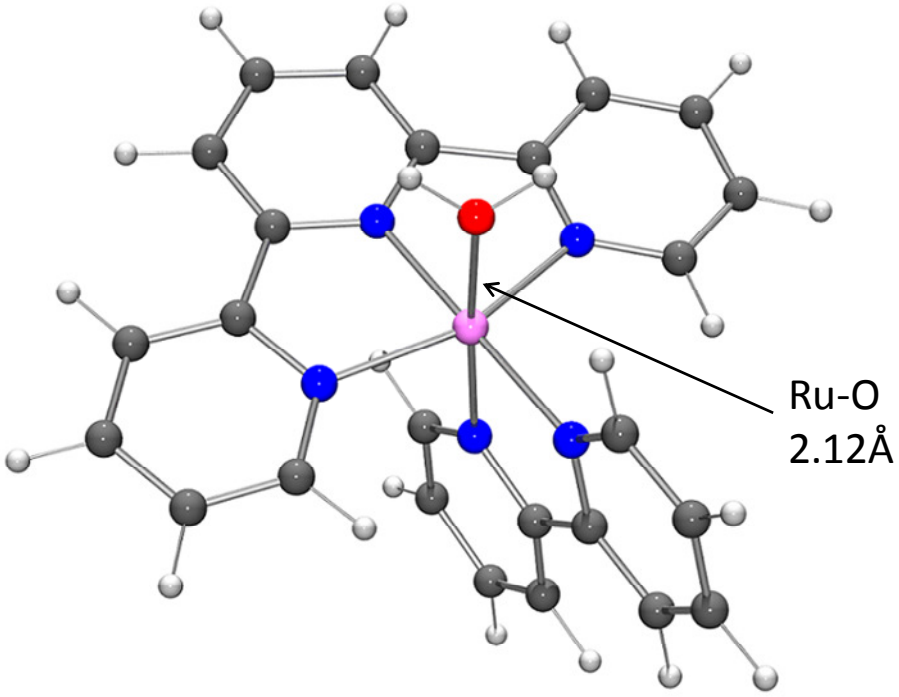

(c) $[Ru^{IV}(terpy)(bpy)(O)]^{2+}$

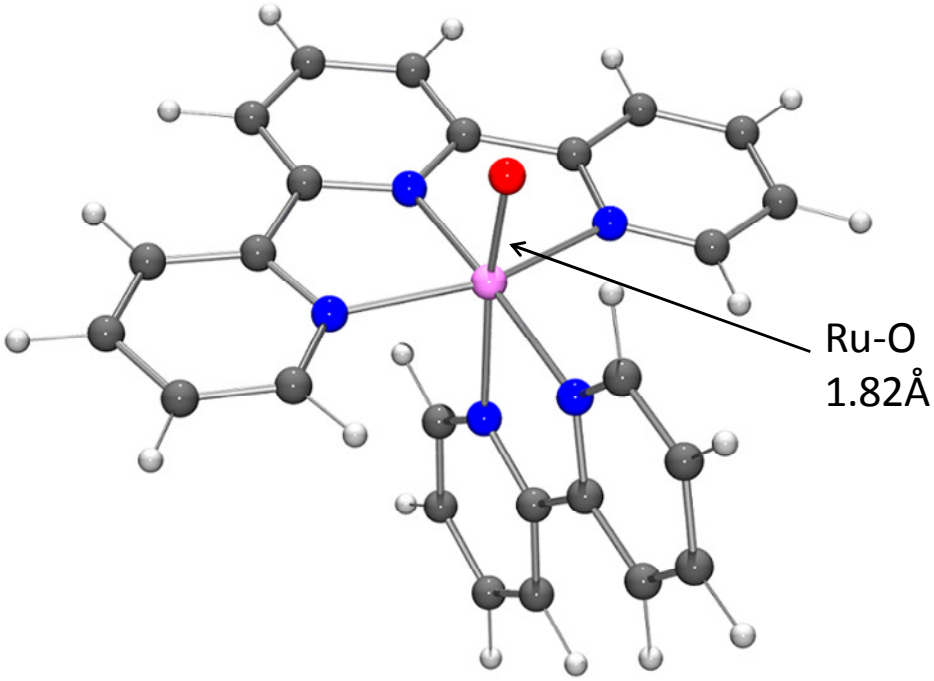

Figure S12. (continued)

(d) $[Ru^{V}(terpy)(bpy)(O)]^{3+}$

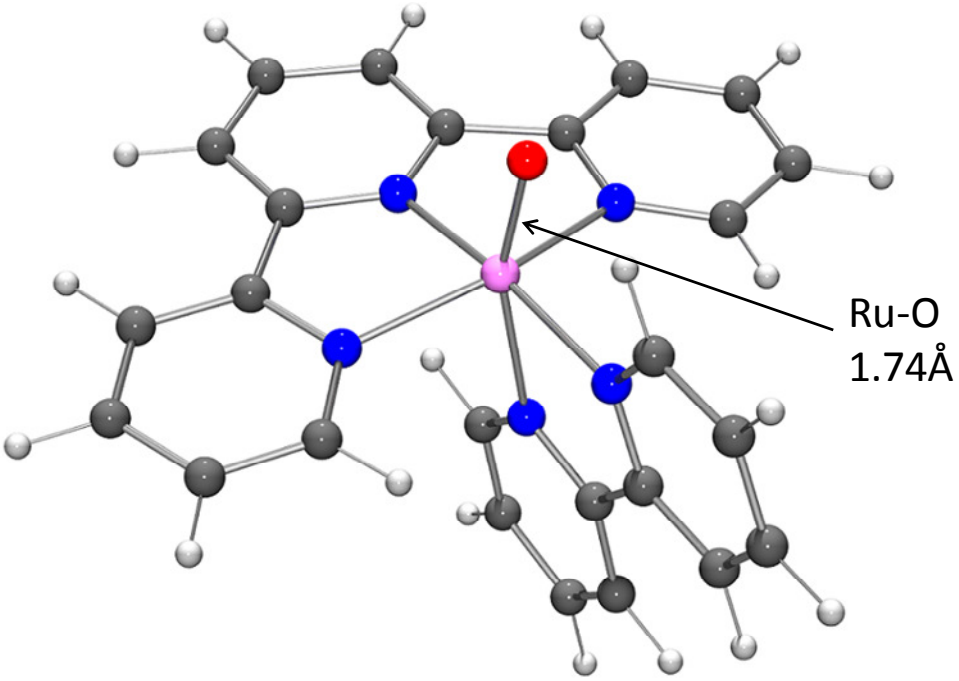

(e) $[Ru^{III}(terpy)(bpy)(OOH)]^{2+}$

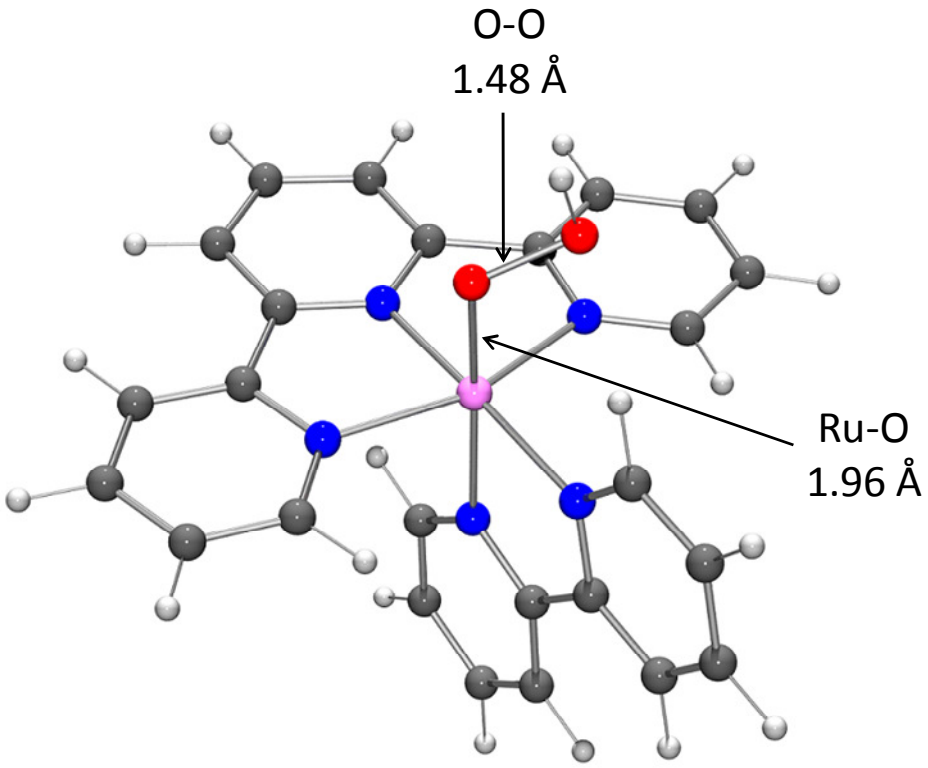

Figure S12. (continued)

(f) $[Ru^{IV}(terpy)(bpy)(OOH)]^{3+}$

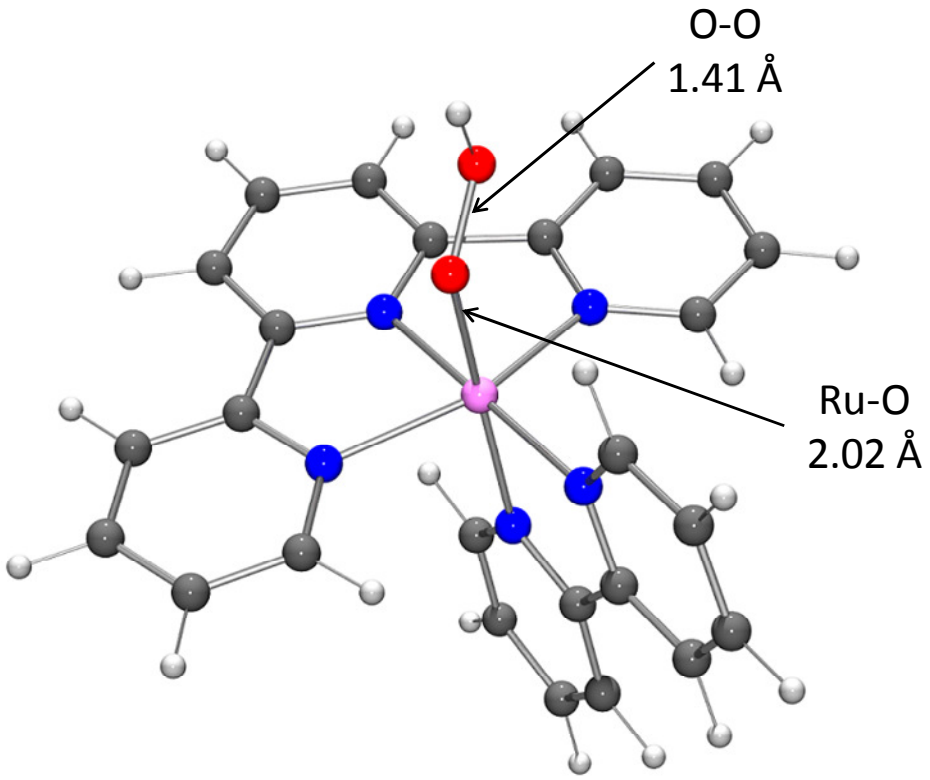

(g) $[Ru^{III}(terpy)(bpy)(OO\bullet)]^{2+}$

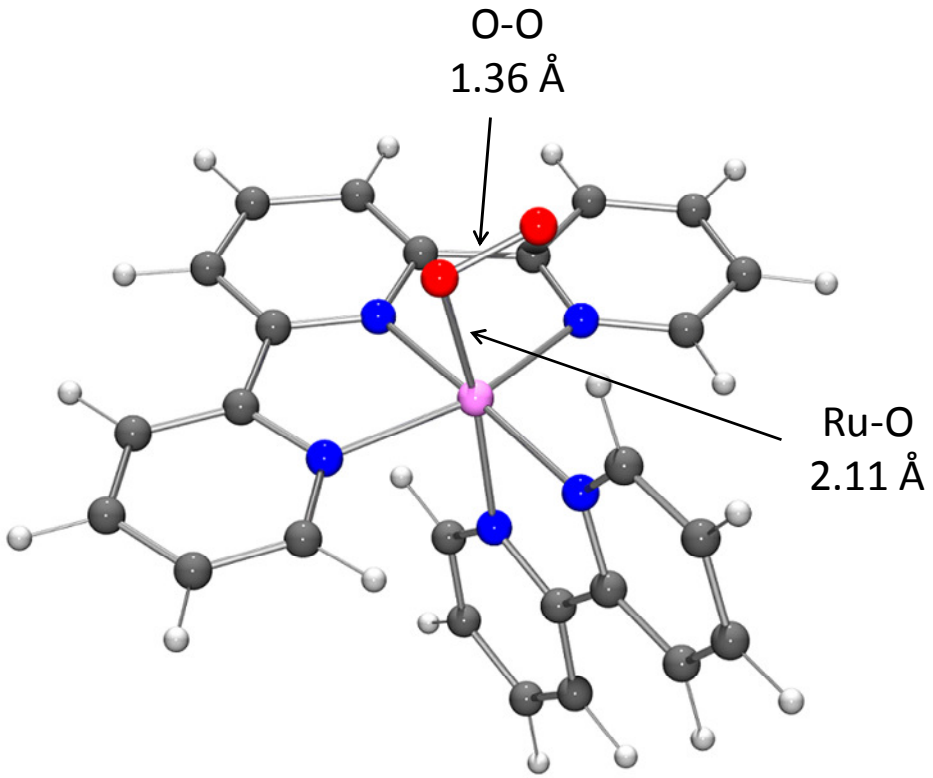

Figure S12.

(a) $[Ru^{III}(terpy)(bpy)(OH_2)]^{3+}$

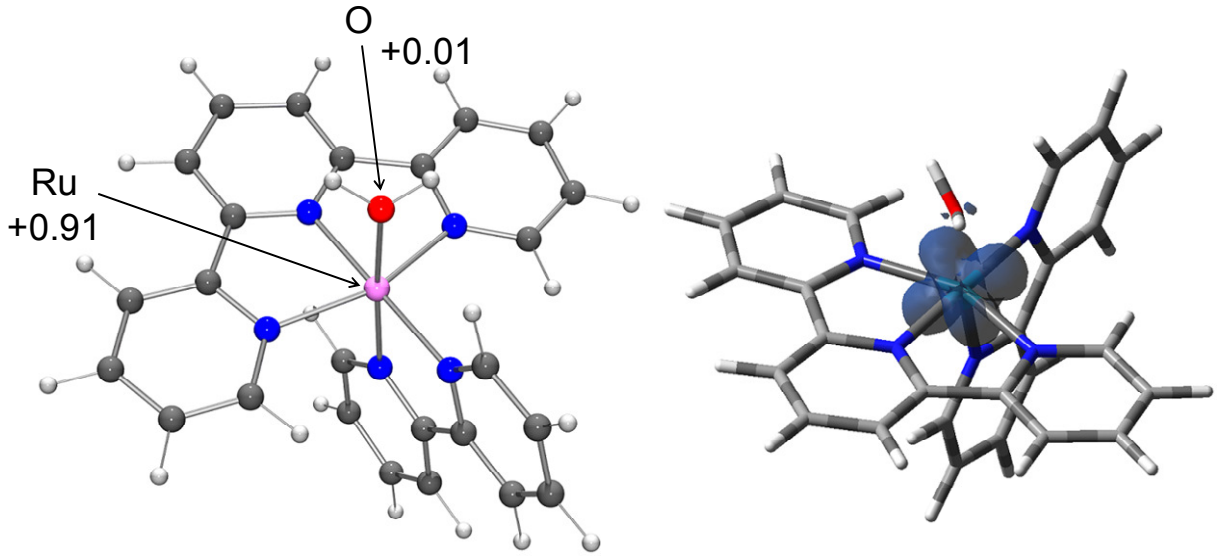

(b) $[Ru^{IV}(terpy)(bpy)(O)]^{2+}$

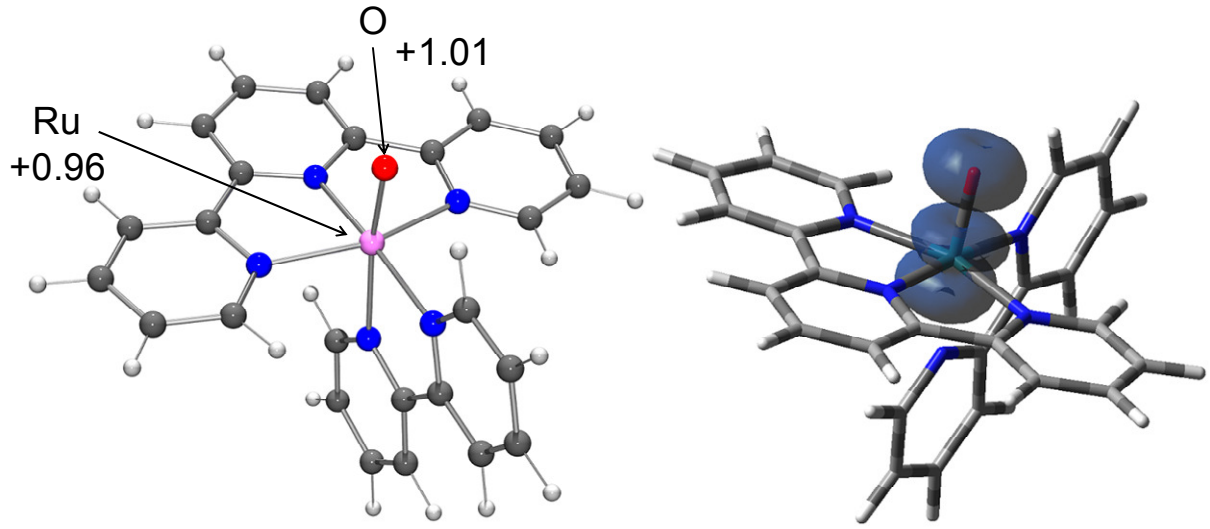

Figure S13. The spin density distributions of (a) $[Ru^{III}(terpy)(bpy)(OH_2)]^{3+}$ in the doublet state (the structure in the Figure S12b), (b) $[Ru^{IV}(terpy)(bpy)(O)]^{2+}$ in the triplet state (the structure in the Figure S12c), (c) $[Ru^{III}(terpy)(bpy)(OOH)]^{2+}$ in the doublet state (the structure in the Figure S12e), (d) $[Ru^{IV}(terpy)(bpy)(OOH)]^{3+}$ in the triplet state (the structure in the Figure S12f).

(c) $[Ru^{III}(terpy)(bpy)(OOH)]^{2+}$

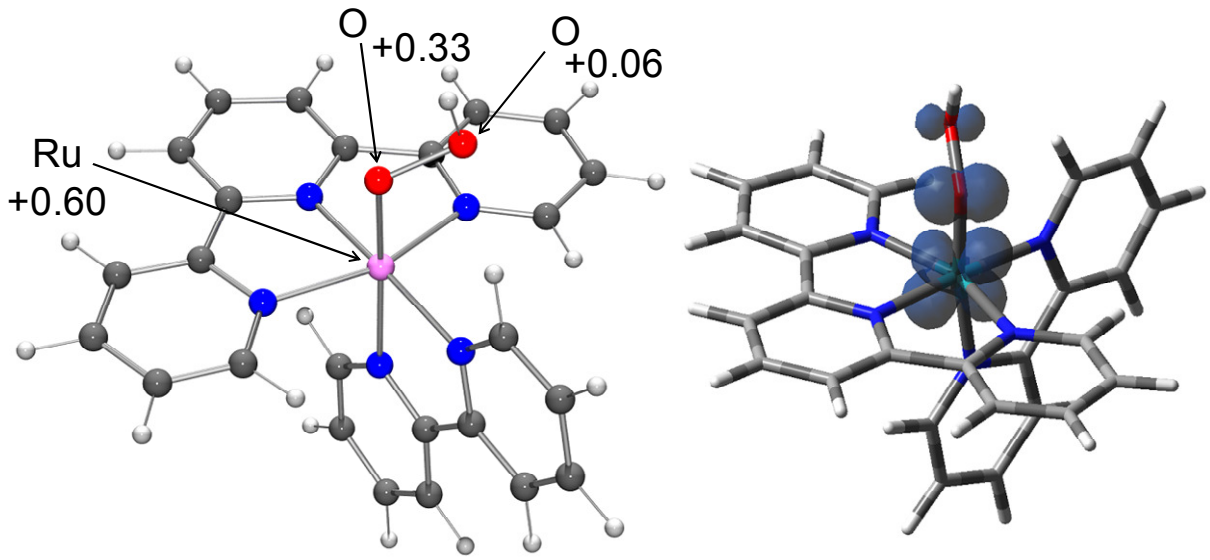

(d) $[Ru^{IV}(terpy)(bpy)(OOH)]^{3+}$

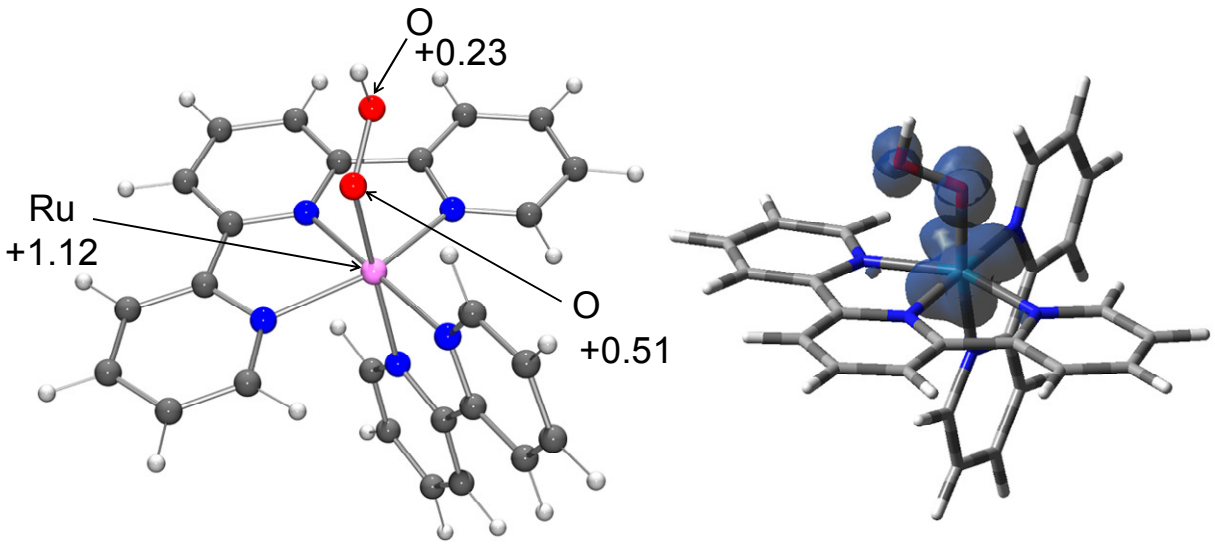

Figure S13. (continued)

(a) $[Ru^{II}(terpy)(bpy)(OH_2)]^{2+}$

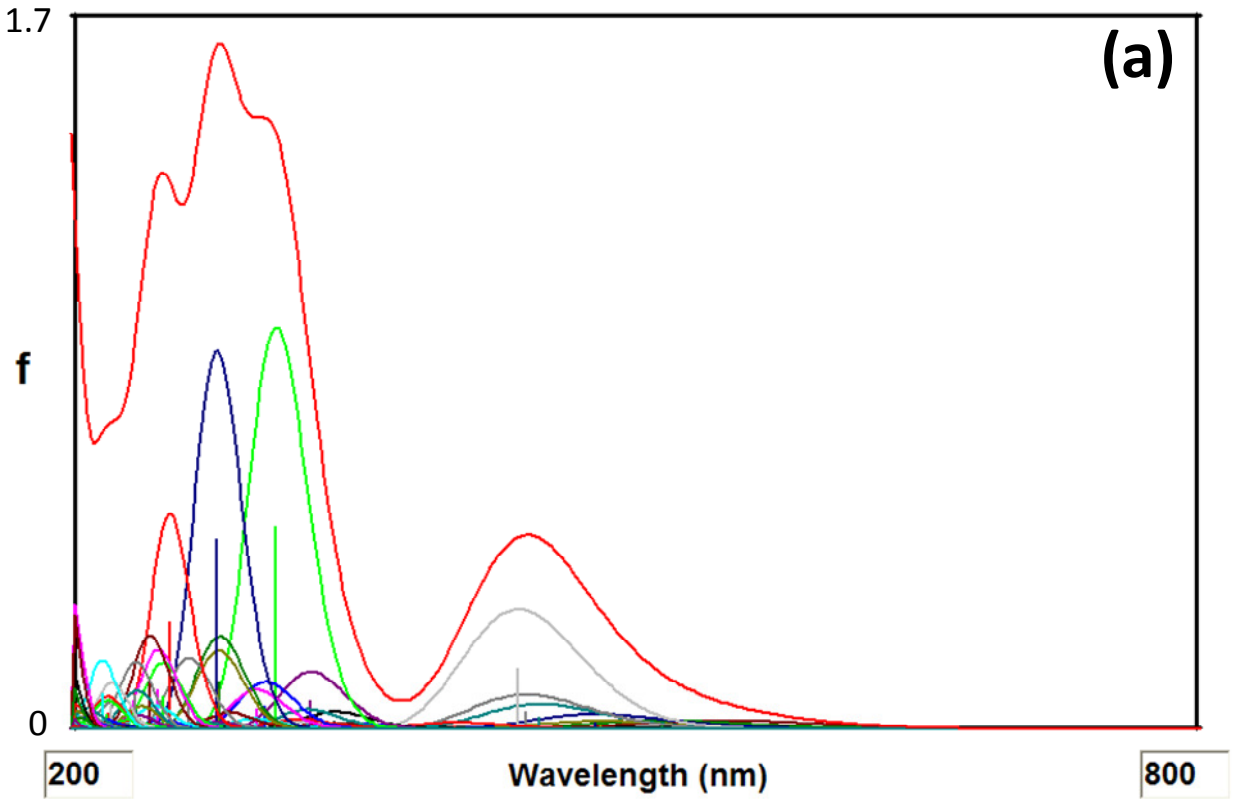

Figure S14. Simulated absorption spectra of (a) $[Ru^{II}(terpy)(bpy)(OH_2)]^{2+}$ (singlet), (b) $[Ru^{III}(terpy)(bpy)(OH_2)]^{3+}$ (doublet), (c) $[Ru^{IV}(terpy)(bpy)(O)]^{2+}$ (triplet), (d) $[Ru^{V}(terpy)(bpy)(O)]^{3+}$ (doublet), (e) $[Ru^{III}(terpy)(bpy)(OOH)]^{2+}$ (doublet), (f) $[Ru^{IV}(terpy)(bpy)(OOH)]^{3+}$ (triplet), and (g) $[Ru^{III}(terpy)(bpy)(OO\bullet)]^{2+}$ (triplet), in aqueous media, based on the results of TD-DFT calculations carried out for the structures shown above. The details of calculated oscillator strengths are summarized in Tables S5a-g.

(b) $[Ru^{III}(terpy)(bpy)(OH_2)]^{3+}$

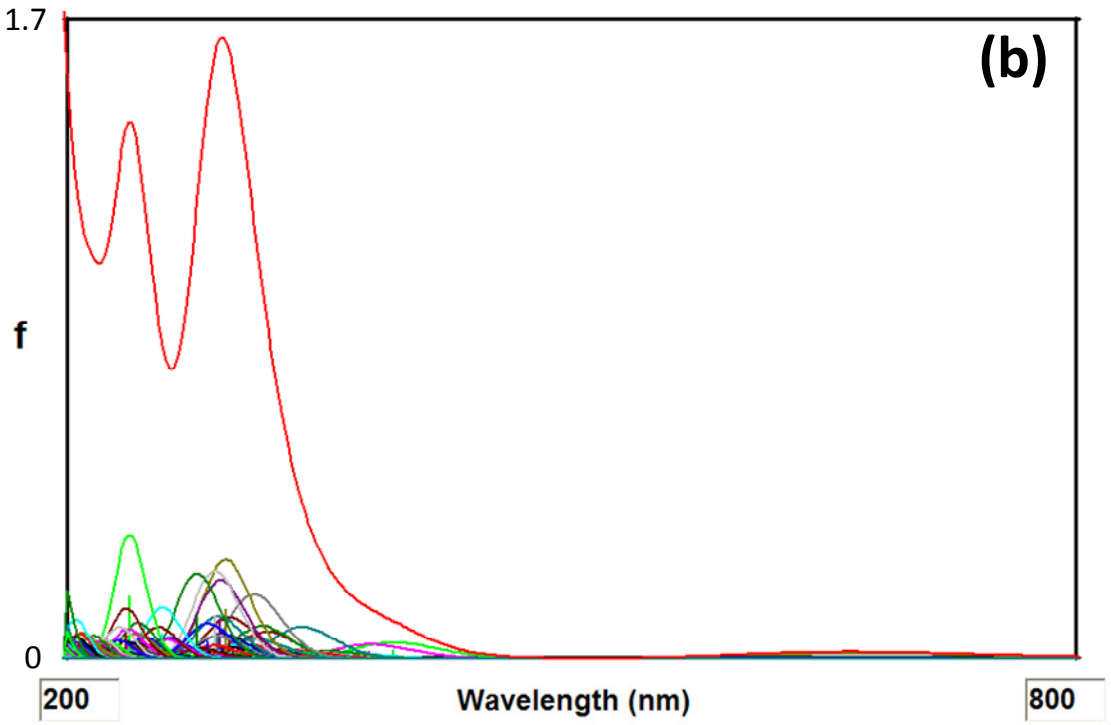

(c) $[Ru^{IV}(terpy)(bpy)(O)]^{2+}$

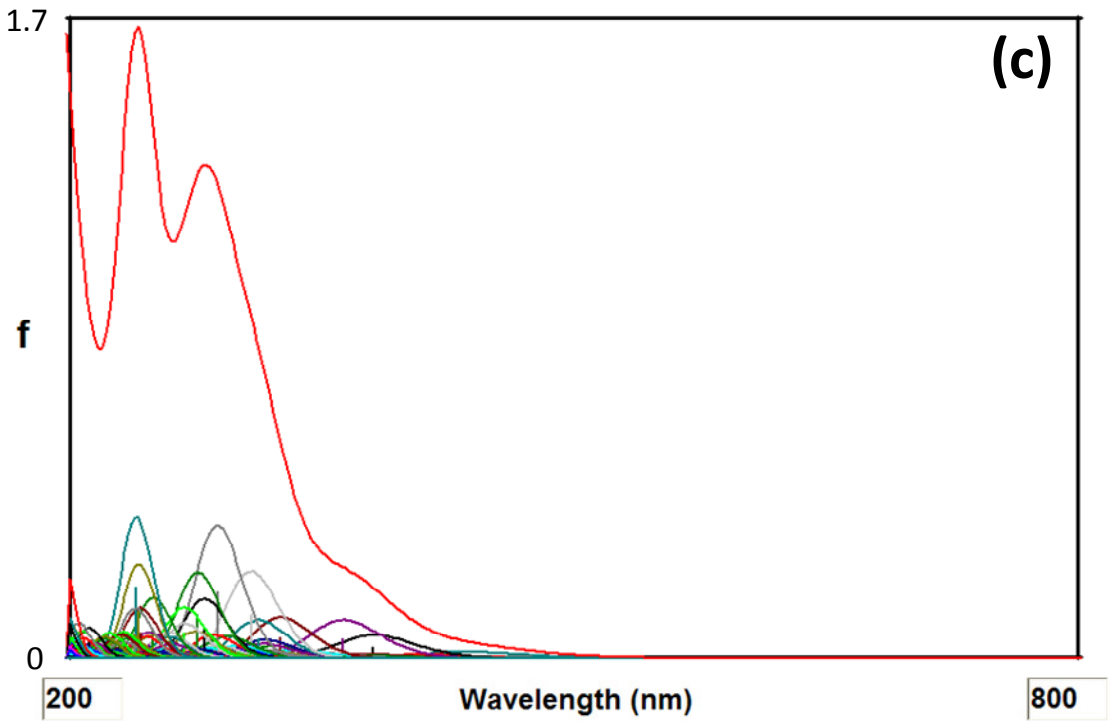

Figure S14. (continued)

(d) $[Ru^{V}(terpy)(bpy)(O)]^{3+}$

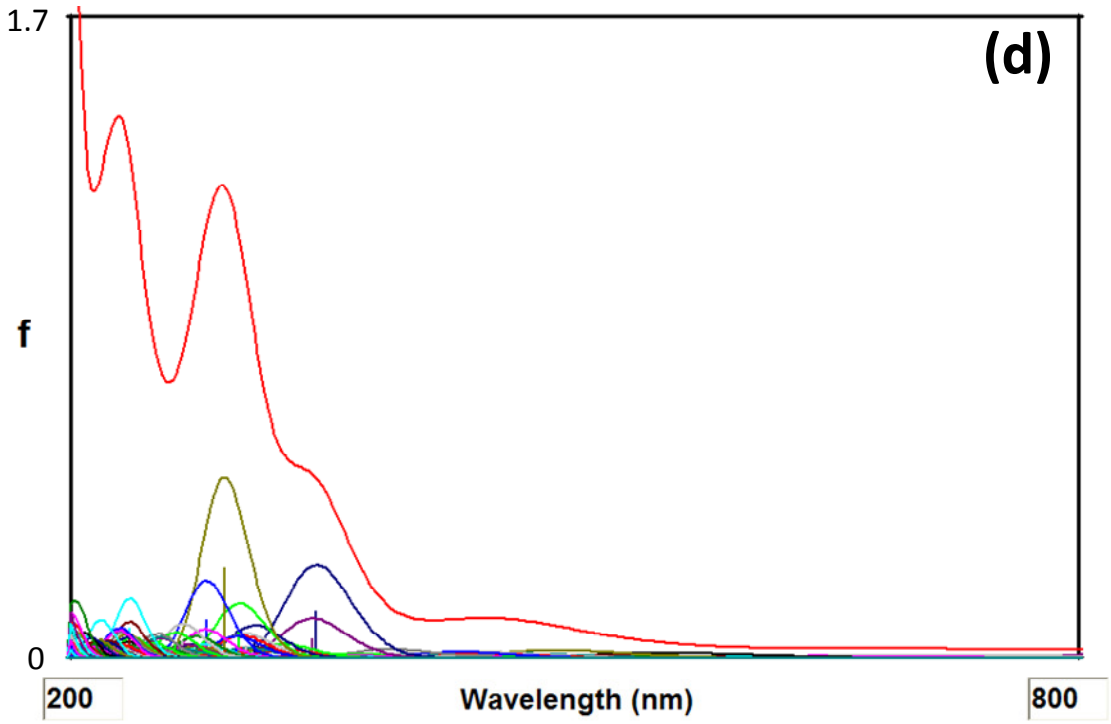

(e) $[Ru^{III}(terpy)(bpy)(OOH)]^{2+}$

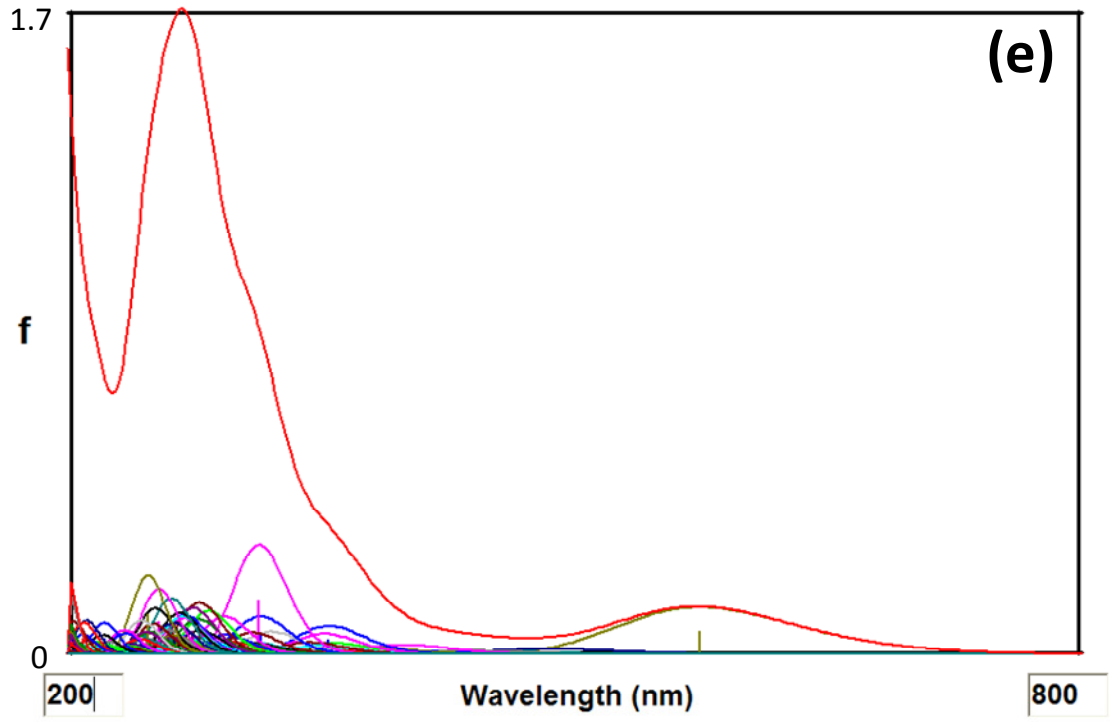

Figure S14. (continued)

(f) $[Ru^{IV}(terpy)(bpy)(OOH)]^{3+}$

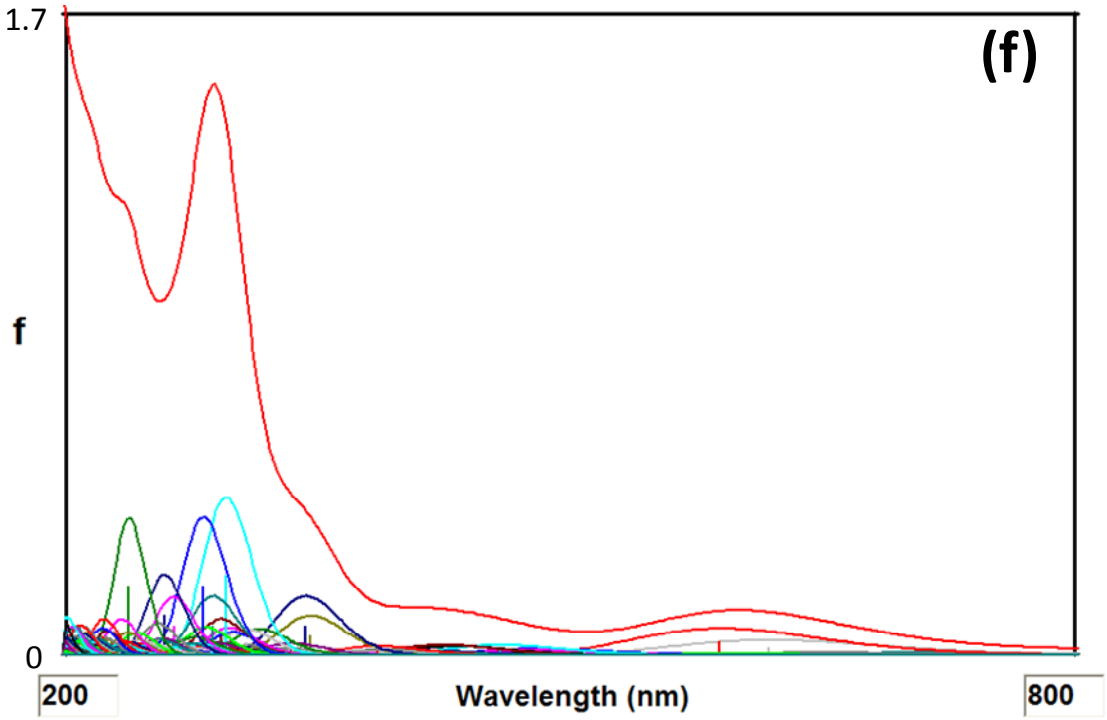

(g) $[Ru^{III}(terpy)(bpy)(OO\bullet)]^{2+}$

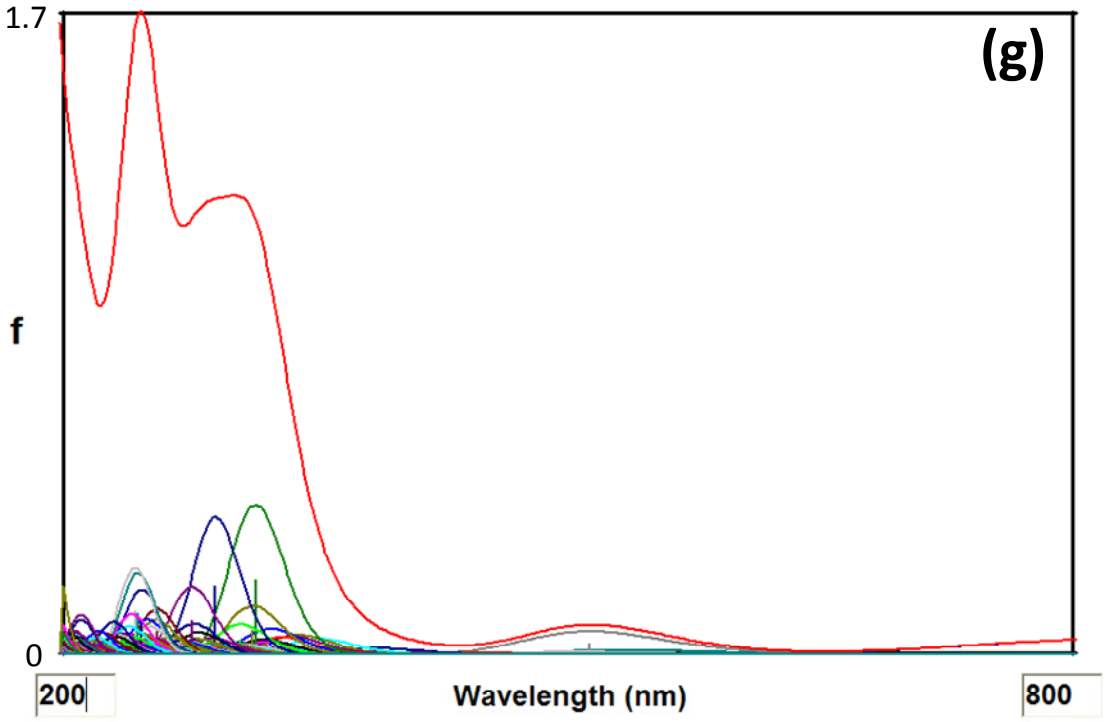

Figure S14.

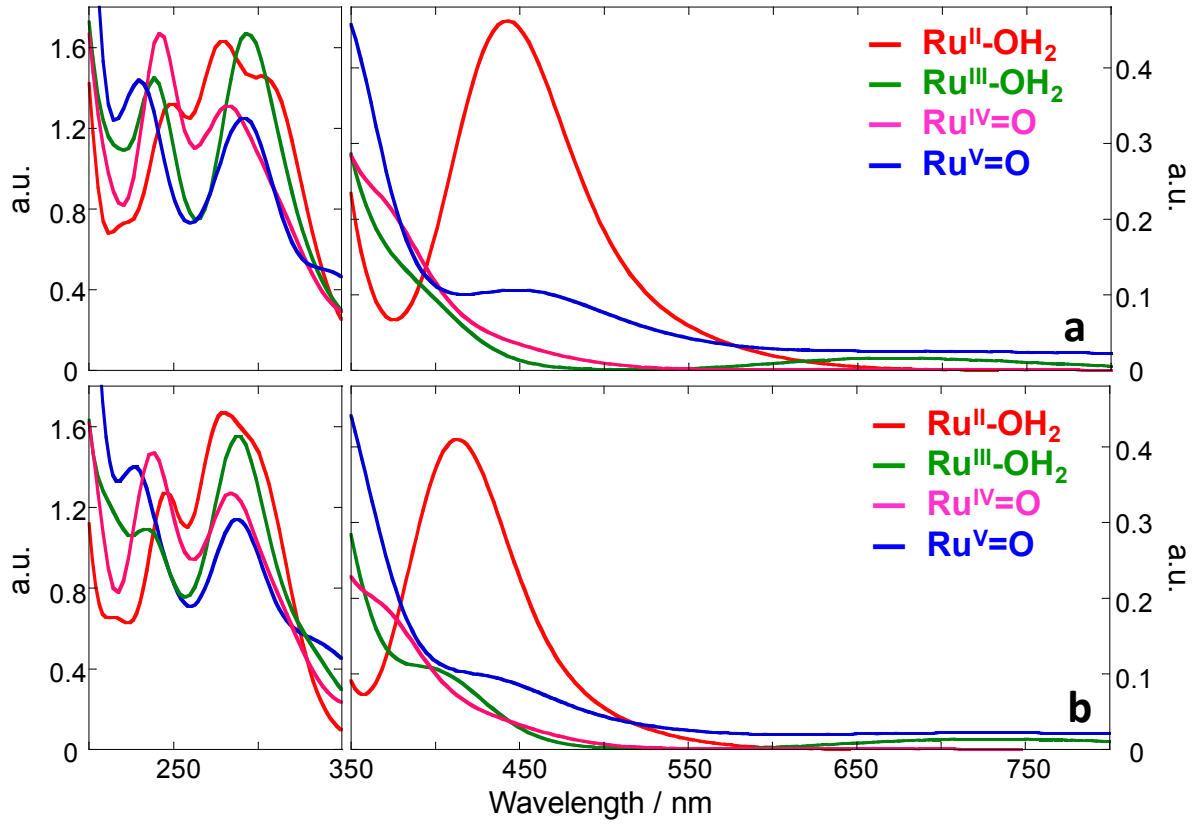

Figure S15. The absorption spectra simulated based on the TD-DFT calculations for the Ru^{II}-OH_2 (singlet), Ru^{III}-OH_2 (doublet), Ru^{IV}=O (triplet) and Ru^{V}=O (doublet). (a) The calculations were performed at the (U)B3LYP/LanL2DZ level using the PCM method, which are same to those used in Figure 2b. (b) The calculations were performed at the (U)B3LYP/LACVP** level (the LanL2DZ basis set for Ru and the 6-31G** basis set for H, C, N and O) using the PCM method. The details are supplied as Tables S5a-k and Figures S18a-g.

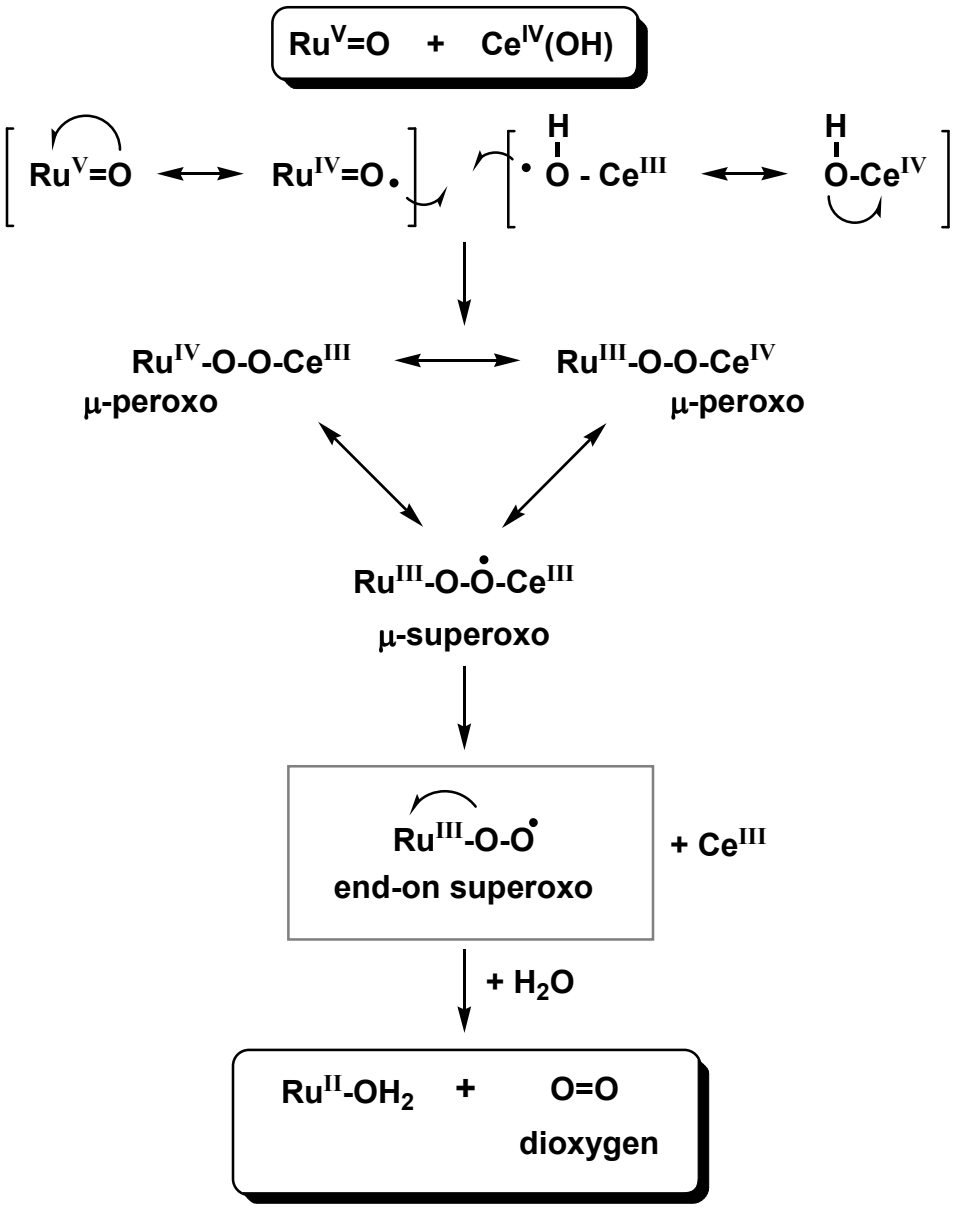

Figure S16. Possible rapid reaction paths after the RDS, in which only the deprotonated product is taken into consideration. The possible peroxo-bridged intermediate may be represented by two resonance structures, i.e., Ru^{IV}-O-O-Ce^{III} and Ru^{III}-O-O-Ce^{IV}, from which another resonance structure, i.e., a superoxo-bridged intermediate Ru^{III}-(OO•)-Ce^{III}, can be yielded. Elimination of Ce^{3+} from this superoxo species must be the more energetically favorable process considering the less negatively charged character of the superoxo bridge compared to the peroxo bridge. As a consequence, the end-on superoxo species proposed above could be given as the final product prior to the elimination of O_2. Finally, elimination of O_2 from the Ru^{III}-(OO•) species may regenerate the original form of the catalyst, i.e., Ru^{II}-OH_2.

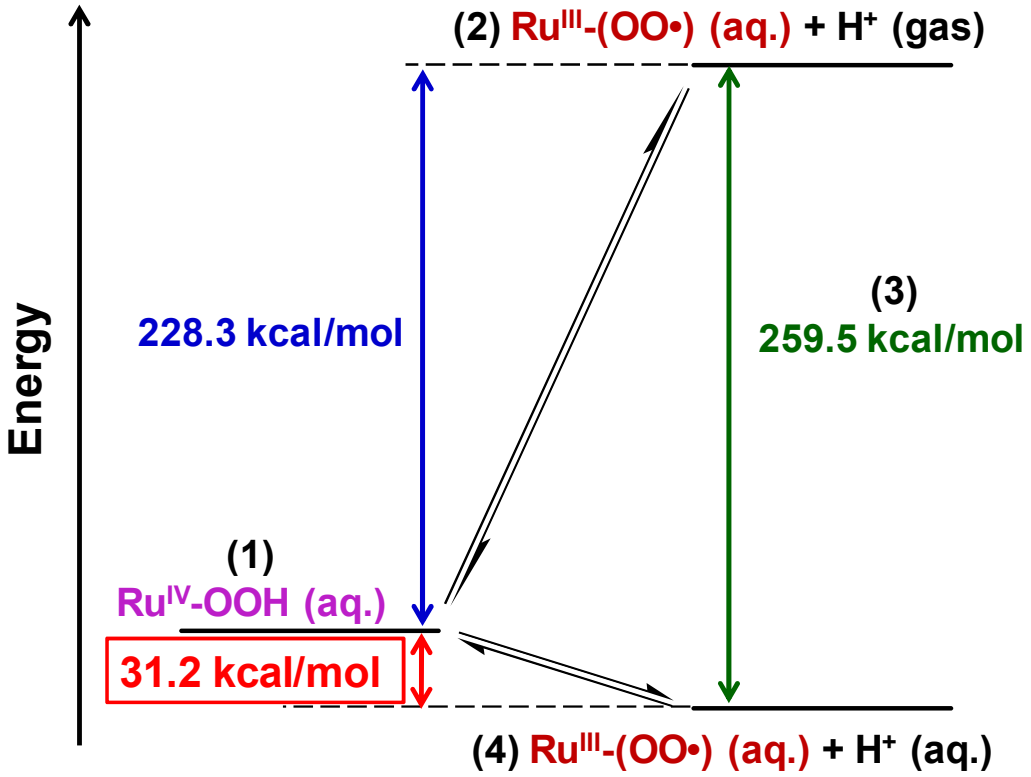

Figure S17. Energy diagram of deprotonation of Ru^{IV}-OOH in aqueous media based on DFT calculation and the reported value for the solvation free energy of proton (see Table S3). The elimination of Ce^{3+} from Ru^{IV}-O-O(H)-Ce^{III} or Ru^{IV}-O-O-Ce^{III} gives Ru^{IV}-OOH or Ru^{III}-(OO•), respectively. These two possible products can be correlated with the following acid dissociation equilibrium, where the notation 'aq.' denotes that the species is solvated in aqueous media:

$$Ru^{IV}\text{-OOH(aq.)} \overset{K_a}{\rightleftharpoons} Ru^{III}\text{-(OO•)(aq.)} + H^{+}\text{(aq.)}$$

By use of the DFT-based energies for these species in aqueous media, together with the solvation free energy of H^+ (–259.5 kcal/mol),[13] the pK_a value is estimated as pK_a = –23 using an equation $\Delta G^\circ = -RT\ln K_a$, where ΔG° = –130.5 kJ/mol in adopted to calculate the K_a value (see Table S3). At pH=1.0, the major species can be undoubtedly considered as Ru^{III}-(OO•), where the concentration of Ru^{IV}-OOH must be negligibly low. It is thus predicted that the end-on superoxo species (i.e, the deprotonated form) is likely to be the major species.

Table S3. The sum of electronic and zero-point energies of Ru^{IV}-OOH and Ru^{III}-(OO•) species based on DFT calculation (see Table S4) and the reported value for the solvation free energy of proton.

		Hartree	kcal/mol	kJ/mol
1	Ru^{IV}-OOH (hydroperoxo)	–1481.713024	–929789.74	-
2	Ru^{III}-(OO•) (superoxo)	–1481.349191	–929561.43	-
	Relative energy of **1** and **2**	-	228.31	-
3	H^+ (solvation free energy)	-	–259.5[a]	-
4	Ru^{III}-(OO•) + H^+	-	–929820.9	-
	Relative energy of **1** and **4**	-	–31.2	–130.5

a: Taken from ref.13.

Table S4(a). The optimized geometry of $[Ru^{II}(terpy)(bpy)(OH_2)]^{2+}$ (charge, +2; singlet), where the optimization was carried for a gaseous state at the B3LYP level of DFT using LanL2DZ basis set.

atom	X	Y	Z	Mulliken Charge
Ru1	-0.035459	-0.007123	-0.497198	-0.285839
N2	0.362015	-2.071657	-0.428188	0.090861
C3	1.222197	-4.741809	-0.240577	0.014539
C4	1.691769	-2.360756	-0.15684	0.18124
C5	-0.516185	-3.094796	-0.603318	-0.073092
C6	-0.124006	-4.439521	-0.517884	-0.090854
C7	2.136038	-3.689154	-0.059713	-0.265015
H8	-1.545847	-2.8261	-0.81712	0.12195
H9	-0.863263	-5.22437	-0.66577	0.14095
H10	3.180906	-3.90445	0.154816	0.155846
H11	1.555562	-5.775894	-0.166585	0.138445
N12	-2.097236	-0.02268	-0.832227	0.124898
C13	-4.896224	-0.042349	-1.042165	-0.011509
C14	-2.876428	-0.013956	0.304121	0.173475
C15	-2.696065	-0.042637	-2.056193	-0.134351
C16	-4.089941	-0.052489	-2.198193	-0.079382
C17	-4.281172	-0.023539	0.219961	-0.25128
H18	-2.032308	-0.049172	-2.91506	0.147245
H19	-4.528239	-0.067792	-3.194187	0.136947
H20	-4.891128	-0.0164	1.120388	0.148626
H21	-5.982197	-0.049542	-1.122318	0.134956
N22	0.335867	2.063293	-0.450438	0.085948
C23	1.159437	4.747104	-0.295368	0.019918
C24	-0.557854	3.07233	-0.626875	-0.077123
C25	1.662991	2.373372	-0.189718	0.18428
C26	2.089163	3.708908	-0.109939	-0.266277
C27	-0.184516	4.423272	-0.557854	-0.092669
H28	-1.585512	2.78722	-0.828615	0.12137
H29	3.132254	3.941015	0.09565	0.155784
H30	-0.936243	5.195959	-0.70684	0.141061
H31	1.479103	5.786375	-0.234699	0.138542
N32	-0.743289	0.009484	1.432369	0.17417
				(continued)

C33	-1.909479	0.041994	3.990431	0.005226
C34	-2.118179	0.00636	1.568464	0.166248
C35	0.035463	0.027274	2.550327	-0.068798
C36	-0.509613	0.043963	3.839758	-0.092752
C37	-2.715568	0.022829	2.841874	-0.238543
H38	1.10961	0.027608	2.404789	0.118198
H39	0.155489	0.058109	4.700908	0.143446
H40	-3.798677	0.021022	2.940434	0.151458
H41	-2.363356	0.055091	4.980099	0.138135
N42	1.923264	0.008275	-0.097042	0.120306
C43	4.646911	0.027843	0.344785	-0.034158
C44	2.564286	1.212682	-0.010629	0.107586
C45	2.578338	-1.186761	0.008486	0.107948
C46	3.965487	-1.200594	0.237248	-0.194437
C47	3.9511	1.246396	0.217561	-0.193675
H48	4.510923	-2.13782	0.325554	0.1651
H49	4.485769	2.191048	0.291262	0.164832
H50	5.72119	0.035603	0.521898	0.139815
O51	0.420931	-0.005604	-2.62533	-0.762735
H52	0.802327	-0.808295	-3.059781	0.475921
H53	0.754359	0.816221	-3.063299	0.477217

Sum of electronic and zero-point Energies = –1407.466620 Hartree

(Uncorrected energies; E(RB+HF-LYP) = –1407.88289956 Hartree)

Table S4(b). The optimized geometry of $[Ru^{III}(terpy)(bpy)(OH_2)]^{3+}$ (charge, +3; doublet), where the optimization was carried for a gaseous state at the UB3LYP level of DFT using LanL2DZ basis set.

atom	X	Y	Z	Mulliken Charge	Spin Density
Ru1	-0.0282	0.004397	-0.51802	1.93531	0.910633
N2	1.959445	0.018099	-0.11295	-0.29126	-0.00693
C3	4.685856	0.041182	0.213821	0.196041	-0.004978
C4	2.588969	1.222736	-0.02531	0.18356	-0.008236
C5	2.612752	-1.17549	-0.04747	0.187825	0.001024
C6	4.008097	-1.18912	0.121278	-0.283263	0.006881
C7	3.982115	1.260287	0.142776	-0.298136	0.012281
H8	4.559024	-2.12588	0.180784	0.188713	-0.000398
H9	4.515057	2.206047	0.220907	0.188265	-0.000733
H10	5.767385	0.051603	0.343219	0.164683	0.000262
N11	0.374881	-2.04323	-0.34357	-0.441959	0.011702
C12	1.197866	-4.7107	-0.17484	0.185207	0.013534
C13	1.717057	-2.344	-0.16318	0.295395	0.012466
C14	-0.54206	-3.04384	-0.41971	-0.025415	0.004979
C15	-0.1613	-4.39129	-0.34548	-0.204544	-0.001991
C16	2.144847	-3.67476	-0.07859	-0.328467	-0.006446
H17	-1.58352	-2.76752	-0.55532	0.153202	-0.000003
H18	-0.92255	-5.16549	-0.41979	0.165532	0.000574
H19	3.198817	-3.9072	0.063453	0.175726	0.000194
H20	1.518118	-5.74999	-0.11057	0.161677	-0.000759
N21	0.331509	2.062628	-0.28581	-0.475632	0.000846
C22	1.119264	4.738694	-0.09656	0.208268	0.021644
C23	1.671392	2.378915	-0.11573	0.313502	0.014875
C24	-0.59928	3.05162	-0.34487	0.002654	0.01479
C25	-0.23664	4.403485	-0.25911	-0.220279	-0.008651
C26	2.08155	3.713902	-0.02149	-0.351873	-0.008301
H27	-1.63794	2.762516	-0.47422	0.152944	-0.000701
H28	-1.00899	5.167863	-0.31742	0.165936	0.000917
H29	3.133398	3.960343	0.112023	0.176015	0.000291
H30	1.427077	5.781263	-0.02381	0.162228	-0.001245
N31	-0.78842	-0.04592	1.390396	-0.2141	-0.007733
C32	-2.00633	-0.08292	3.905836	0.159178	0.004951
C33	-0.02627	-0.08138	2.516552	-0.035845	-0.002332
					(continued)

C34	-2.16534	-0.0328	1.484787	0.263773	0.005121
C35	-2.79136	-0.04968	2.741712	-0.298498	-0.002332
C36	-0.6038	-0.10011	3.791347	-0.171147	0.001846
H37	1.051401	-0.09137	2.396873	0.144897	-0.000146
H38	-3.87644	-0.03795	2.818554	0.170828	-0.000097
H39	0.039909	-0.12613	4.668332	0.166305	-0.000215
H40	-2.48241	-0.09651	4.885457	0.158958	-0.000299
N41	-2.07197	0.00531	-0.91594	-0.387533	-0.006633
C42	-4.85102	-0.01065	-1.21604	0.1633	0.014684
C43	-2.88401	-0.01297	0.200122	0.281349	0.011907
C44	-2.62338	0.008911	-2.16102	-0.009673	0.003329
C45	-4.01137	0.000788	-2.34615	-0.2178	-0.003901
C46	-4.28106	-0.01937	0.06888	-0.343056	-0.006559
H47	-1.94209	0.007808	-3.00632	0.164103	-0.000365
H48	-4.41699	0.002508	-3.35591	0.161706	0.000139
H49	-4.92284	-0.03246	0.947242	0.167408	0.000214
H50	-5.93422	-0.01571	-1.33158	0.160301	-0.000878
O51	0.539236	0.037329	-2.56493	-0.973053	0.010182
H52	0.375861	0.824032	-3.1523	0.518886	0.001027
H53	1.27163	-0.52676	-2.93199	0.527858	-0.000434

Sum of electronic and zero-point Energies = –1407.262604 Hartree

(Uncorrected energies; E(UB+HF-LYP) = –1407.67927110 Hartree)

Table S4(c). The optimized geometry of $[Ru^{IV}(terpy)(bpy)(O)]^{2+}$ (charge, +2; triplet), where the optimization was carried for a gaseous state at the UB3LYP level of DFT using LanL2DZ basis set.

atom	X	Y	Z	Mulliken Charge	Spin Density
Ru1	-0.00587	-0.00412	-0.61156	1.368118	0.95684
N2	0.380141	-2.08108	-0.45151	-0.257458	-0.004261
C3	1.240686	-4.73535	-0.24869	0.148369	0.006613
C4	1.714427	-2.35708	-0.20496	0.221117	0.001601
C5	-0.50651	-3.09521	-0.5892	-0.025711	0.007843
C6	-0.11115	-4.43957	-0.49372	-0.164698	-0.001732
C7	2.161856	-3.6813	-0.10162	-0.296431	-0.000039
H8	-1.54066	-2.83127	-0.78641	0.134199	-0.000541
H9	-0.85352	-5.22634	-0.61235	0.154845	0.000091
H10	3.211337	-3.89673	0.089984	0.167194	-0.00009
H11	1.577261	-5.76851	-0.1727	0.150062	-0.000414
N12	1.960279	0.016935	-0.17091	-0.310121	-0.018179
C13	4.660018	0.0446	0.285619	0.242574	0.017173
C14	2.57878	1.22576	-0.06537	0.261034	0.013963
C15	2.602214	-1.17884	-0.05872	0.260311	0.013918
C16	3.98751	-1.18895	0.175957	-0.335665	-0.005826
C17	3.963813	1.264196	0.167905	-0.335654	-0.005821
H18	4.538138	-2.12268	0.270333	0.179596	0.000231
H19	4.496454	2.208793	0.256803	0.179228	0.000231
H20	5.73437	0.055579	0.465302	0.15782	-0.001067
N21	0.337958	2.081284	-0.45827	-0.256882	-0.004037
C22	1.144375	4.753344	-0.2686	0.148645	0.006387
C23	-0.56974	3.076378	-0.59798	-0.027739	0.007637
C24	1.667039	2.385298	-0.21597	0.221616	0.00142
C25	2.087357	3.718929	-0.11936	-0.296491	0.000095
C26	-0.20169	4.428908	-0.50895	-0.165306	-0.001587
H27	-1.59953	2.790963	-0.79095	0.136961	-0.000528
H28	3.132548	3.956693	0.069233	0.16705	-0.000097
H29	-0.96033	5.199827	-0.6288	0.154624	0.000084
H30	1.45977	5.793519	-0.19754	0.149959	-0.0004
N31	-0.73433	-0.00443	1.438592	-0.366296	-0.024536
C32	-1.90632	0.003617	3.980485	0.15409	0.014658
C33	-2.10348	-0.00993	1.560861	0.315788	0.012659
					(continued)

C34	0.043791	0.003654	2.553096	0.011586	0.010191
C35	-0.50604	0.008072	3.842181	-0.18941	-0.008504
C36	-2.71094	-0.00585	2.829476	-0.308886	-0.00834
H37	1.120894	0.00564	2.416039	0.127711	-0.001251
H38	0.152562	0.014769	4.708319	0.153081	0.000503
H39	-3.79386	-0.01028	2.928313	0.159961	0.000272
H40	-2.36618	0.006821	4.96789	0.145615	-0.000862
N41	-2.1073	-0.02446	-0.85717	-0.21659	0.005112
C42	-4.89846	-0.04149	-1.03463	0.12226	-0.005285
C43	-2.71507	-0.03692	-2.07459	-0.064637	0.002882
C44	-2.8634	-0.0216	0.291452	0.253627	-0.007326
C45	-4.26795	-0.03021	0.220553	-0.303745	0.004758
C46	-4.11044	-0.04581	-2.20051	-0.1602	0.003338
H47	-2.06217	-0.03858	-2.94265	0.179987	-0.000829
H48	-4.86957	-0.02775	1.126267	0.157344	-0.000465
H49	-4.55976	-0.05523	-3.19152	0.151747	0.000344
H50	-5.98573	-0.04772	-1.09923	0.146636	0.000312
O51	0.285603	-0.00151	-2.40265	-0.600833	1.012858

Sum of electronic and zero-point Energies = –1406.213120 Hartree

(Uncorrected energies; E(UB+HF-LYP) = –1406.60857794 Hartree)

Table S4(d). The optimized geometry of $[Ru^{V}(terpy)(bpy)(O)]^{3+}$ (charge, +3; doublet), where the optimization was carried for a gaseous state at the UB3LYP level of DFT using LanL2DZ basis set.

atom	X	Y	Z	Mulliken Charge	Spin Density
Ru1	-0.00981	0.056122	-0.68909	2.447823	0.404697
N2	-0.23252	2.064561	-0.25558	-0.53522	-0.016026
C3	-0.83802	4.765713	0.069731	0.331458	-0.006644
C4	-1.55837	2.459777	-0.10307	0.370277	-0.004808
C5	0.772925	2.982134	-0.22071	0.021883	0.000833
C6	0.498109	4.346213	-0.06547	-0.254116	0.001286
C7	-1.87481	3.810824	0.051969	-0.442618	0.003371
H8	1.792966	2.63069	-0.33131	0.172361	-0.000284
H9	1.322868	5.056426	-0.05253	0.181397	-0.000361
H10	-2.91154	4.125166	0.165739	0.192374	-0.000293
H11	-1.07439	5.822203	0.196068	0.18822	0.000311
N12	-1.97334	0.131714	-0.24727	-0.502137	-0.004225
C13	-4.68285	0.257031	0.099743	0.364593	0.01893
C14	-2.66657	-1.04328	-0.20061	0.30193	0.004977
C15	-2.54193	1.360918	-0.08968	0.172301	0.017525
C16	-3.92947	1.451186	0.085945	-0.350672	-0.01406
C17	-4.05956	-0.99967	-0.02996	-0.343233	-0.004727
H18	-4.42253	2.41397	0.212642	0.20577	0.000829
H19	-4.65049	-1.91352	0.01159	0.205731	0.000215
H20	-5.76359	0.307961	0.230386	0.188413	-0.001121
N21	-0.45483	-1.98443	-0.45164	-0.293668	-0.012138
C22	-1.34656	-4.61562	-0.26875	0.202837	0.00265
C23	0.443232	-2.99745	-0.49871	-0.134383	0.007589
C24	-1.80991	-2.23723	-0.30073	0.181421	-0.004301
C25	-2.27159	-3.55537	-0.21164	-0.264034	0.002834
C26	0.023499	-4.33414	-0.41034	-0.143449	-0.005318
H27	1.493378	-2.7522	-0.63058	0.175707	-0.000749
H28	-3.33439	-3.75932	-0.08865	0.19041	-0.0003
H29	0.766708	-5.12772	-0.46354	0.178703	0.000101
H30	-1.69473	-5.64589	-0.20147	0.17812	-0.000202
N31	0.666076	-0.16192	1.347261	-0.500391	-0.017
C32	1.735396	-0.4579	3.909483	0.243394	0.002703
C33	2.030899	-0.22431	1.513135	0.380952	0.001592
					(continued)

C34	-0.16186	-0.24762	2.425043	-0.051286	0.003656
C35	0.34162	-0.39289	3.72251	-0.226271	-0.003967
C36	2.585336	-0.37175	2.79485	-0.332419	-0.001863
H37	-1.23319	-0.19534	2.261271	0.150686	-0.000597
H38	-0.35072	-0.45178	4.560174	0.171111	0.000245
H39	3.66346	-0.42131	2.930616	0.178248	-0.00009
H40	2.155262	-0.57509	4.907992	0.170168	-0.000164
N41	2.10941	0.011558	-0.88544	-0.3484	0.010873
C42	4.897902	-0.06697	-0.98692	0.188376	-0.001603
C43	2.748298	0.11265	-2.08317	-0.105357	0.007679
C44	2.83011	-0.12738	0.27942	0.228641	-0.003602
C45	4.232621	-0.16981	0.246515	-0.296094	0.001621
C46	4.146289	0.077014	-2.167	-0.176917	-0.001216
H47	2.132822	0.221708	-2.97248	0.201492	-0.000866
H48	4.806681	-0.27962	1.163994	0.174755	-0.000175
H49	4.624099	0.159563	-3.14136	0.171358	0.000739
H50	5.986253	-0.09883	-1.02332	0.16584	0.000078
O51	-0.11868	-0.13867	-2.41703	-0.576088	0.611364

Sum of electronic and zero-point Energies = –1405.962330 Hartree

(Uncorrected energies; E(UB+HF-LYP) = –1406.35759444 Hartree)

Table S4(e). The optimized geometry of $[Ru^{III}(terpy)(bpy)(OOH)]^{2+}$ (charge, +2; doublet), where the optimization was carried for a gaseous state at the UB3LYP level of DFT using LanL2DZ basis set.

atom	X	Y	Z	Mulliken Charge	Spin Density
Ru1	-0.02712	0.009999	-0.46693	0.888616	0.597749
N2	-2.12031	-0.05407	-0.7181	-0.33369	0.004109
C3	-4.91727	-0.17152	-0.84869	-0.208934	-0.003638
C4	-2.75629	0.071989	-1.91484	-0.200801	-0.003195
C5	-2.85532	-0.23495	0.430869	0.277771	-0.00298
C6	-4.25969	-0.29576	0.386309	-0.299617	0.002487
C7	-4.15356	0.015406	-2.01644	-0.20547	0.003824
H8	-2.12765	0.234418	-2.7816	0.308076	-0.000095
H9	-4.83834	-0.43722	1.296095	0.295985	-0.000266
H10	-4.62405	0.11863	-2.99224	0.296065	-0.000127
H11	-6.00437	-0.21798	-0.89655	0.303009	0.000222
N12	-0.69972	-0.26944	1.515476	-0.299335	-0.009758
C13	-1.79831	-0.63316	4.069068	-0.205784	0.004966
C14	-2.06495	-0.35062	1.671643	0.267168	0.005251
C15	0.10818	-0.36945	2.605074	-0.182099	0.002047
C16	-0.40416	-0.54897	3.896357	-0.214637	-0.00263
C17	-2.63317	-0.53384	2.94474	-0.289143	-0.0032
H18	1.178243	-0.30079	2.446467	0.287457	-0.000451
H19	0.28027	-0.62074	4.739207	0.29956	0.00022
H20	-3.71208	-0.5978	3.064897	0.297429	0.000106
H21	-2.22867	-0.77405	5.059613	0.305972	-0.000286
N22	0.494977	-2.03458	-0.54268	-0.283877	0.001144
C23	1.514021	-4.64651	-0.58992	-0.203395	-0.003673
C24	1.841456	-2.25871	-0.30646	0.283655	-0.003706
C25	-0.32516	-3.08442	-0.79314	-0.20843	-0.004065
C26	0.148993	-4.40607	-0.82577	-0.198301	0.004642
C27	2.36726	-3.55917	-0.32676	-0.306044	0.003448
H28	-1.37386	-2.86524	-0.9711	0.285594	0.000197
H29	-0.54434	-5.219	-1.03254	0.299126	-0.000247
H30	3.425745	-3.72894	-0.13908	0.299955	-0.000285
H31	1.910715	-5.66061	-0.60976	0.305587	0.000219
N32	1.936097	0.105963	-0.03018	-0.379165	-0.011863
C33	4.634275	0.258575	0.42984	-0.193638	0.011706
					(continued)

C34	2.48174	1.336703	0.181191	0.269703	0.004771
C35	2.654527	-1.05101	-0.03454	0.263227	0.014017
C36	4.040205	-0.99756	0.20187	-0.305895	-0.006411
C37	3.861901	1.439042	0.421551	-0.305658	-0.002501
H38	4.647455	-1.90036	0.206934	0.305951	0.000347
H39	4.336035	2.402886	0.594513	0.305347	0.000045
H40	5.706129	0.320412	0.613498	0.305589	-0.000713
N41	0.196381	2.093007	-0.17713	-0.287963	-0.015177
C42	0.852911	4.786971	0.223586	-0.201477	0.011616
C43	-0.75823	3.049266	-0.27086	-0.200335	0.013559
C44	1.502323	2.451439	0.113334	0.285491	0.005403
C45	1.847293	3.794448	0.318427	-0.308674	-0.00297
C46	-0.46699	4.409996	-0.07741	-0.201414	-0.006763
H47	-1.76621	2.724962	-0.50926	0.285956	-0.000949
H48	2.873993	4.072517	0.548245	0.300326	0.00007
H49	-1.26375	5.146252	-0.16219	0.299181	0.000309
H50	1.109648	5.833764	0.380837	0.306004	-0.000707
O51	0.441486	0.069757	-2.36635	-0.280252	0.333634
O52	-0.11922	1.215854	-3.12302	-0.389835	0.063178
H53	0.206186	1.025062	-4.06244	0.466065	-0.002632

Sum of electronic and zero-point Energies = –1481.980980 Hartree

(Uncorrected energies; E(UB+HF-LYP) = –1482.38908068 Hartree)

Table S4(f). The optimized geometry of $[Ru^{IV}(terpy)(bpy)(OOH)]^{3+}$ (charge, +3; triplet), where the optimization was carried for a gaseous state at the UB3LYP level of DFT using LanL2DZ basis set.

atom	X	Y	Z	Mulliken Charge	Spin Density
Ru1	0.056881	-0.01033	-0.45879	1.002466	1.119435
N2	2.071063	-0.17808	-0.90799	-0.410159	-0.006244
C3	4.82204	-0.35699	-1.32863	-0.152887	0.038512
C4	2.558845	-0.31681	-2.17545	-0.113152	0.020537
C5	2.932781	-0.12328	0.171705	0.338505	0.021053
C6	4.31724	-0.21337	-0.02405	-0.259759	-0.011439
C7	3.932156	-0.40876	-2.4187	-0.169919	-0.013449
H8	1.832988	-0.34563	-2.97851	0.289661	-0.001734
H9	4.997368	-0.1747	0.817214	0.277299	0.000405
H10	4.289041	-0.51698	-3.43577	0.283556	0.00083
H11	5.89229	-0.42688	-1.4898	0.288188	-0.002311
N12	0.898267	0.073745	1.442808	-0.312405	-0.013046
C13	2.22141	0.216233	3.897808	-0.162378	0.000564
C14	2.274693	0.020207	1.481114	0.304116	0.000128
C15	0.185656	0.18585	2.592956	-0.13024	-0.001609
C16	0.817558	0.260198	3.840631	-0.183156	0.004109
C17	2.954657	0.092926	2.706162	-0.251408	0.002767
H18	-0.89269	0.21745	2.513387	0.286207	-0.000424
H19	0.21528	0.350479	4.736593	0.282149	-0.000379
H20	4.036033	0.053648	2.7379	0.276039	-0.000397
H21	2.73721	0.274056	4.850014	0.287786	-0.000051
N22	-0.22176	2.071372	-0.3534	-0.331535	0.033611
C23	-0.83499	4.792976	-0.29511	-0.156494	0.006895
C24	-1.52669	2.476353	-0.14204	0.331224	0.005899
C25	0.764993	2.990073	-0.51178	-0.136352	0.001799
C26	0.488279	4.36442	-0.49407	-0.173526	0.002487
C27	-1.85112	3.837255	-0.11305	-0.263974	-0.000961
H28	1.7715	2.62544	-0.66816	0.285151	0.000549
H29	1.297982	5.070256	-0.63496	0.28359	0.000936
H30	-2.87362	4.153035	0.053418	0.279077	-0.000114
H31	-1.07474	5.85046	-0.27542	0.289145	-0.000272
N32	-1.92187	0.141256	0.038685	-0.408332	-0.007847
C33	-4.62916	0.331365	0.483975	-0.152859	0.000567
					(continued)

C34	-2.63495	-1.00791	0.212612	0.300791	0.002694
C35	-2.49024	1.38092	0.069617	0.275553	0.000792
C36	-3.87011	1.501613	0.295273	-0.25702	0.006361
C37	-4.0166	-0.93479	0.44747	-0.258156	0.005549
H38	-4.34783	2.472739	0.325821	0.281758	-0.00021
H39	-4.60337	-1.83162	0.600144	0.281414	-0.000242
H40	-5.69617	0.406657	0.661299	0.287948	-0.000067
N41	-0.46609	-2.00769	-0.08785	-0.335405	0.028985
C42	-1.40529	-4.6124	0.263796	-0.156157	0.008922
C43	0.401894	-3.05085	-0.12733	-0.14833	0.003505
C44	-1.8109	-2.22733	0.145645	0.343405	0.006306
C45	-2.29851	-3.52676	0.320259	-0.267042	-0.001951
C46	-0.03931	-4.37106	0.040037	-0.170023	0.000656
H47	1.445663	-2.83025	-0.30662	0.284833	0.00033
H48	-3.3532	-3.69632	0.499465	0.278903	-0.000029
H49	0.680025	-5.17994	-0.00592	0.283298	0.000977
H50	-1.77126	-5.62441	0.397884	0.288865	-0.000408
O51	-0.51187	-0.00735	-2.39309	-0.15384	0.513912
O52	-1.44058	-0.99918	-2.7833	-0.240304	0.231843
H53	-1.56902	-0.84546	-3.75891	0.463888	-0.008732

Sum of electronic and zero-point Energies = –1481.713024 Hartree

(Uncorrected energies; E(UB+HF-LYP) = –1482.12676096 Hartree)

Table S4(g). The optimized geometry of $[Ru^{III}(terpy)(bpy)(OO\bullet)]^{2+}$ (charge, +2; triplet), where the optimization was carried for a gaseous state at the UB3LYP level of DFT using LanL2DZ basis set.

atom	X	Y	Z	Mulliken Charge	Spin Density
Ru1	0.028361	0.010125	-0.47526	0.821463	0.645858
N2	2.102463	-0.02434	-0.8298	-0.331845	0.001242
C3	4.894818	-0.10058	-1.05152	-0.204599	-0.001709
C4	2.693733	-0.00226	-2.05476	-0.193449	-0.003656
C5	2.88296	-0.07742	0.303891	0.284095	-0.000688
C6	4.285216	-0.1182	0.21387	-0.297623	0.001678
C7	4.087124	-0.03935	-2.20267	-0.201339	0.004289
H8	2.041728	0.045233	-2.92019	0.295735	-0.001175
H9	4.899331	-0.16297	1.110302	0.298282	-0.000192
H10	4.520434	-0.02023	-3.20067	0.29981	-0.000333
H11	5.980238	-0.1322	-1.13583	0.305795	0.000086
N12	0.764124	-0.04567	1.460725	-0.306086	-0.005054
C13	1.943351	-0.11222	3.996166	-0.197646	0.010662
C14	2.137016	-0.08232	1.575826	0.278304	0.009851
C15	-0.01336	-0.03827	2.577203	-0.170592	0.005082
C16	0.542776	-0.07167	3.861302	-0.214116	-0.004056
C17	2.744224	-0.11687	2.842937	-0.288336	-0.005205
H18	-1.08954	-0.00664	2.441803	0.299104	-0.000491
H19	-0.11356	-0.06659	4.729159	0.303515	0.000165
H20	3.82738	-0.14547	2.936403	0.301566	0.000288
H21	2.405115	-0.13857	4.982306	0.309145	-0.000643
N22	-0.26429	2.088175	-0.27575	-0.303663	-0.008031
C23	-0.99871	4.782222	-0.09601	-0.194715	0.010025
C24	-1.59331	2.430333	-0.08462	0.297855	0.008654
C25	0.678772	3.05904	-0.36841	-0.196384	0.006876
C26	0.346952	4.419778	-0.28334	-0.197296	-0.003815
C27	-1.97665	3.775839	0.005319	-0.302826	-0.004894
H28	1.706701	2.745606	-0.51958	0.290385	-0.00045
H29	1.132053	5.168803	-0.36525	0.302906	0.000303
H30	-3.02107	4.043156	0.154168	0.302982	0.000153
H31	-1.2859	5.830775	-0.02791	0.309155	-0.000592
N32	-1.94624	0.073422	-0.06064	-0.364782	-0.001688
C33	-4.66492	0.177	0.319512	-0.194759	-0.007005
					(continued)

C34	-2.63012	-1.10004	0.039042	0.251227	-0.007569
C35	-2.53945	1.296663	0.029958	0.267269	-0.003457
C36	-3.92905	1.374582	0.224157	-0.30178	0.006746
C37	-4.02184	-1.07309	0.233418	-0.301834	0.006795
H38	-4.43493	2.334927	0.300412	0.306479	-0.00037
H39	-4.59735	-1.99299	0.31528	0.307236	-0.000484
H40	-5.74326	0.218555	0.46665	0.30702	0.00042
N41	-0.42379	-2.0462	-0.28232	-0.302469	0.010693
C42	-1.33543	-4.68345	-0.0694	-0.196273	0.012182
C43	0.4514	-3.07852	-0.37779	-0.196395	0.008535
C44	-1.76859	-2.29798	-0.07096	0.295422	0.011141
C45	-2.24217	-3.61325	0.035471	-0.303788	-0.006109
C46	0.029075	-4.41287	-0.27718	-0.198388	-0.004698
H47	1.495948	-2.83568	-0.54868	0.292947	-0.000271
H48	-3.30049	-3.80715	0.199165	0.303072	0.000327
H49	0.76055	-5.21393	-0.36321	0.302025	0.000624
H50	-1.6907	-5.70997	0.01158	0.308493	-0.000704
O51	-0.53405	0.437746	-2.45965	-0.144069	0.539328
O52	-0.26462	-0.77532	-2.99893	-0.136232	0.771337

Sum of electronic and zero-point Energies = –1481.349191 Hartree

(Uncorrected energies; E(UB+HF-LYP) = –1481.74665993 Hartree)

Table S4(h). The optimized geometry of $[Ru^{II}(terpy)(bpy)(OH_2)]^{2+}$ (charge, +2; singlet), where the optimization was carried for a gaseous state at the B3LYP level of DFT using LACVP** basis set.

atom	X	Y	Z	Mulliken Charge
Ru1	0.043094	-0.000528	-0.510804	0.811957
N2	-0.364276	2.082945	-0.446449	-0.533295
C3	-1.222859	4.728682	-0.260694	-0.062157
C4	-1.678234	2.363258	-0.174394	0.288881
C5	0.496742	3.098881	-0.623241	0.098596
C6	0.109581	4.433851	-0.539303	-0.090089
C7	-2.124148	3.681636	-0.077562	-0.096445
H8	1.521932	2.820665	-0.837130	0.160363
H9	0.844706	5.215734	-0.689860	0.147118
H10	-3.164374	3.890670	0.139584	0.148870
H11	-1.560328	5.756644	-0.186271	0.150412
N12	-1.926628	0.001625	-0.108894	-0.625834
C13	-4.621700	0.004000	0.371045	-0.076633
C14	-2.566977	-1.185502	-0.000980	0.289090
C15	-2.565041	1.189894	-0.001619	0.288737
C16	-3.939727	1.214830	0.245507	-0.091964
C17	-3.941723	-1.208022	0.246055	-0.091977
H18	-4.473277	2.152563	0.335991	0.152401
H19	-4.476829	-2.144814	0.337034	0.152397
H20	-5.688787	0.004930	0.562822	0.152013
N21	-0.367208	-2.082770	-0.442668	-0.533876
C22	-1.230562	-4.726824	-0.254682	-0.062161
C23	0.492403	-3.100469	-0.616679	0.098576
C24	-1.682074	-2.360512	-0.172053	0.288831
C25	-2.130332	-3.678006	-0.074237	-0.096305
C26	0.102831	-4.434651	-0.531509	-0.089990
H27	1.518377	-2.824295	-0.829459	0.160494
H28	-3.171237	-3.884997	0.141615	0.148927
H29	0.836853	-5.217984	-0.679885	0.147177
H30	-1.569942	-5.754102	-0.179513	0.150475
N31	0.756095	0.001709	1.428751	-0.562208
C32	1.903260	0.002805	3.969327	-0.063831
C33	2.115190	0.000674	1.564867	0.301108
C34	-0.014279	0.003140	2.533747	0.111714

C35	0.517933	0.003772	3.817287	-0.094863
C36	2.704479	0.001209	2.832017	-0.096031
H37	-1.084257	0.003628	2.372176	0.155823
H38	-0.148425	0.004915	4.671791	0.146675
H39	3.782249	0.000308	2.930491	0.147030
H40	2.354908	0.003198	4.955194	0.148876
N41	2.130234	-0.001981	-0.826597	-0.528692
C42	4.907899	-0.003695	-1.000366	-0.066883
C43	2.884056	-0.001175	0.306737	0.286567
C44	2.741055	-0.003383	-2.026466	0.094368
C45	4.125540	-0.004331	-2.155221	-0.089502
C46	4.280567	-0.002042	0.242111	-0.097205
H47	2.083665	-0.003575	-2.888368	0.163804
H48	4.572743	-0.005525	-3.142443	0.143188
H49	4.874557	-0.001409	1.147163	0.145338
H50	5.990609	-0.004421	-1.063390	0.146419
O51	-0.355332	-0.007333	-2.691427	-0.542816
H52	-0.864801	0.747862	-3.020910	0.383277
H53	-0.812631	-0.796895	-3.016982	0.383256

Sum of electronic and zero-point Energies = –1407.643603 Hartree

(Uncorrected energies; E(RB3LYP) = –1408.06256781 Hartree)

Table S4(i). The optimized geometry of $[Ru^{III}(terpy)(bpy)(OH_2)]^{3+}$ (charge, +3; doublet), where the optimization was carried for a gaseous state at the UB3LYP level of DFT using LACVP** basis set.

atom	X	Y	Z	Mulliken Charge	Spin Density
Ru1	-0.03567	0.008805	-0.53578	0.101608	0.905282
N2	1.962739	0.043565	-0.13987	-0.65534	-0.00875
C3	4.662863	0.092469	0.236349	-0.07532	-0.00485
C4	2.574642	1.242372	-0.04061	0.30795	-0.00594
C5	2.620773	-1.13249	-0.05551	0.303059	-7E-06
C6	4.003639	-1.13319	0.137312	-0.09398	0.006512
C7	3.955516	1.293553	0.15284	-0.0936	0.010379
H8	4.559223	-2.06555	0.213824	0.19758	-0.0002
H9	4.475285	2.245014	0.243129	0.19731	-0.00034
H10	5.741132	0.112926	0.3875	0.191898	0.000169
N11	0.409087	-2.03987	-0.3288	-0.58753	0.016383
C12	1.269963	-4.67101	-0.15866	-0.06089	0.011953
C13	1.742906	-2.31243	-0.16247	0.314014	0.009134
C14	-0.48052	-3.04727	-0.3926	0.109891	0.005099
C15	-0.08355	-4.37907	-0.31666	-0.09692	-0.00079
C16	2.192198	-3.62702	-0.07743	-0.09888	-0.00538
H17	-1.52691	-2.78182	-0.51706	0.195269	0.000373
H18	-0.83428	-5.16401	-0.38148	0.187167	0.000764
H19	3.2513	-3.83834	0.054847	0.193229	0.000054
H20	1.61044	-5.7035	-0.09316	0.189596	-0.00039
N21	0.326258	2.07317	-0.28206	-0.59209	0.009842
C22	1.093359	4.73087	-0.08077	-0.0597	0.019039
C23	1.65141	2.391038	-0.12569	0.321088	0.011561
C24	-0.5998	3.049299	-0.31709	0.11259	0.012331
C25	-0.25048	4.393053	-0.22587	-0.0972	-0.00587
C26	2.053711	3.719166	-0.02609	-0.09974	-0.00687
H27	-1.63798	2.748711	-0.42897	0.193946	0.00004
H28	-1.02982	5.151178	-0.26683	0.187316	0.000917
H29	3.105774	3.96743	0.09758	0.193491	0.000096
H30	1.397718	5.773724	-0.00302	0.190213	-0.00069
N31	-0.7971	-0.05356	1.380686	-0.59227	-0.00776
C32	-1.99728	-0.12516	3.878956	-0.06376	0.00351
C33	-0.04104	-0.09199	2.494507	0.113911	-0.00253
C34	-2.1597	-0.05096	1.47651	0.310284	0.003474

C35	-2.77836	-0.08589	2.726806	-0.09921	-0.00174
C36	-0.60788	-0.12904	3.762449	-0.09951	0.002564
H37	1.036546	-0.08995	2.366186	0.188842	-0.00019
H38	-3.86297	-0.08505	2.803846	0.190744	-0.00017
H39	0.040552	-0.15957	4.635525	0.185683	-0.00022
H40	-2.47261	-0.15361	4.858287	0.187114	-0.00015
N41	-2.09692	-0.01926	-0.91523	-0.57617	-0.00586
C42	-4.85572	-0.02184	-1.18315	-0.06433	0.016172
C43	-2.8868	-0.02691	0.198428	0.295908	0.011658
C44	-2.65881	-0.02434	-2.14001	0.108117	0.005236
C45	-4.03746	-0.02562	-2.31283	-0.0935	-0.00424
C46	-4.27633	-0.02388	0.084466	-0.10065	-0.0069
H47	-1.9837	-0.03516	-2.99082	0.191486	-0.00039
H48	-4.45196	-0.03007	-3.31867	0.183777	0.000058
H49	-4.9063	-0.0261	0.970635	0.189649	0.000105
H50	-5.9401	-0.01958	-1.28416	0.186611	-0.00067
O51	0.496887	-0.07679	-2.61846	-0.57681	0.007361
H52	0.363165	0.742036	-3.15364	0.430219	0.001519
H53	1.387919	-0.4124	-2.87389	0.427838	-0.0007

Sum of electronic and zero-point Energies = – 1407.467233 Hartree

(Uncorrected energies; E(UB+HF-LYP) = – 1407.88154920 Hartree)

Table S4(j). The optimized geometry of $[Ru^{IV}(terpy)(bpy)(OH_2)]^{2+}$ (charge, +2; triplet), where the optimization was carried for a gaseous state at the UB3LYP level of DFT using LACVP** basis set.

atom	X	Y	Z	Mulliken Charge	Spin Density
Ru1	0.000661	0.000057	-0.6333	1.063866	0.978243
N2	0.402122	-2.08865	-0.46923	-0.55374	-0.00204
C3	1.28152	-4.7141	-0.26044	-0.06492	0.006094
C4	1.722214	-2.34794	-0.21328	0.31261	0.001295
C5	-0.46029	-3.105	-0.61463	0.106813	0.006852
C6	-0.05829	-4.43587	-0.5171	-0.10214	-0.00139
C7	2.181194	-3.65874	-0.10501	-0.10789	0.000121
H8	-1.49427	-2.84532	-0.81998	0.180774	-0.00047
H9	-0.79251	-5.22854	-0.6439	0.176865	0.00014
H10	3.230327	-3.86041	0.099178	0.183541	-5.2E-05
H11	1.630043	-5.74252	-0.17902	0.179776	-0.00027
N12	1.964233	0.019551	-0.17125	-0.67414	-0.01642
C13	4.633505	0.046934	0.339224	-0.07402	0.018641
C14	2.573954	1.217539	-0.04666	0.322651	0.014624
C15	2.599712	-1.1657	-0.05265	0.321607	0.014611
C16	3.970736	-1.17552	0.210179	-0.10474	-0.00699
C17	3.944498	1.255422	0.215889	-0.10473	-0.007
H18	4.518305	-2.10956	0.312916	0.19009	0.000216
H19	4.471963	2.200495	0.322844	0.189884	0.000216
H20	5.70342	0.058006	0.541757	0.185729	-0.00081
N21	0.357231	2.095633	-0.45964	-0.55425	-0.00207
C22	1.181422	4.738097	-0.24002	-0.06494	0.006067
C23	-0.52606	3.094266	-0.60289	0.104841	0.006838
C24	1.67157	2.381625	-0.20168	0.312582	0.001271
C25	2.102793	3.701212	-0.08743	-0.10809	0.00014
C26	-0.15179	4.432887	-0.50041	-0.10242	-0.00137
H27	-1.55463	2.814489	-0.80987	0.184847	-0.00047
H28	3.14725	3.923912	0.118661	0.183466	-5.3E-05
H29	-0.90216	5.210477	-0.62593	0.176656	0.000138
H30	1.508318	5.773184	-0.15416	0.179638	-0.00027
N31	-0.7676	-0.01363	1.450554	-0.52225	-0.02118
C32	-1.9604	-0.03843	3.959414	-0.06722	0.0117
C33	-2.12275	-0.02649	1.554989	0.298108	0.00972
C34	-0.0163	-0.01297	2.565132	0.102198	0.01012

C35	-0.5719	-0.02465	3.840016	-0.10858	-0.00664
C36	-2.7432	-0.03946	2.80741	-0.11299	-0.00665
H37	1.062169	-0.00363	2.434499	0.168488	-0.00094
H38	0.078133	-0.02349	4.712146	0.171219	0.000279
H39	-3.82644	-0.05072	2.89177	0.177025	0.000096
H40	-2.43447	-0.04846	4.939589	0.174261	-0.00046
N41	-2.12752	-0.02008	-0.8569	-0.54798	0.004839
C42	-4.89681	-0.02629	-1.03352	-0.07002	-0.00416
C43	-2.73338	-0.01883	-2.05918	0.102177	0.001398
C44	-2.87426	-0.02567	0.280265	0.299273	-0.00571
C45	-4.27011	-0.02857	0.210293	-0.11136	0.003501
C46	-4.11718	-0.02165	-2.18887	-0.10248	0.002503
H47	-2.07607	-0.01462	-2.92429	0.188127	0.000328
H48	-4.8699	-0.03167	1.116158	0.176032	-0.00029
H49	-4.56408	-0.01997	-3.18061	0.171344	0.000426
H50	-5.98388	-0.0278	-1.09505	0.174117	0.000136
O51	0.2697	0.007656	-2.40008	-0.49973	0.98514

Sum of electronic and zero-point Energies = – 1406.408716 Hartree

(Uncorrected energies; E(UB+HF-LYP) = – 1406.8014761 Hartree)

Table S4(k). The optimized geometry of $[Ru^{V}(terpy)(bpy)(O)]^{3+}$ (charge, +3; doublet), where the optimization was carried for a gaseous state at the UB3LYP level of DFT using LACVP** basis set.

atom	X	Y	Z	Mulliken Charge	Spin Density
Ru1	-0.00915	0.04675	-0.69663	1.33546	0.45388
N2	-0.06020	2.08353	-0.25146	-0.62287	-0.00822
C3	-0.43241	4.80397	0.06878	-0.03111	-0.00400
C4	-1.33123	2.57985	-0.09056	0.34974	-0.00168
C5	1.00375	2.90859	-0.23307	0.15775	-0.00147
C6	0.85007	4.28147	-0.07801	-0.08019	0.00250
C7	-1.53414	3.94421	0.06348	-0.07319	0.00160
H8	1.97867	2.45801	-0.35718	0.19453	-0.00026
H9	1.72774	4.91570	-0.07443	0.18146	-0.00029
H10	-2.53593	4.33621	0.18347	0.18325	-0.00012
H11	-0.58150	5.87032	0.19437	0.18495	0.00009
N12	-1.95457	0.30257	-0.23158	-0.72071	-0.00690
C13	-4.61342	0.67437	0.17898	-0.04267	0.01586
C14	-2.74859	-0.79437	-0.17723	0.34196	0.00490
C15	-2.40198	1.56868	-0.06383	0.35429	0.01532
C16	-3.76133	1.78250	0.14435	-0.06887	-0.01064
C17	-4.11714	-0.62115	0.02904	-0.07071	-0.00290
H18	-4.15449	2.78119	0.28274	0.18764	0.00040
H19	-4.78364	-1.47213	0.07973	0.18696	0.00002
H20	-5.67496	0.82328	0.33902	0.18857	-0.00066
N21	-0.66813	-1.95896	-0.48375	-0.56981	-0.00008
C22	-1.82244	-4.46408	-0.33839	-0.03594	0.00243
C23	0.10226	-3.05118	-0.57603	0.14704	0.00477
C24	-2.02276	-2.06662	-0.31270	0.33761	-0.00303
C25	-2.61860	-3.32196	-0.24068	-0.07548	0.00208
C26	-0.44730	-4.32955	-0.50352	-0.08168	-0.00300
H27	1.16321	-2.89835	-0.72557	0.19810	-0.00030
H28	-3.68864	-3.41023	-0.10263	0.18058	-0.00011
H29	0.20346	-5.19093	-0.58942	0.17862	0.00015
H30	-2.27806	-5.44615	-0.28437	0.18007	-0.00011
N31	0.68318	-0.26559	1.35060	-0.56001	-0.01831
C32	1.71730	-0.66466	3.88913	-0.04082	0.00272
C33	2.02636	-0.39752	1.51596	0.33402	0.00157
C34	-0.13949	-0.34223	2.41430	0.14031	0.00334

C35	0.34218	-0.53772	3.70142	-0.08774	-0.00300
C36	2.56562	-0.59415	2.78779	-0.08240	-0.00200
H37	-1.19989	-0.23633	2.23101	0.17751	-0.00050
H38	-0.35465	-0.58507	4.52919	0.17108	0.00003
H39	3.63430	-0.69572	2.91993	0.17102	-0.00010
H40	2.12825	-0.82025	4.88021	0.17351	-0.00013
N41	2.13211	-0.14014	-0.86428	-0.55678	0.01365
C42	4.89050	-0.36129	-0.96182	-0.04281	-0.00120
C43	2.83174	-0.32771	0.28642	0.31040	-0.00261
C44	2.77469	-0.06518	-2.04544	0.13698	0.00466
C45	4.15734	-0.17077	-2.13112	-0.08120	-0.00063
C46	4.22217	-0.44189	0.25705	-0.08433	0.00115
H47	2.15774	0.07865	-2.92353	0.19316	-0.00004
H48	4.63657	-0.10636	-3.10032	0.16956	0.00072
H49	4.78010	-0.59110	1.17174	0.16984	-0.00011
H50	5.97072	-0.44747	-0.99369	0.17176	0.00001
O51	-0.07653	-0.18996	-2.39387	-0.37841	0.54054

Sum of electronic and zero-point Energies = –1406.139185 Hartree

(Uncorrected energies; E(UB3LYP) = –1406.53700968 Hartree)

Table S5(a). Oscillator strengths for the electronic transitions of $[Ru^{II}(terpy)(bpy)(OH_2)]^{2+}$ calculated by the UB3LYP level of TD-DFT using LanL2DZ basis set.

Excited State	E (cm^{-1})	λ (nm)	f[a] (> 0.01)	Major contributions	|CI coef| (> 0.2)
1	19436	514.5	0.0104	MO112 -> MO115 (HOMO-2 -> LUMO)	0.65614
3	20886	478.78	0.0179	MO113 -> MO115 (HOMO-1 -> LUMO)	0.48323
				MO114 -> MO117 (HOMO -> LUMO+2)	0.46098
5	22272	448.99	0.0297	MO112 -> MO117 (HOMO-2 -> LUMO+2)	0.44052
				MO114 -> MO116 (HOMO -> LUMO+1)	0.30032
				MO114 -> MO117 (HOMO -> LUMO+2)	0.35652
6	22630	441.9	0.0409	MO113 -> MO116 (HOMO-1 -> LUMO+1)	0.37858
				MO113 -> MO117 (HOMO-1 -> LUMO+2)	0.55789
7	22846	437.71	0.143	MO112 -> MO116 (HOMO-2 -> LUMO+1)	0.6361

[a]Oscillator strength

Table S5(b). Oscillator strengths for the electronic transitions of $[Ru^{III}(terpy)(bpy)(OH_2)]^{3+}$ calculated by the UB3LYP level of TD-DFT using LanL2DZ basis set.

Excited State	E (cm^{-1})	λ (nm)	f[a] (> 0.01)	Major contributions	|CI coef| (> 0.2)
9	25330	394.79	0.0218	MO108B -> MO114B (HOMO-6_B -> HOMO_B)	0.97305
11	26273	380.62	0.0194	MO107B -> MO114B (HOMO-7_B -> HOMO_B)	0.95626
15	28171	354.97	0.0102	MO111A -> MO115A (HOMO-3_A -> LUMO_A)	0.22753
				MO114A -> MO115A (HOMO_A -> LUMO_A)	0.33078
				MO110B -> MO115B (HOMO-4_B -> LUMO_B)	0.61597
				MO111B -> MO115B (HOMO-3_B -> LUMO_B)	0.21669
				MO113B -> MO115B (HOMO-1_B -> LUMO_B)	0.45613

[a]Oscillator strength

Table S5(c). Oscillator strengths for the electronic transitions of $[Ru^{IV}(terpy)(bpy)(O)]^{2+}$ calculated by the UB3LYP level of TD-DFT using LanL2DZ basis set.

Excited State	E (cm^{-1})	λ (nm)	f[a] (> 0.01)	Major contributions	|CI coef| (> 0.2)
13	26232	381.22	0.0308	MO113A -> MO115A (HOMO-1_A -> LUMO_A)	0.57101
				MO114A -> MO117A (HOMO_A -> LUMO+2_A)	0.22622
				MO111B -> MO114B (HOMO-3_B -> HOMO_B)	0.50989
				MO111B -> MO116B (HOMO-3_B -> LUMO+1_B)	0.27321
				MO111B -> MO117B (HOMO-3_B -> LUMO+2_B)	0.2694
18	27519	363.39	0.0508	MO111A -> MO115A (HOMO-3_A -> LUMO_A)	0.3085
				MO112A -> MO115A (HOMO-2_A -> LUMO_A)	0.51339
				MO105B -> MO114B (HOMO-9_B -> HOMO_B)	0.26639
				MO111B -> MO113B (HOMO-3_B -> HOMO-2_B)	0.32613
				MO111B -> MO115B (HOMO-3_B -> LUMO_B)	0.43878

[a]Oscillator strength

Table S5(d). Oscillator strengths for the electronic transitions of $[Ru^{V}(terpy)(bpy)(O)]^{3+}$ calculated by the UB3LYP level of TD-DFT using LanL2DZ basis set.

Excited State	E (cm^{-1})	λ (nm)	f[a] (> 0.01)	Major contributions	|CI coef| (> 0.2)
16	20408	490	0.0106	MO105A -> MO114A (HOMO-8_A -> LUMO_A)	0.30604
				MO104B -> MO113B (HOMO-9_B -> HOMO_B)	0.32134
				MO104B -> MO114B (HOMO-9_B -> LUMO_B)	0.23665
				MO109B -> MO114B (HOMO-4_B -> LUMO_B)	0.50057
				MO110B -> MO114B (HOMO-3_B -> LUMO_B)	0.48807
34	25576	390.99	0.012	MO99A -> MO114A (HOMO-14_A -> LUMO_A)	0.28363
				MO103A -> MO114A (HOMO-10_A -> LUMO_A)	0.25153
				MO102B -> MO113B (HOMO-11_B -> HOMO_B)	0.52241
				MO103B -> MO113B (HOMO-10_B -> HOMO_B)	0.4012
				MO106B -> MO113B (HOMO-7_B -> HOMO_B)	0.23599

[a]Oscillator strength

Table S5(e). Oscillator strengths for the electronic transitions of $[Ru^{III}(terpy)(bpy)(OOH)]^{2+}$ calculated by the UB3LYP level of TD-DFT using LanL2DZ basis set.

Excited State	E (cm^{-1})	λ (nm)	f[a] (> 0.01)	Major contributions	|CI coef| (> 0.2)
2	17419	574.07	0.0623	MO115B -> MO118B (HOMO-3_B -> HOMO_B)	0.91894
11	25042	399.33	0.0121	MO116A -> MO119A (HOMO-2_A -> LUMO_A)	0.23767
				MO116A -> MO120A (HOMO-2_A -> LUMO+1_A)	0.2382
				MO117A -> MO119A (HOMO-1_A -> LUMO_A)	0.60223
				MO116B -> MO120B (HOMO-2_B -> LUMO+1_B)	0.41133
				MO116B -> MO121B (HOMO-2_B -> LUMO+2_B)	0.29079
				MO117B -> MO119B (HOMO-1_B -> LUMO_B)	0.20609
				MO117B -> MO121B (HOMO-1_B -> LUMO+2_B)	0.31152
21	27637	361.84	0.0103	MO118A -> MO121A (HOMO_A -> LUMO+2_A)	0.55282
				MO112B -> MO118B (HOMO-6_B -> HOMO_B)	0.41224
				MO115B -> MO119B (HOMO-3_B -> LUMO_B)	0.3019
				MO116B -> MO120B (HOMO-2_B -> LUMO+1_B)	0.27296
				MO116B -> MO121B (HOMO-2_B -> LUMO+2_B)	0.3778
				MO117B -> MO121B (HOMO-1_B -> LUMO+2_B)	0.20406
23	28028	356.79	0.015	MO115A -> MO121A (HOMO-3_A -> LUMO+2_A)	0.2264
				MO117A -> MO121A (HOMO-1_A -> LUMO+2_A)	0.42594
				MO118A -> MO121A (HOMO_A -> LUMO+2_A)	0.31382
				MO112B -> MO118B (HOMO-6_B -> HOMO_B)	0.35385
				MO114B -> MO121B (HOMO-4_B -> LUMO+2_B)	0.31267
				MO116B -> MO120B (HOMO-2_B -> LUMO+1_B)	0.21382
				MO116B -> MO121B (HOMO-2_B -> LUMO+2_B)	0.35175
				MO117B -> MO121B (HOMO-1_B -> LUMO+2_B)	0.25849
24	28221	354.34	0.0379	MO115A -> MO119A (HOMO-3_A -> LUMO_A)	0.32951
				MO116A -> MO120A (HOMO-2_A -> LUMO+1_A)	0.23946
				MO118A -> MO126A (HOMO_A -> LUMO+7_A)	0.27781
				MO112B -> MO118B (HOMO-6_B -> HOMO_B)	0.36053
				MO114B -> MO119B (HOMO-4_B -> LUMO_B)	0.24896
				MO115B -> MO119B (HOMO-3_B -> LUMO_B)	0.45047
25	28462	351.35	0.0272	MO116A -> MO120A (HOMO-2_A -> LUMO+1_A)	0.3759
				MO116A -> MO121A (HOMO-2_A -> LUMO+2_A)	0.20439
				MO117A -> MO128A (HOMO-1_A -> LUMO+9_A)	0.28244
				MO118A -> MO126A (HOMO_A -> LUMO+7_A)	0.49479
				MO115B -> MO119B (HOMO-3_B -> LUMO_B)	0.27472
				MO117B -> MO126B (HOMO-1_B -> LUMO+7_B)	0.21931
				MO117B -> MO128B (HOMO-1_B -> LUMO+9_B)	0.26235

(continued)

[a]Oscillator strength

Table S5(f). Oscillator strengths for the electronic transitions of $[Ru^{IV}(terpy)(bpy)(OOH)]^{3+}$ calculated by the UB3LYP level of TD-DFT using LanL2DZ basis set.

Excited State	E(cm^{-1})	λ (nm)	f[a] (> 0.01)	Major contributions	|CI coef| (> 0.2)
7	16198	617.36	0.0198	MO112B -> MO117B (HOMO-6_B -> HOMO-2_B)	0.51425
				MO113B -> MO117B (HOMO-5_B -> HOMO-2_B)	0.47846
				MO113B -> MO118B (HOMO-5_B -> HOMO_B)	0.52438
8	16990	588.57	0.0352	MO107B -> MO117B (HOMO-11_B -> HOMO-2_B)	0.20658
				MO112B -> MO117B (HOMO-6_B -> HOMO-2_B)	0.61646
				MO113B -> MO118B (HOMO-5_B -> HOMO_B)	0.6236
				MO114B -> MO118B (HOMO-4_B -> HOMO_B)	0.23182

[a]Oscillator strength

Table S5(g). Oscillator strengths for the electronic transitions of $[Ru^{III}(terpy)(bpy)(OO\bullet)]^{2+}$ calculated by the UB3LYP level of TD-DFT using LanL2DZ basis set.

Excited State	E (cm^{-1})	λ (nm)	f[a] (>0.01)	Major contributions	|CI coef| (> 0.2)
3	11828	845.48	0.0213	MO114B -> MO117B (HOMO-4_B -> HOMO-2_B)	0.35143
				MO115B -> MO117B (HOMO-3_B -> HOMO-2_B)	0.34297
				MO115B -> MO118B (HOMO-3_B -> HOMO_B)	0.46682
				MO116B -> MO117B (HOMO-2_B -> HOMO-2_B)	0.62365
				MO116B -> MO118B (HOMO-2_B -> HOMO_B)	0.33346
6	19510	512.56	0.0306	MO113B -> MO117B (HOMO-5_B -> HOMO-2_B)	0.31821
				MO114B -> MO118B (HOMO-4_B -> HOMO_B)	0.52476
				MO115B -> MO118B (HOMO-3_B -> HOMO_B)	0.62677
				MO116B -> MO117B (HOMO-2_B -> HOMO-1_B)	0.20834
26	28385	352.3	0.0212	MO115A -> MO119A (HOMO-3_A -> LUMO_A)	0.23727
				MO116A -> MO119A (HOMO-2_A -> LUMO_A)	0.59747
				MO110B -> MO117B (HOMO-8_B -> HOMO-2_B)	0.26221
				MO114B -> MO119B (HOMO-4_B -> LUMO_B)	0.25737
				MO115B -> MO119B (HOMO-3_B -> LUMO_B)	0.22521
				MO115B -> MO121B (HOMO-3_B -> LUMO+2_B)	0.26161
				MO116B -> MO121B (HOMO-2_B -> LUMO+2_B)	0.29001

[a]Oscillator strength

Table S5(h). Oscillator strengths for the electronic transitions of $[Ru^{II}(terpy)(bpy)(OH_2)]^{2+}$ calculated by the B3LYP level of TD-DFT using LACVP** basis set.

Excited State	E (cm^{-1})	λ (nm)	f[a] (> 0.01)	Major contributions	|CI coef| (> 0.2)
3	22637	441.76	0.0264	MO112 -> MO115 (HOMO-2 -> LUMO)	0.53925
				MO114 -> MO116 (HOMO -> LUMO+1)	0.39026
6	23828	419.68	0.023	MO113 -> MO117 (HOMO-1 -> LUMO+2)	0.42315
				MO114 -> MO116 (HOMO -> LUMO+1)	0.34087
				MO114 -> MO117 (HOMO -> LUMO+2)	0.34803
7	24405	409.75	0.1286	MO113 -> MO116 (HOMO-1 -> LUMO+1)	0.65132
8	24489	408.34	0.0335	MO112 -> MO116 (HOMO-2 -> LUMO+1)	0.44872
				MO112 -> MO117 (HOMO-2 -> LUMO+2)	0.51923

[a]Oscillator strength

Table S5(i). Oscillator strengths for the electronic transitions of $[Ru^{III}(terpy)(bpy)(OH_2)]^{3+}$ calculated by the UB3LYP level of TD-DFT using LACVP** basis set.

Excited State	E (cm^{-1})	λ (nm)	f[a] (> 0.01)	Major contributions	|CI coef| (> 0.2)
8	24303	411.48	0.0208	MO108B -> MO114B (HOMO-6_B -> HOMO_B)	0.94444
12	25320	394.95	0.0183	MO111A -> MO118A (HOMO-3_A -> LUMO+3_A)	0.249
				MO107B -> MO114B (HOMO-7_B -> HOMO_B)	0.87557
				MO110B -> MO118B (HOMO-4_B -> LUMO+3_B)	0.28811

[a]Oscillator strength

Table S5(j). Oscillator strengths for the electronic transitions of $[Ru^{IV}(terpy)(bpy)(OH_2)]^{2+}$ calculated by the UB3LYP level of TD-DFT using LACVP** basis set.

Excited State	E (cm^{-1})	λ (nm)	f[a] (> 0.01)	Major contributions	|CI coef| (> 0.2)
15	26353	379.46	0.0215	MO113A -> MO115A (HOMO-1_A -> LUMO_A)	0.43902
				MO110B -> MO114B (HOMO-4_B -> HOMO_B)	0.31078
				MO111B -> MO114B (HOMO-3_B -> HOMO_B)	0.53836
				MO111B -> MO116B (HOMO-3_B -> LUMO+1_B)	0.32683
				MO112B -> MO114B (HOMO-2_B -> HOMO_B)	0.25131
17	27507	363.55	0.0523	MO111A -> MO115A (HOMO-3_A -> LUMO_A)	0.51777
				MO112A -> MO115A (HOMO-2_A -> LUMO_A)	0.38843
				MO111B -> MO113B (HOMO-3_B -> HOMO-2_B)	0.3638
				MO111B -> MO115B (HOMO-3_B -> LUMO_B)	0.39057
				MO112B -> MO115B (HOMO-2_B -> LUMO_B)	0.31402

[a]Oscillator strength

Table S5(k). Oscillator strengths for the electronic transitions of $[Ru^{V}(terpy)(bpy)(O)]^{3+}$ calculated by the UB3LYP level of TD-DFT using LACVP** basis set.

Excited State	E (cm^{-1})	λ (nm)	f[a] (> 0.01)	Major contributions	|CI coef| (> 0.2)
42	27935	357.98	0.0359	MO112A -> MO115A (HOMO-1_A -> LUMO+1_A)	0.52223
				MO112A -> MO116A (HOMO-1_A -> LUMO+2_A)	0.49845
				MO100B -> MO113B (HOMO-13_B -> HOMO_B)	0.22487
				MO109B -> MO116B (HOMO-4_B -> LUMO+2_B)	0.23813
				MO111B -> MO115B (HOMO-2_B -> LUMO+1_B)	0.36354

[a]Oscillator strength

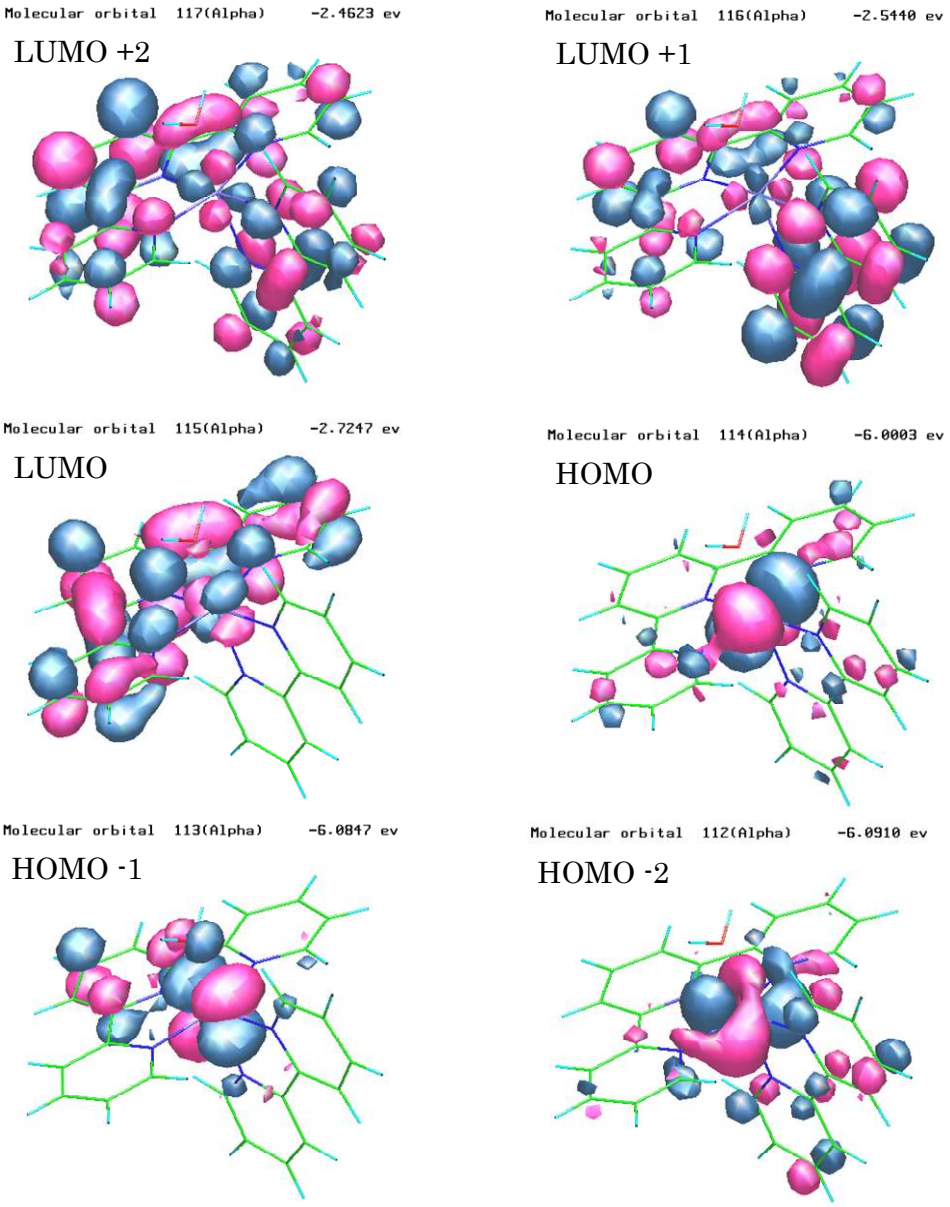

Figure S18(a). Frontier molecular orbitals of $[Ru^{II}(terpy)(bpy)(OH_2)]^{2+}$ for the optimized structure given Table S4a and Figure S12a.

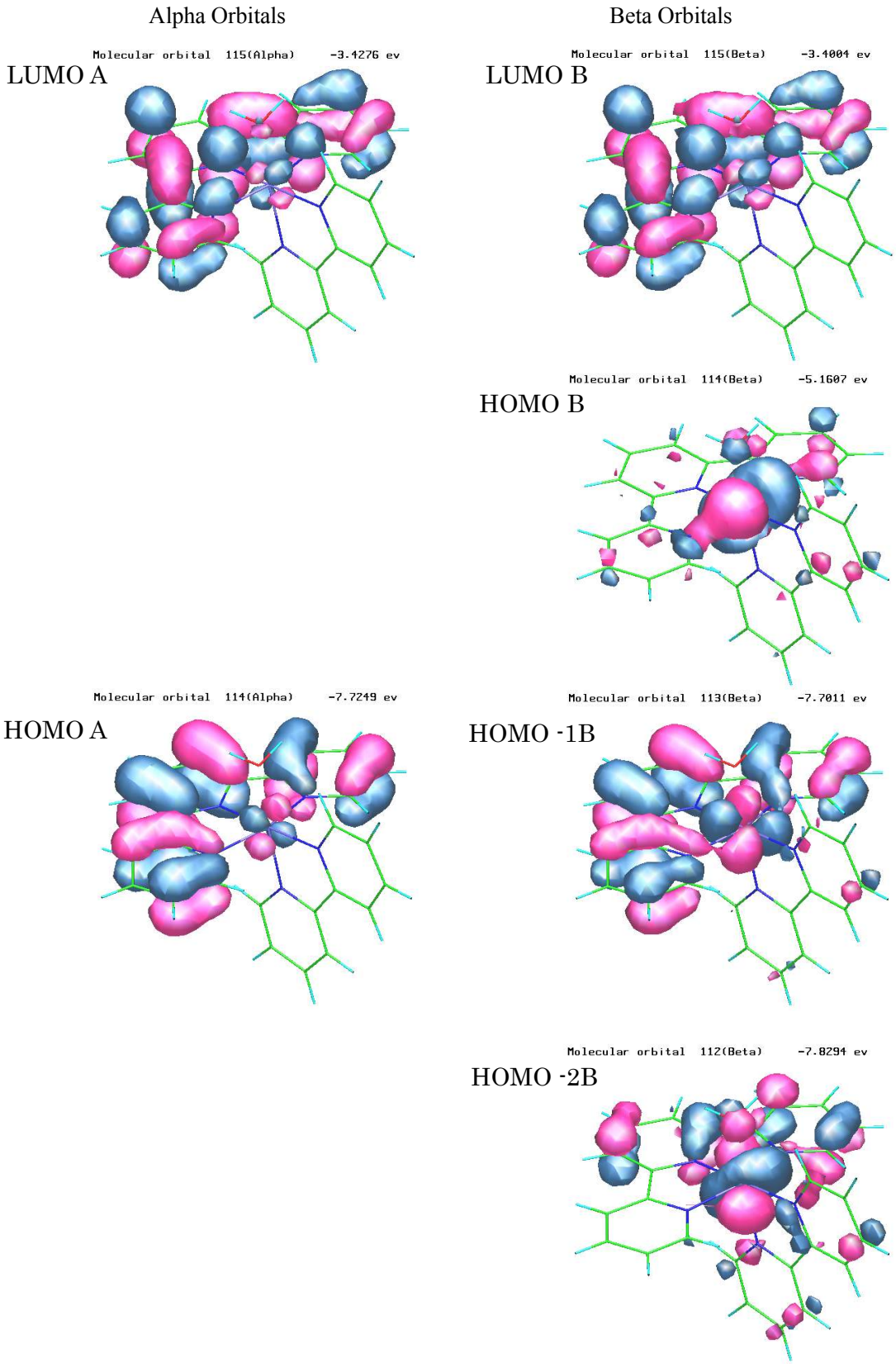

Figure S18(b). Frontier molecular orbitals of $[Ru^{III}(terpy)(bpy)(OH_2)]^{3+}$ for the optimized structure given Table S4b and Figure S12b.

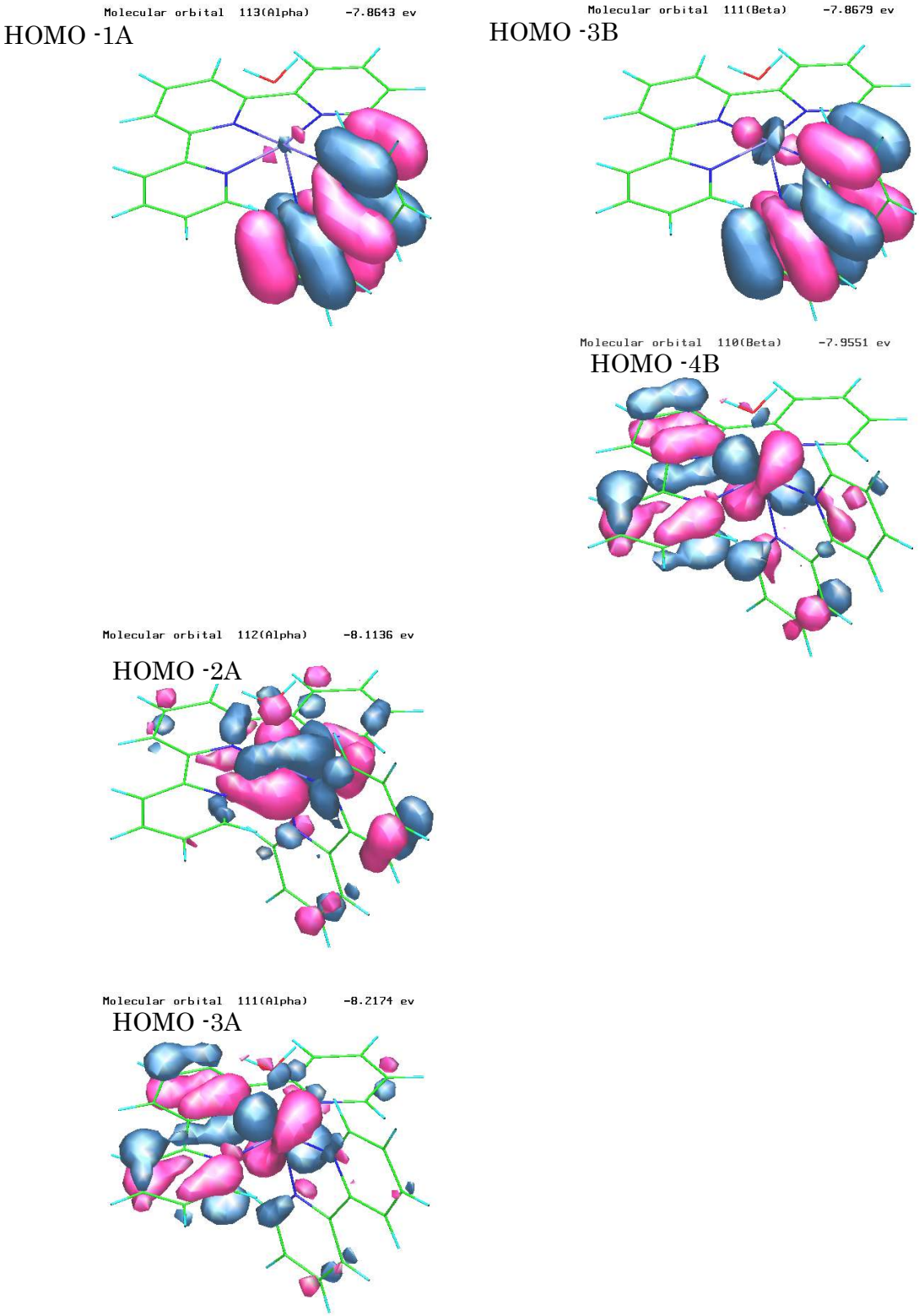

Figure S18(b). (continued)

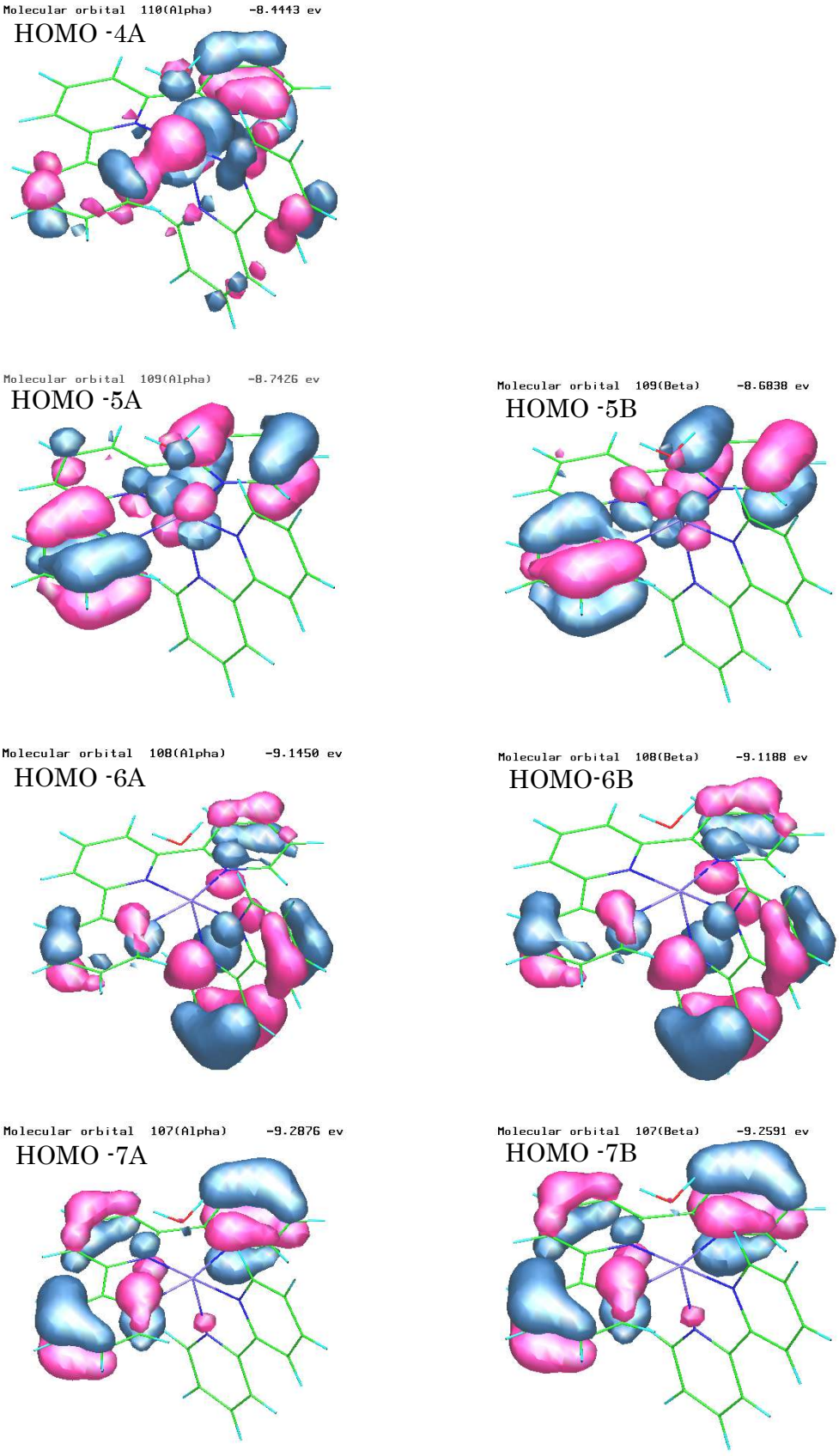
Molecular orbital 110(Alpha) -8.4443 ev
HOMO -4A
Molecular orbital 109(Alpha) -8.7426 ev
HOMO -5A
Molecular orbital 109(Beta) -8.6838 ev
HOMO -5B
Molecular orbital 108(Alpha) -9.1450 ev
HOMO -6A
Molecular orbital 108(Beta) -9.1188 ev
HOMO-6B
Molecular orbital 107(Alpha) -9.2876 ev
HOMO -7A
Molecular orbital 107(Beta) -9.2591 ev
HOMO -7B

Figure S18(b).

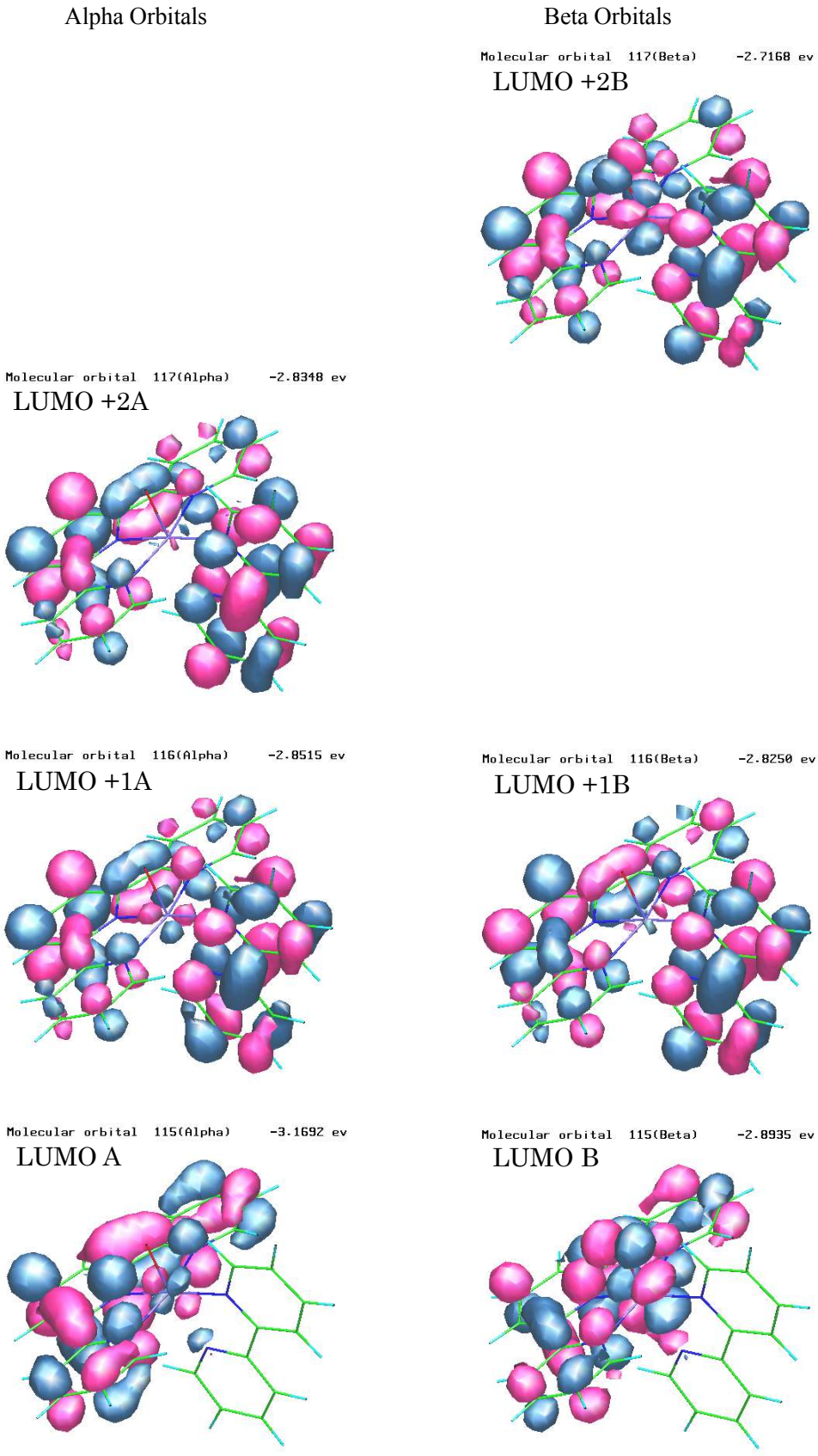

Figure S18(c). Frontier molecular orbitals of $[Ru^{IV}(terpy)(bpy)(O)]^{2+}$ for the optimized structure given Table S4c and Figure S12c.

Molecular orbital 114(Alpha) -7.1392 ev

HOMO A

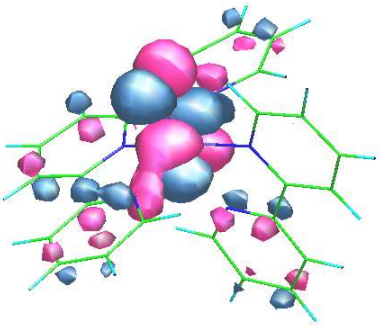

Molecular orbital 114(Beta) -3.7111 ev

HOMO B

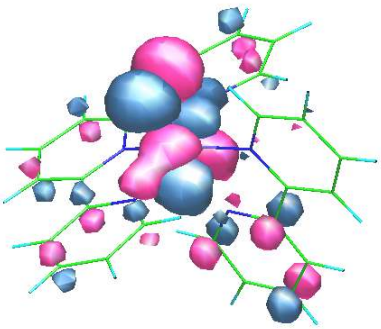

Molecular orbital 113(Alpha) -7.2626 ev

HOMO -1A

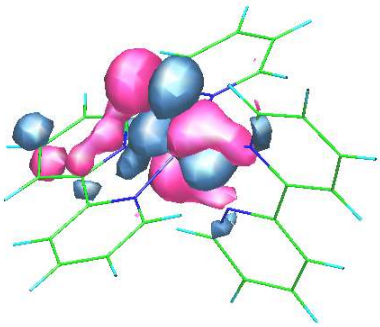

Molecular orbital 113(Beta) -3.8441 ev

HOMO -1B

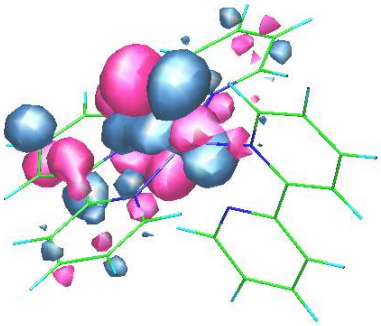

Molecular orbital 112(Beta) -7.3401 ev

HOMO -2B

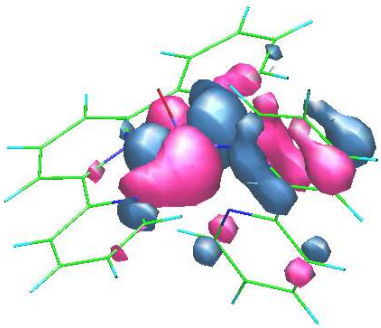

Molecular orbital 111(Beta) -7.5448 ev

HOMO -3B

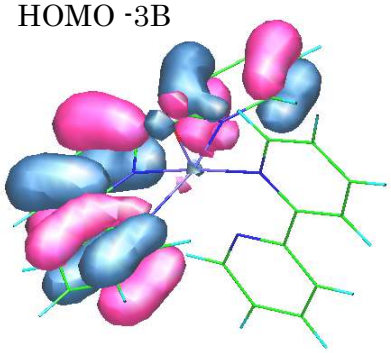

Figure S18(c). (continued)

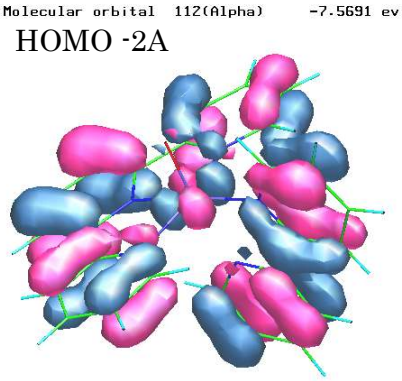

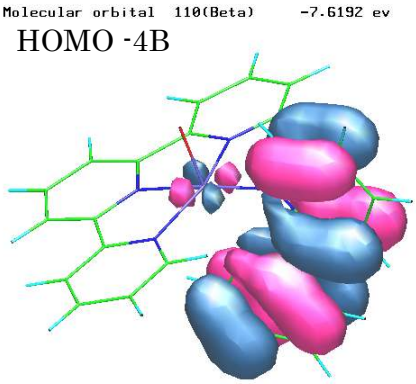

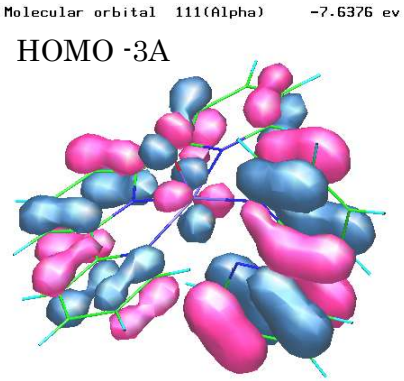

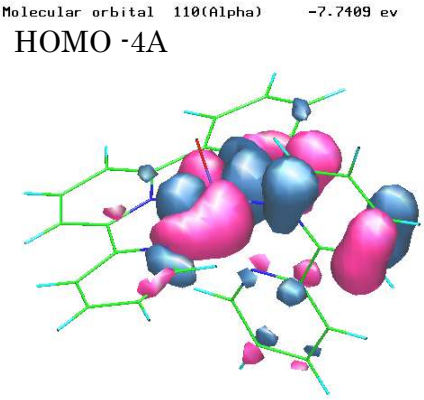

Figure S18(c). (continued)

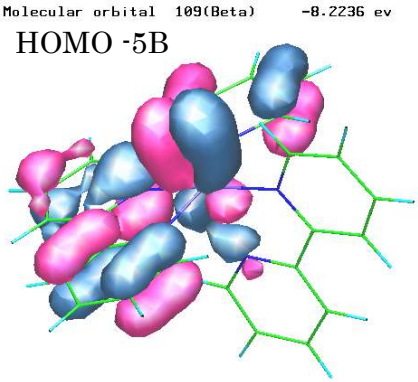

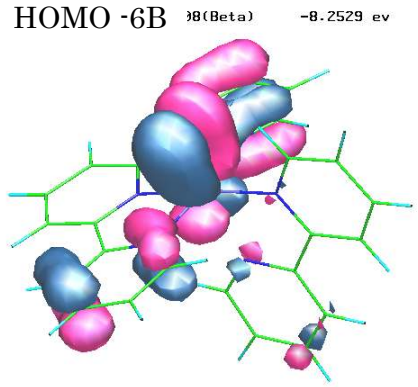

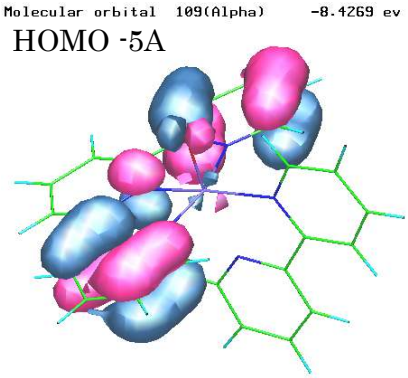

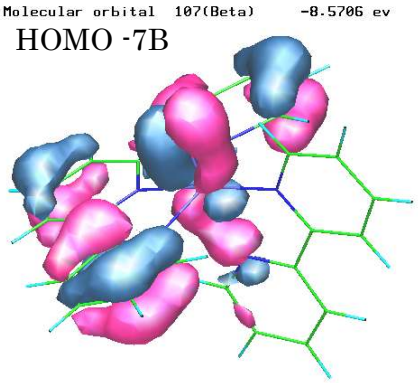

Figure S18(c). (continued)

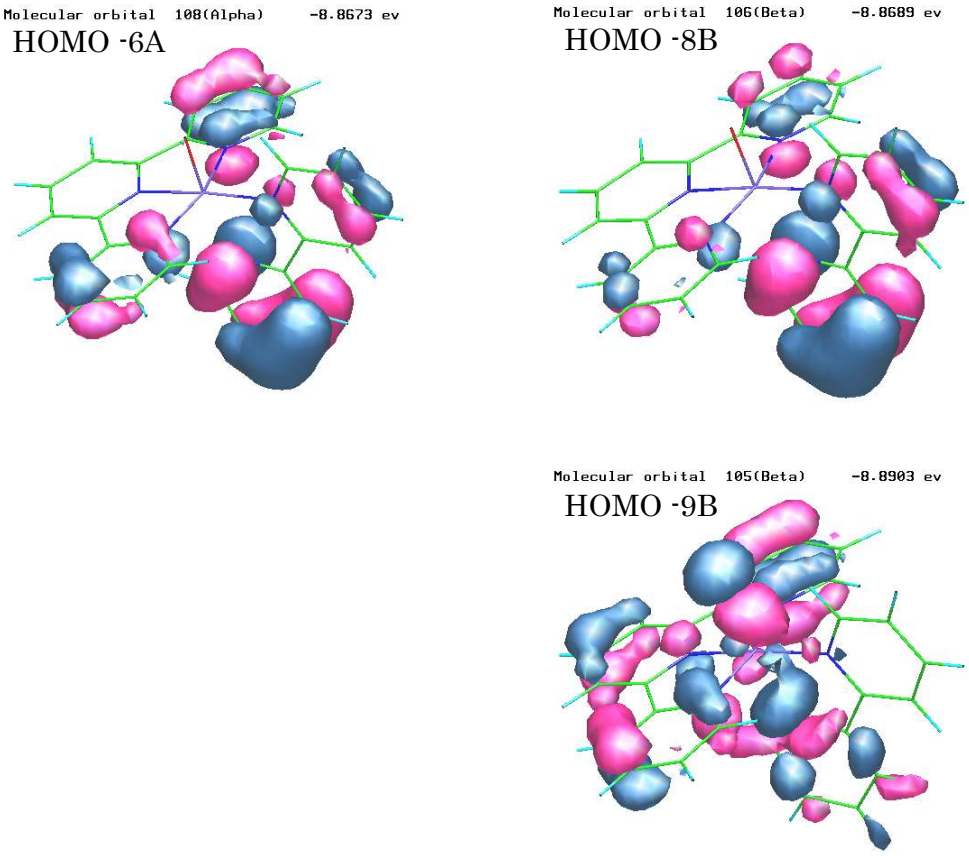
Molecular orbital 108(Alpha) -8.8673 ev
HOMO -6A
Molecular orbital 106(Beta) -8.8689 ev
HOMO -8B
Molecular orbital 105(Beta) -8.8903 ev
HOMO -9B

Figure S18(c).

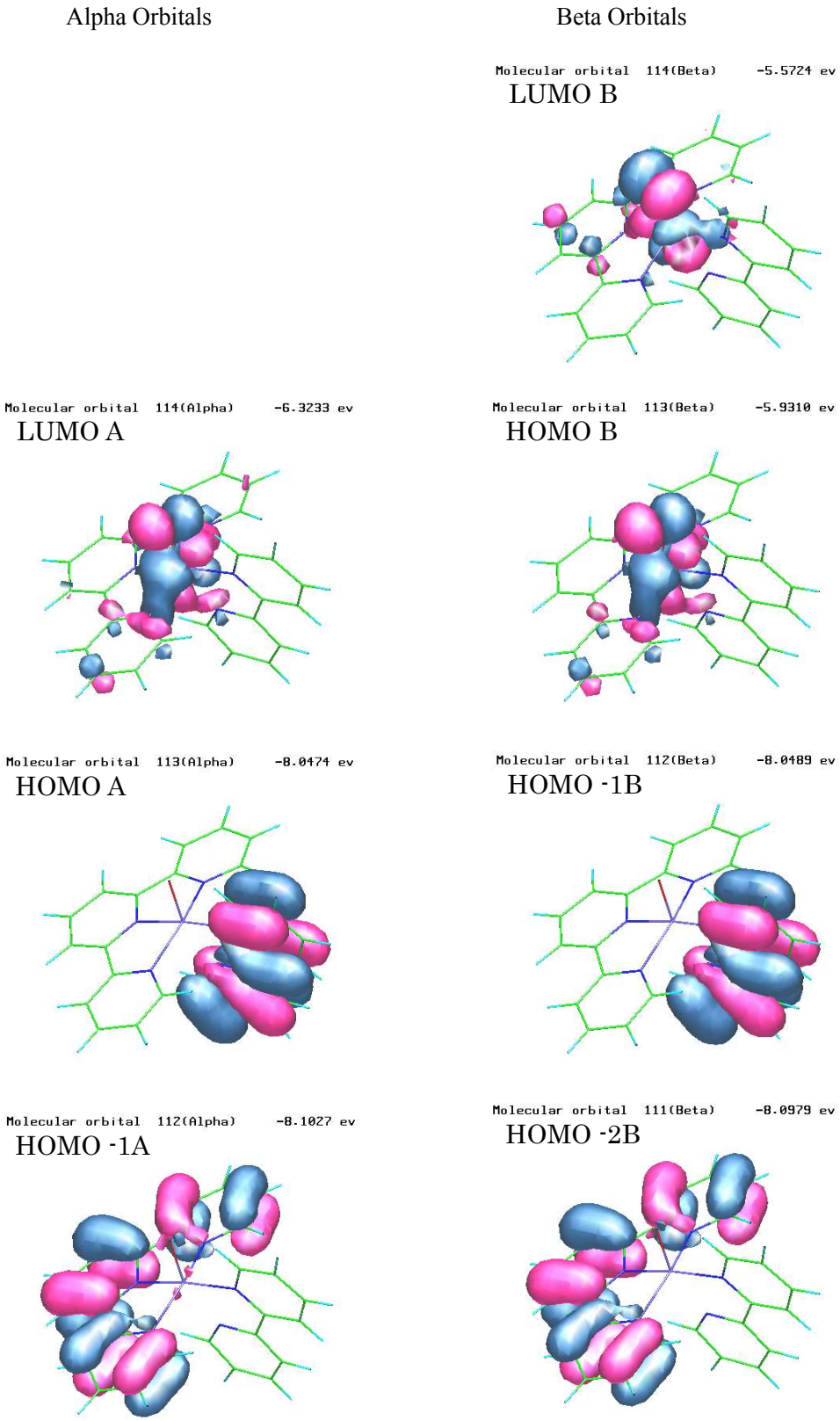

Figure S18(d). Frontier molecular orbitals of $[Ru^{V}(terpy)(bpy)(O)]^{3+}$ for the optimized structure given Table S4d and Figure S12d.

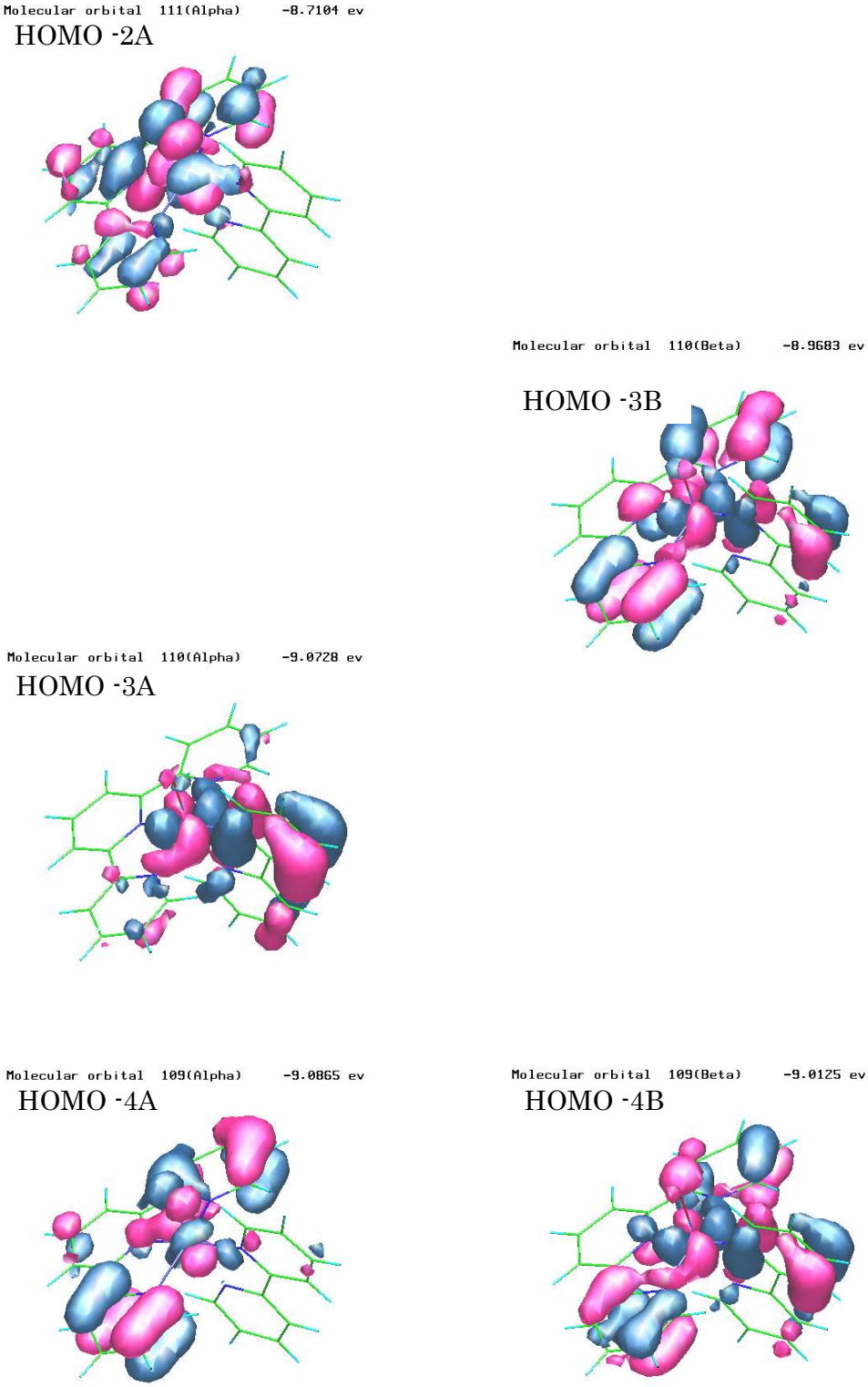

Figure S18(d). (continued)

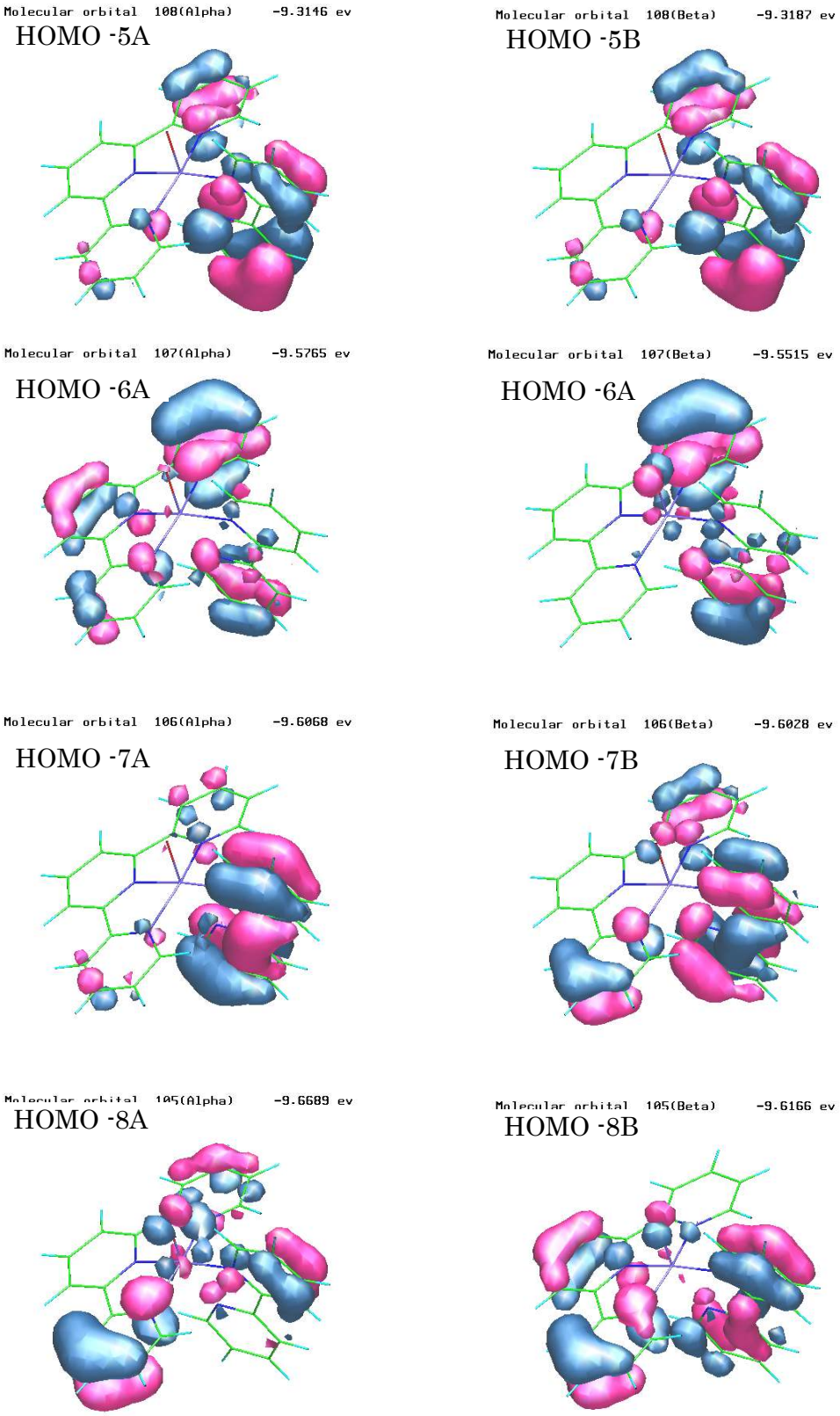

Figure S18(d). (continued)

Molecular orbital 104(Alpha) -9.9206 ev
HOMO -9A

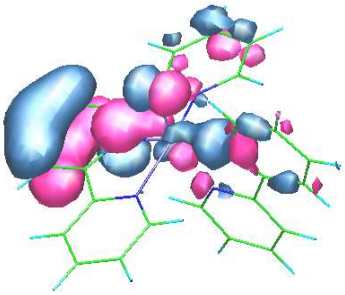

Molecular orbital 104(Beta) -9.6636 ev
HOMO -9B

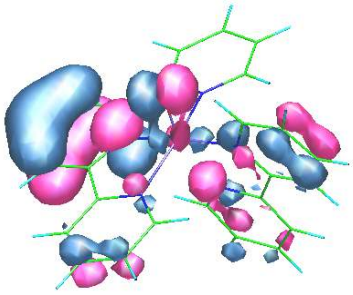

Molecular orbital 103(Alpha) -10.2391 ev
HOMO -10A

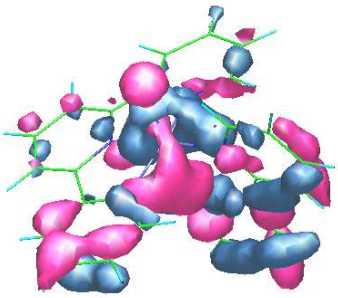

Molecular orbital 103(Beta) -10.1484 ev
HOMO -10B

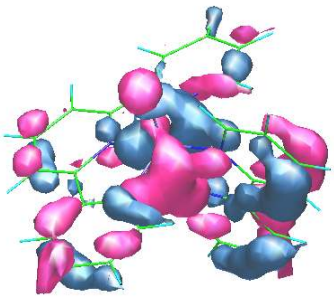

Molecular orbital 102(Beta) -10.2218 ev
HOMO -11B

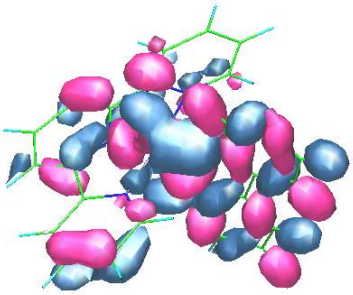

Molecular orbital 102(Alpha) -10.2665 ev
HOMO -11A

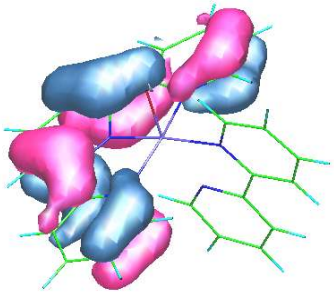

Molecular orbital 101(Beta) -10.2600 ev
HOMO -12B

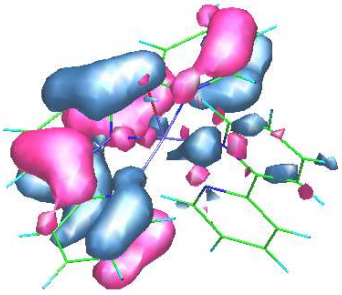

Figure S18(d). (continued)

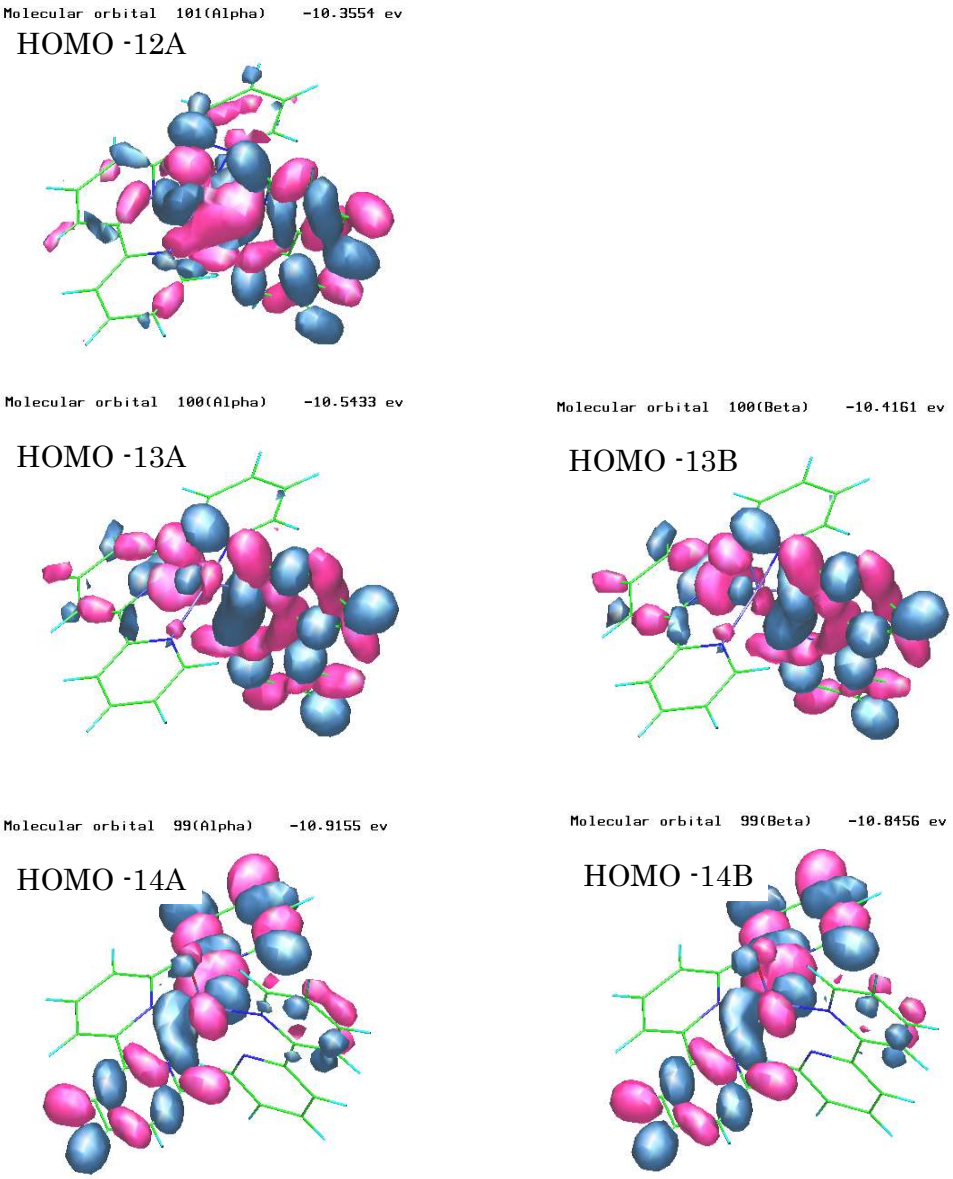

Figure S18(d). (continued)

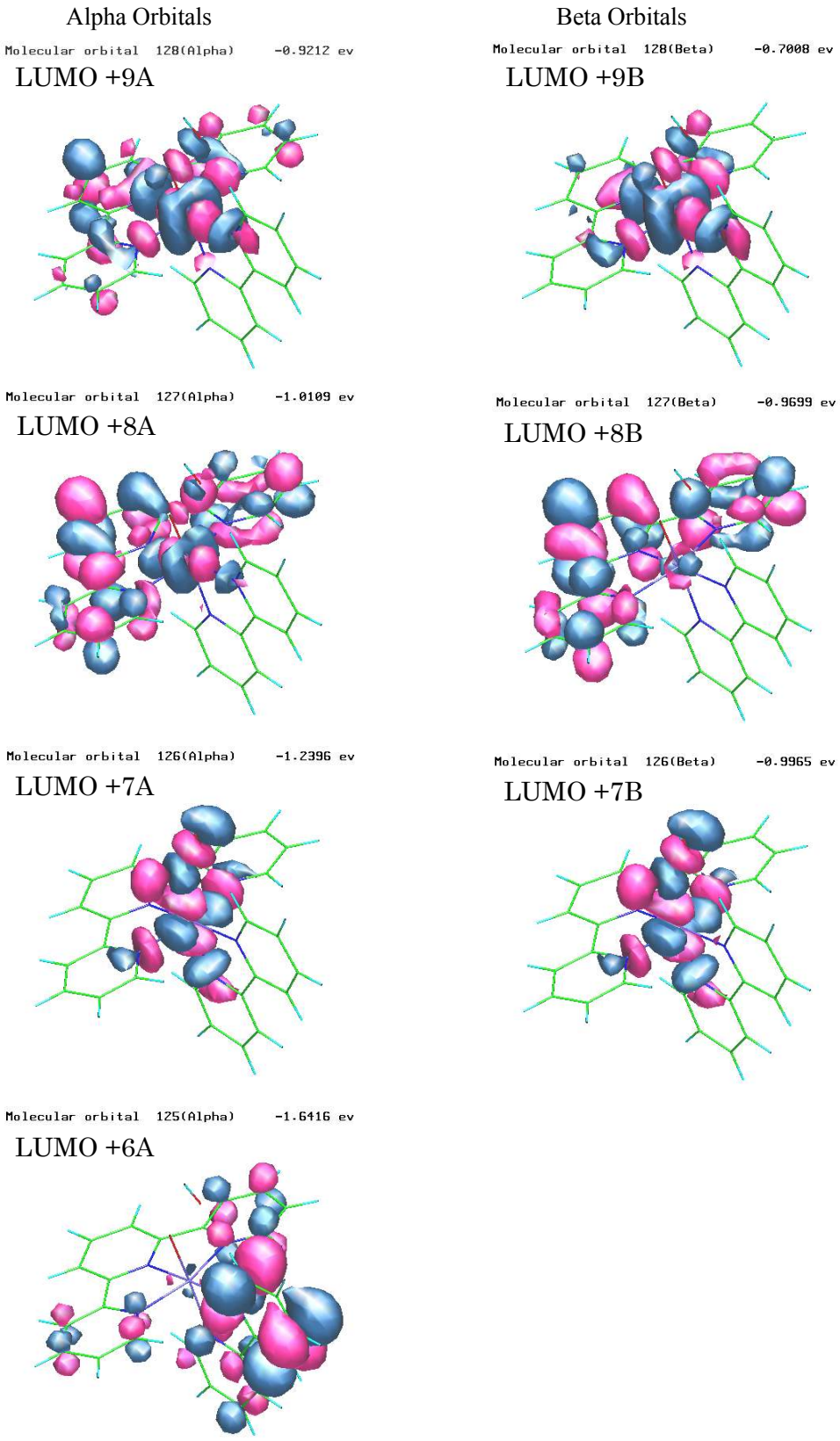

Figure S18(e). Frontier molecular orbitals of $[Ru^{III}(terpy)(bpy)(OOH)]^{2+}$ for the optimized structure given Table S4e and Figure S12e.

Molecular orbital 124(Alpha) -1.6820 ev

LUMO +5A

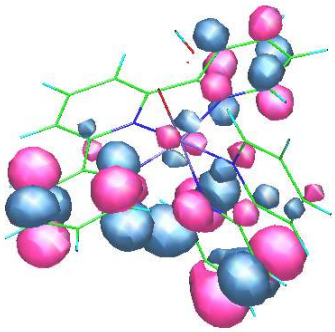

Molecular orbital 125(Beta) -1.6314 ev

LUMO +6B

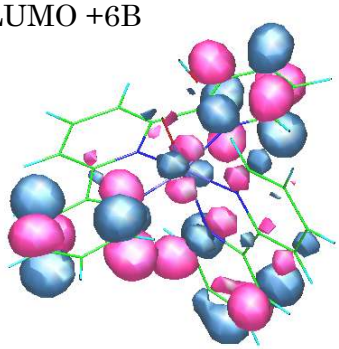

Molecular orbital 124(Beta) -1.6384 ev

LUMO +5B

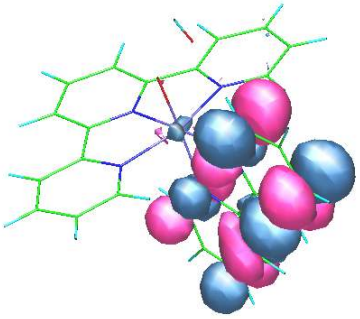

Molecular orbital 123(Alpha) -1.7509 ev

LUMO +4A

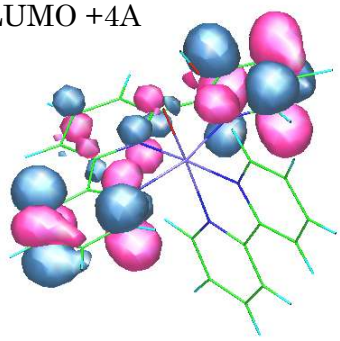

Molecular orbital 123(Beta) -1.7402 ev

LUMO +4B

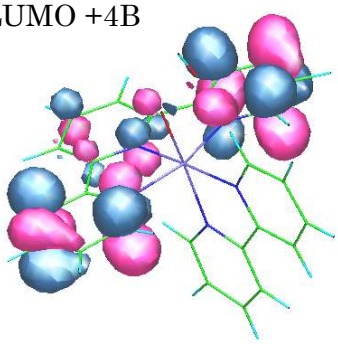

Figure S18(e). (continued)

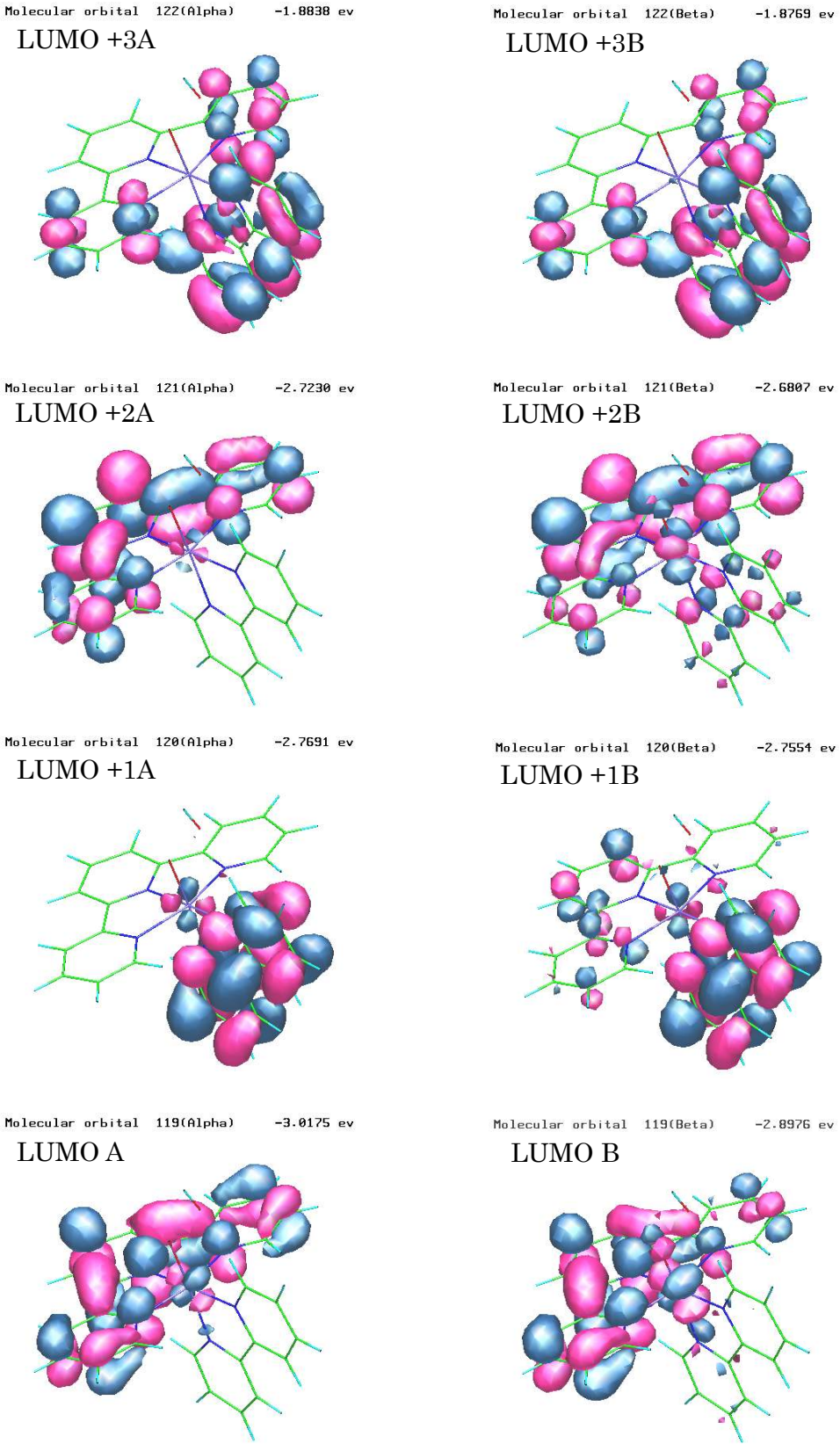

Figure S18(e). (continued)

Molecular orbital 118(Alpha) -6.9011 ev
HOMO A

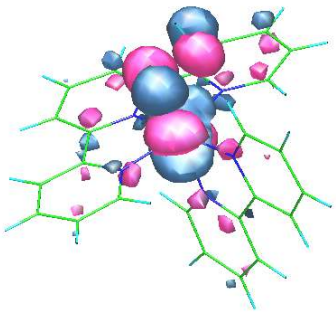

Molecular orbital 118(Beta) -4.0808 ev
HOMO B

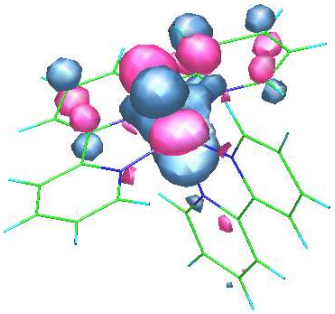

Molecular orbital 117(Alpha) -7.0580 ev
HOMO -1A

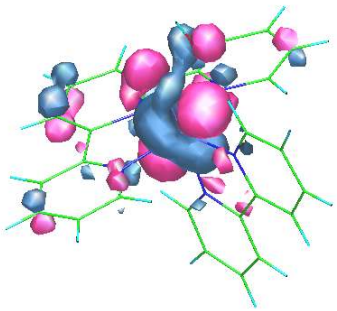

Molecular orbital 117(Beta) -6.7860 ev
HOMO -1B

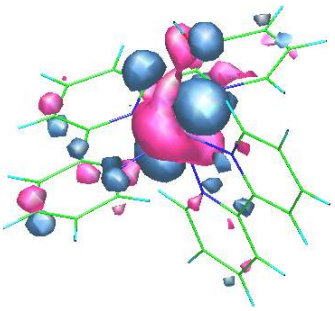

Molecular orbital 116(Alpha) -7.1355 ev
HOMO -2A

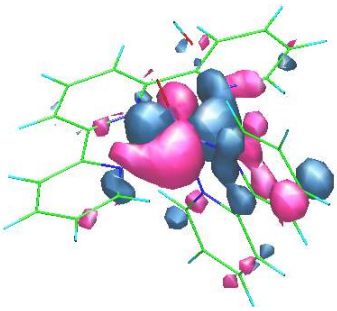

Molecular orbital 116(Beta) -6.9035 ev
HOMO -2B

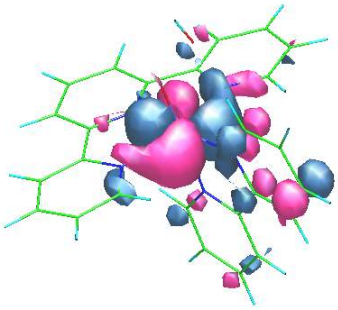

Molecular orbital 115(Beta) -7.2479 ev
HOMO -3B

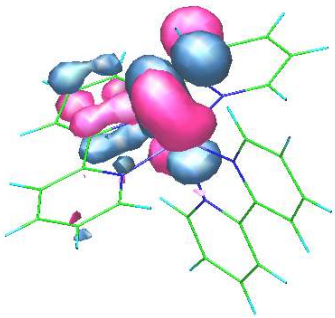

Figure S18(e). (continued)

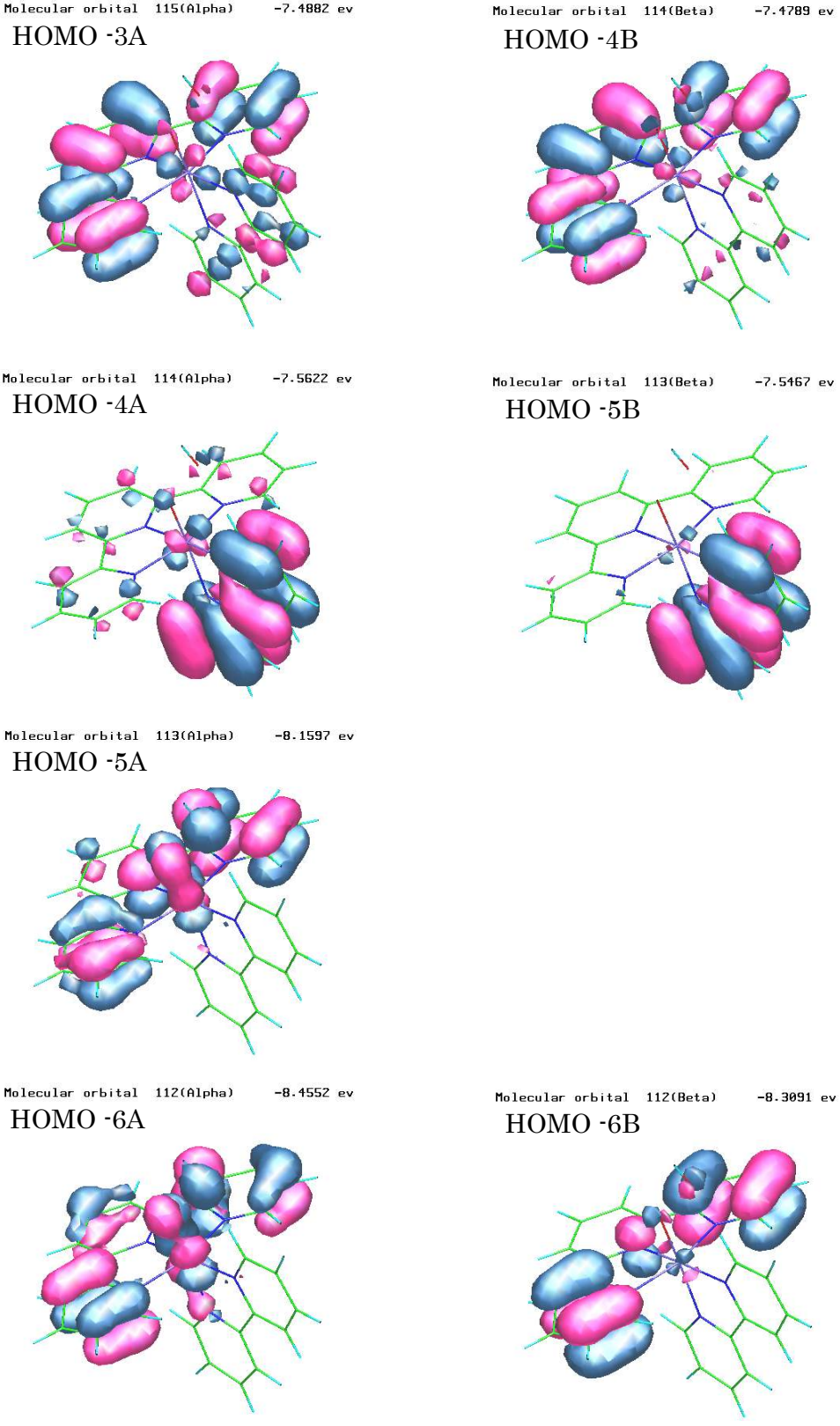
Molecular orbital 115(Alpha) -7.4882 ev
HOMO -3A
Molecular orbital 114(Beta) -7.4789 ev
HOMO -4B
Molecular orbital 114(Alpha) -7.5622 ev
HOMO -4A
Molecular orbital 113(Beta) -7.5467 ev
HOMO -5B
Molecular orbital 113(Alpha) -8.1597 ev
HOMO -5A
Molecular orbital 112(Alpha) -8.4552 ev
HOMO -6A
Molecular orbital 112(Beta) -8.3091 ev
HOMO -6B

Figure S18(e).

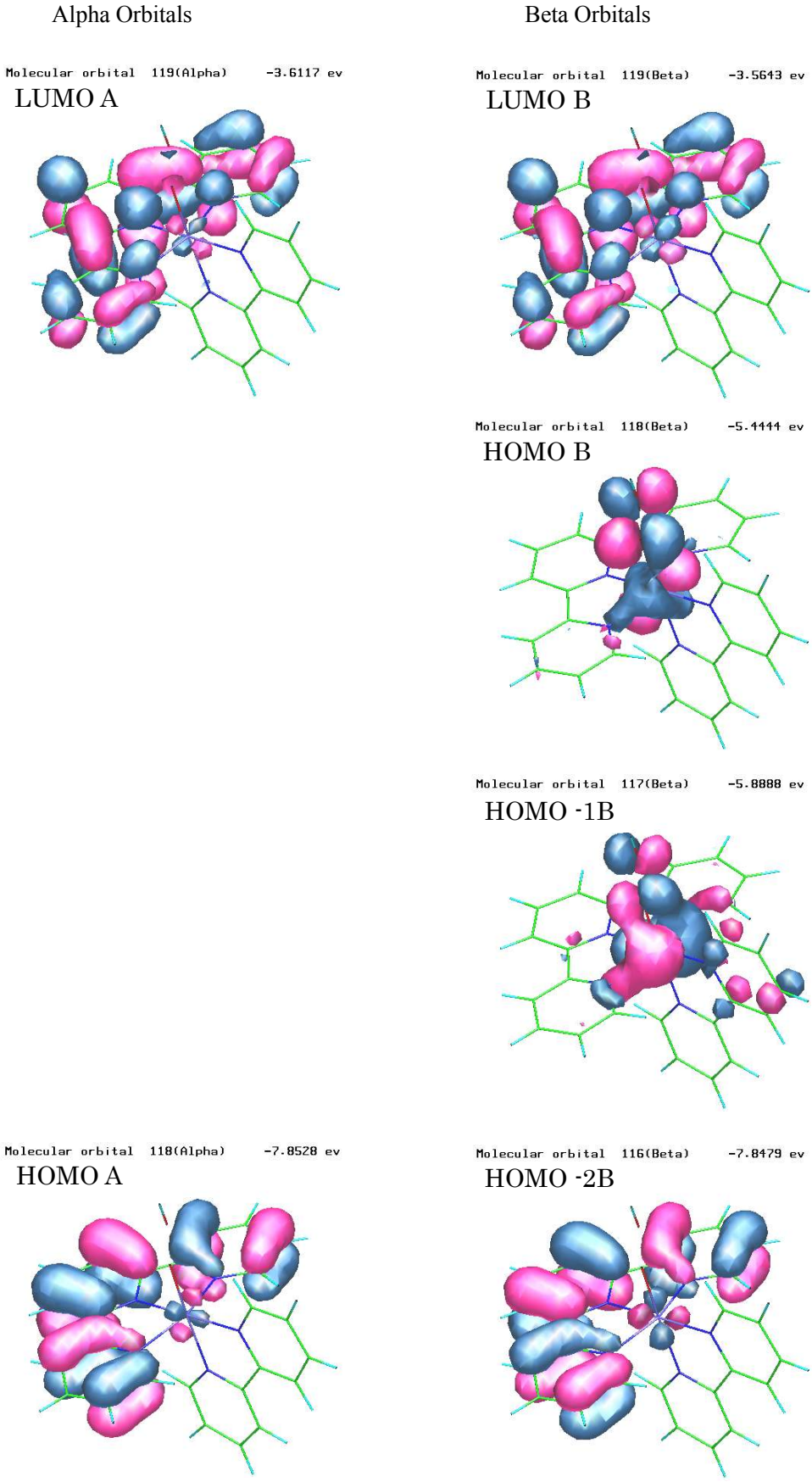

Figure S18(f). Frontier molecular orbitals of $[Ru^{IV}(terpy)(bpy)(OOH)]^{3+}$ for the optimized structure given Table S4f and Figure S12f.

Molecular orbital 117(Alpha) -8.0127 ev

HOMO -1A

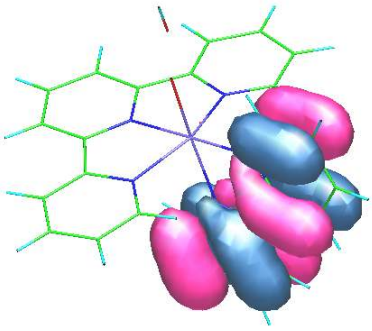

Molecular orbital 115(Beta) -8.0123 ev

HOMO -3B

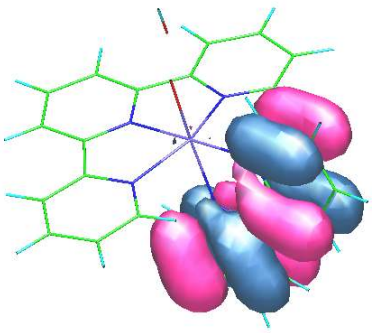

Molecular orbital 114(Beta) -8.3044 ev

HOMO -4B

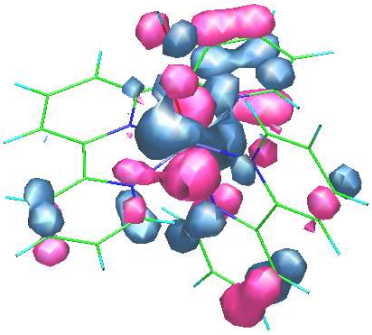

Molecular orbital 113(Beta) -8.4673 ev

HOMO -5B

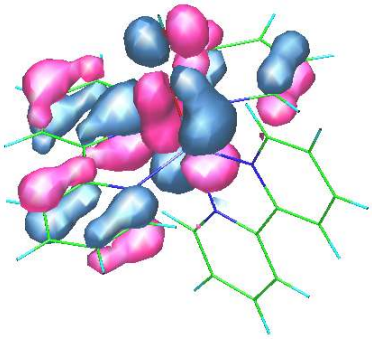

Molecular orbital 116(Alpha) -8.5488 ev

HOMO -2A

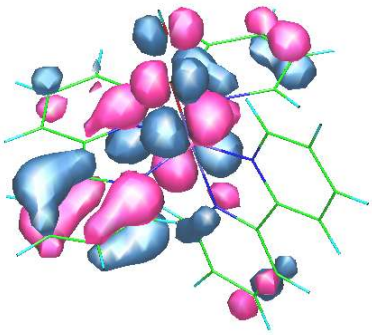

Figure S18(f).(continued)

Molecular orbital 115(Alpha) -8.6286 ev
HOMO -3A

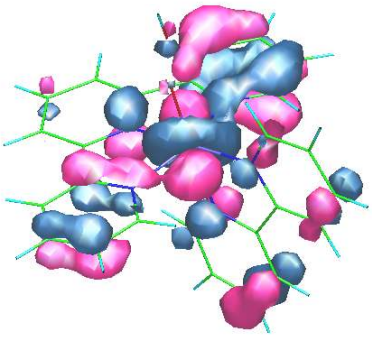

Molecular orbital 112(Beta) -8.8584 ev
HOMO -6B

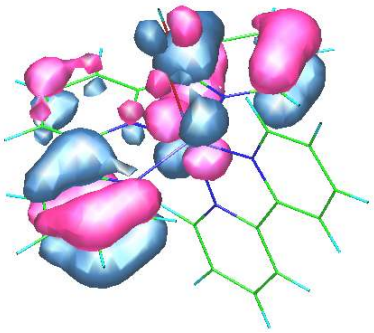

Molecular orbital 114(Alpha) -8.7909 ev
HOMO -4A

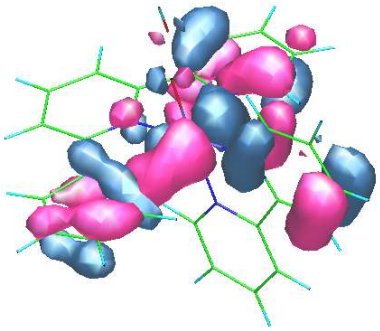

Molecular orbital 113(Alpha) -8.9873 ev
HOMO -5A

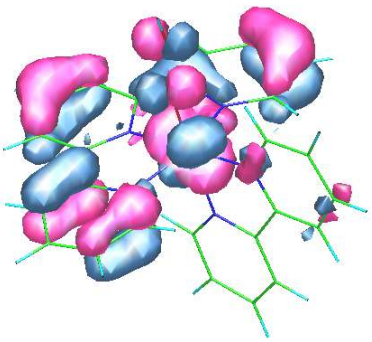

Figure S18(f). (continued)

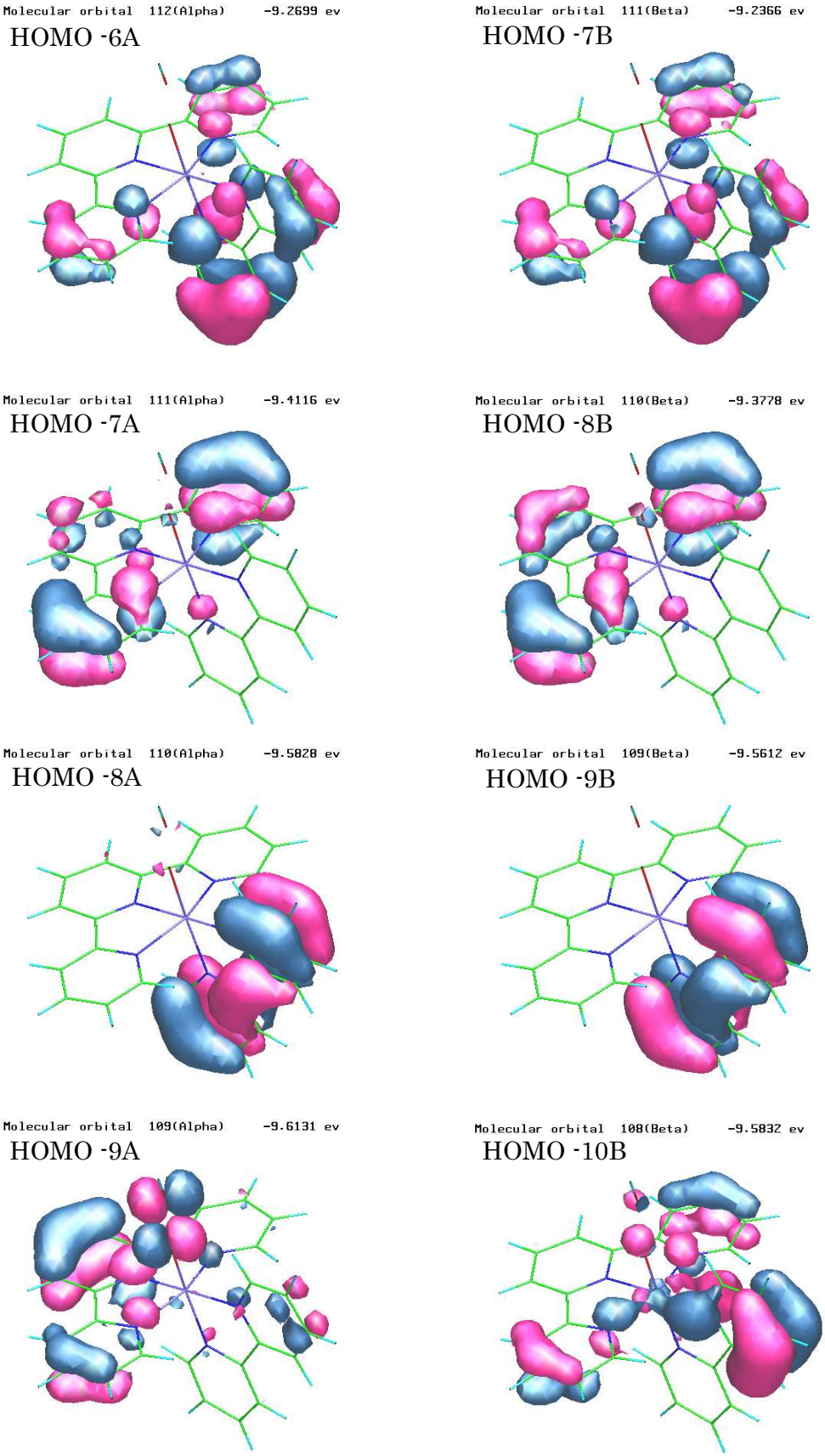

Figure S18(f). (continued)

Molecular orbital 107(Beta) -9.8018 ev

HOMO -11B

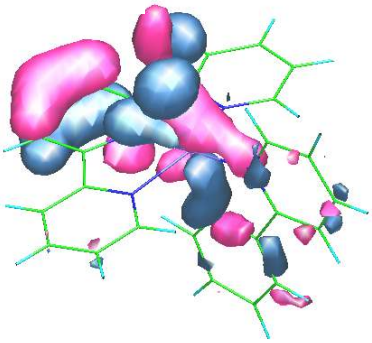

Molecular orbital 106(Beta) -9.9623 ev

HOMO -12B

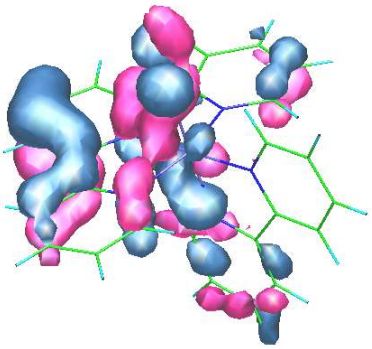

Molecular orbital 105(Beta) -9.9764 ev

HOMO -13B

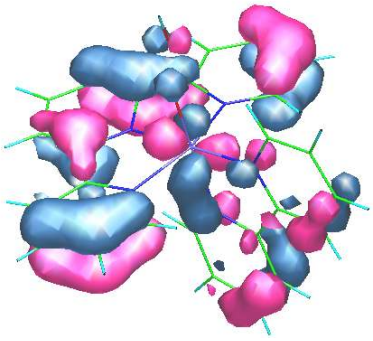

Molecular orbital 104(Beta) -10.1869 ev

HOMO -14B

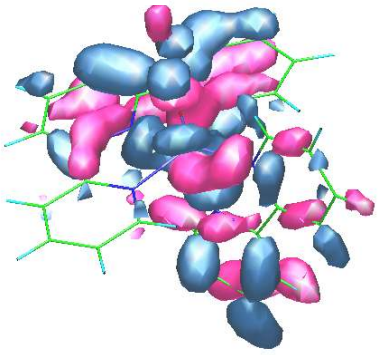

Figure S18(f). (continued)

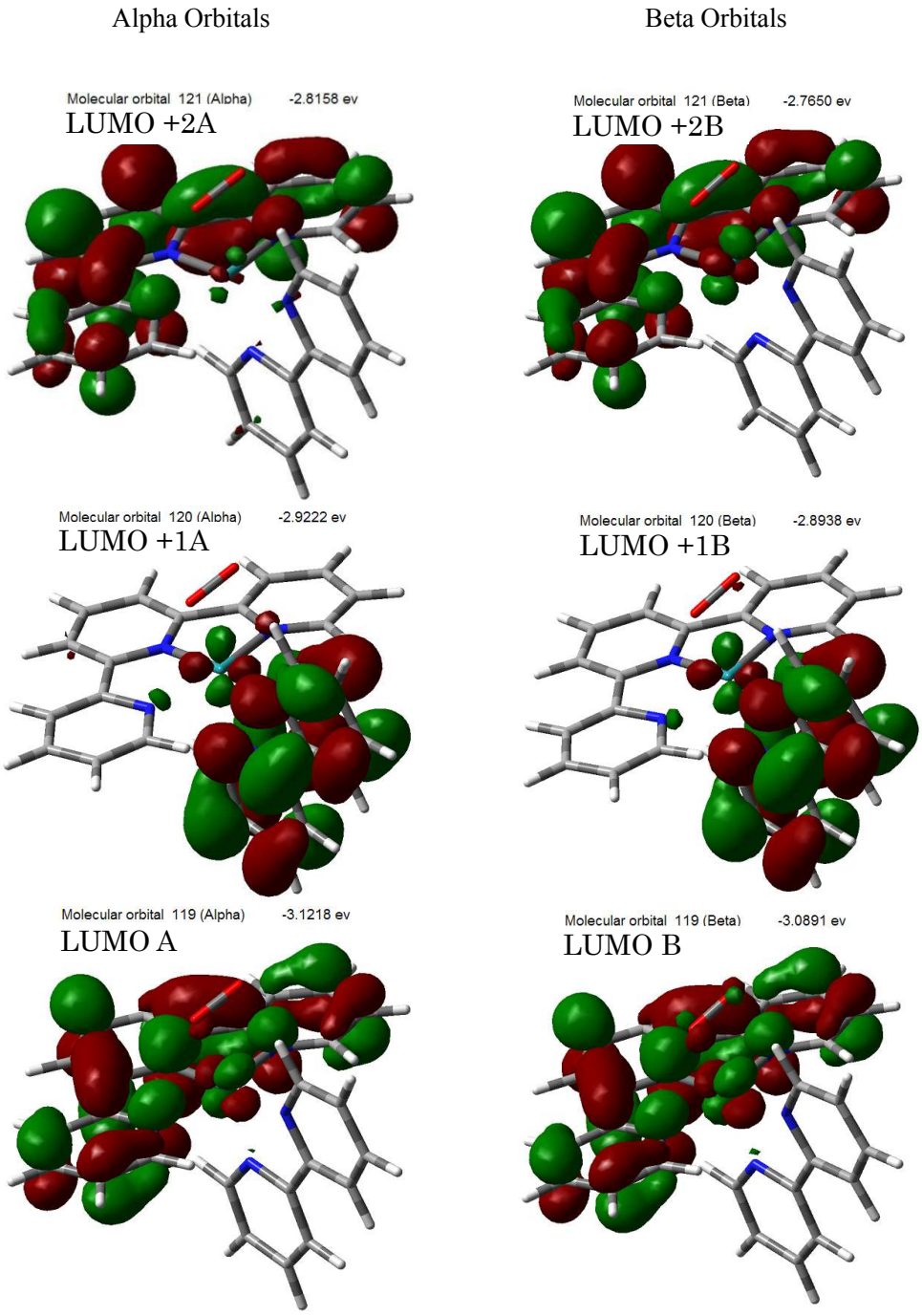

Figure S18(g). Frontier molecular orbitals of $[Ru^{III}(terpy)(bpy)(OO\bullet)]^{2+}$ for the optimized structure given Table S4g and Figure S12g. HOMO A, HOMO -1B, HOMO -2B and HOMO -3B show the character of π back bonding from the metal d orbitals to the $\pi^*(O_2)$ orbitals.

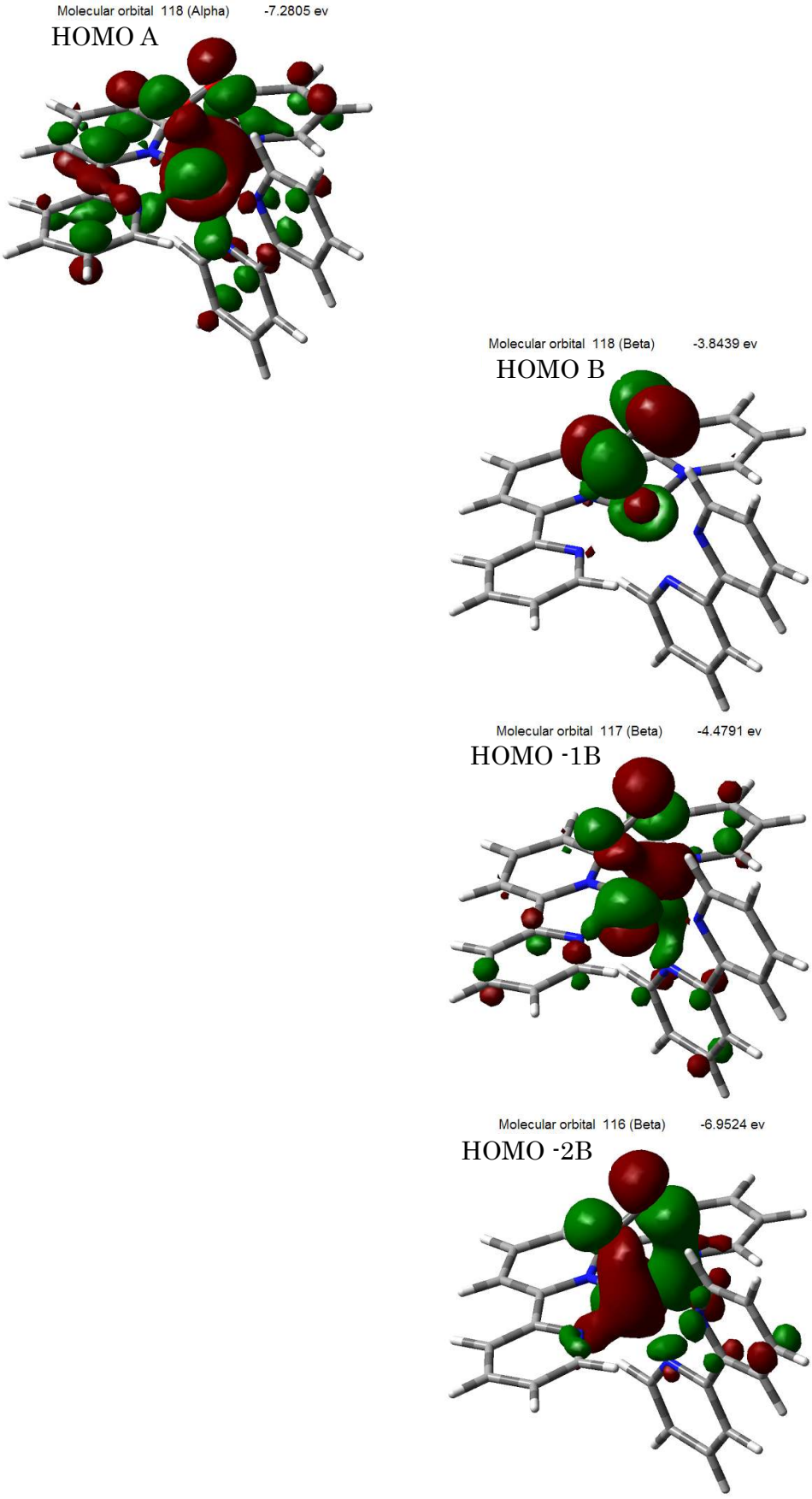

Figure S18(g). (continued)

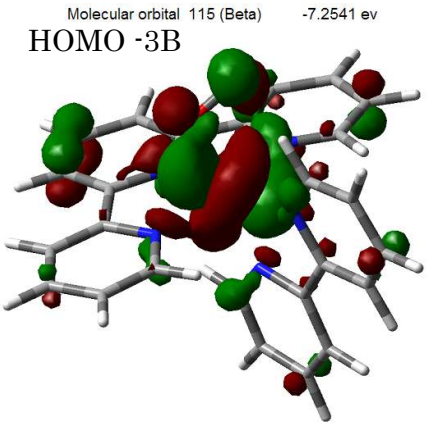

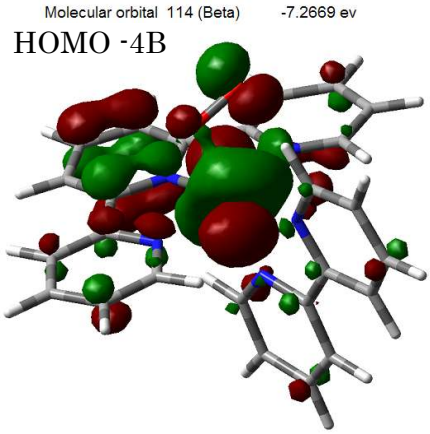

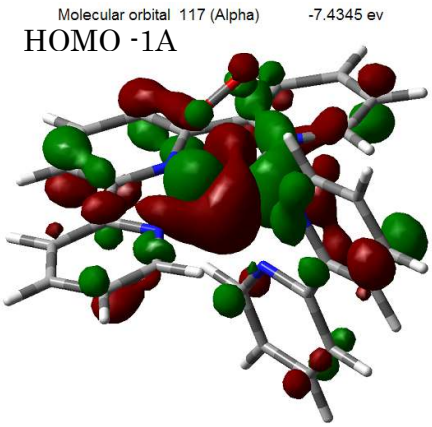

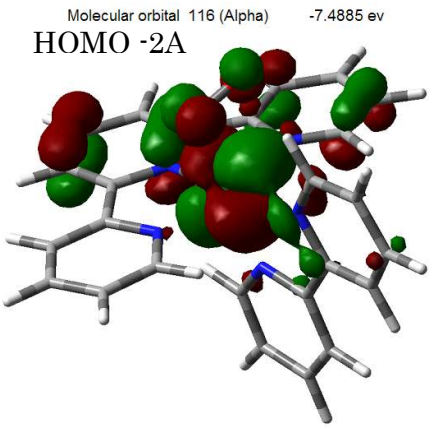

Figure S18(g). (continued)

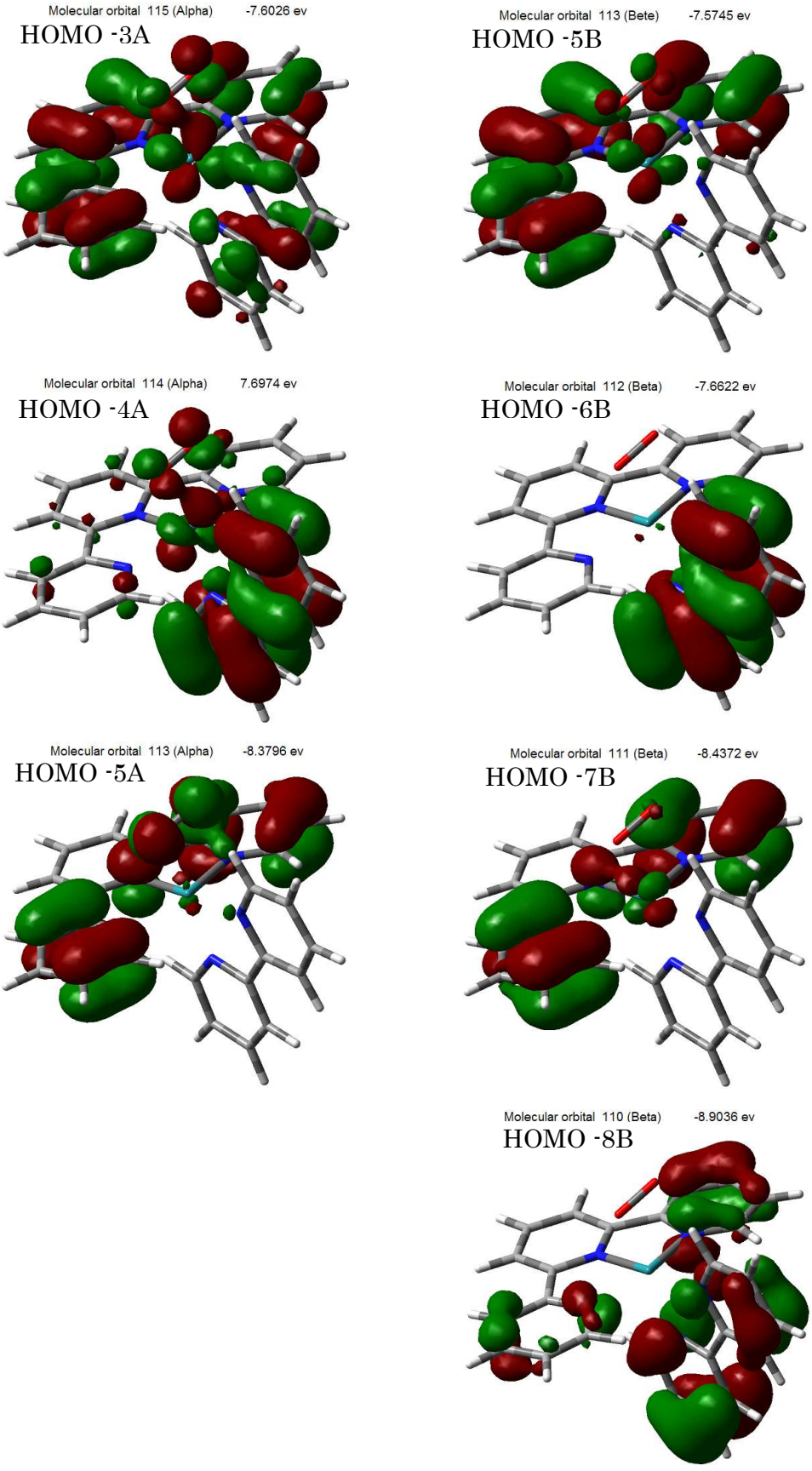
Molecular orbital 115 (Alpha) -7.6026 ev
HOMO -3A
Molecular orbital 113 (Bete) -7.5745 ev
HOMO -5B
Molecular orbital 114 (Alpha) 7.6974 ev
HOMO -4A
Molecular orbital 112 (Beta) -7.6622 ev
HOMO -6B
Molecular orbital 113 (Alpha) -8.3796 ev
HOMO -5A
Molecular orbital 111 (Beta) -8.4372 ev
HOMO -7B
Molecular orbital 110 (Beta) -8.9036 ev
HOMO -8B

Figure S18(g).

References

(1) K. J. Takeuchi, M. S. Thompson, D. W. Pipes, T. J. Meyer, *Inorg. Chem.* 1984, **23**, 1845.

(2) SPECFIT; Spectrum Research Associate: Chapel Hill, NC.

(3) S. Masaoka, K. Sakai, *Chem. Lett.* 2009, **38**, 182.

(4) Gaussian 03, Revision C.02, M. J. Frisch, G. W. Trucks, H. B. Schlegel, G. E. Scuseria, M. A. Robb, J. R. Cheeseman, , J. A. Montgomery, Jr., T. Vreven, K. N. Kudin, J. C. Burant, J. M. Millam, S. S. Iyengar, J. Tomasi, V. Barone, B. Mennucci, M. Cossi, G. Scalmani, N. Rega, G. A. Petersson, H. Nakatsuji, M. Hada, M. Ehara, K. Toyota, R. Fukuda, J. Hasegawa, M. Ishida, T. Nakajima, Y. Honda, O. Kitao, H. Nakai, M. Klene, X. Li, J. E. Knox, H. P. Hratchian, J. B. Cross, V. Bakken, C. Adamo, J. Jaramillo, R. Gomperts, R. E. Stratmann, O. Yazyev, A. J. Austin, R. Cammi, C. Pomelli, J. W. Ochterski, P. Y. Ayala, K. Morokuma, G. A. Voth, P. Salvador, J. J. Dannenberg, V. G. Zakrzewski, S. Dapprich, A. D. Daniels, M. C. Strain, O. Farkas, D. K. Malick, A. D. Rabuck, K. Raghavachari, J. B. Foresman, J. V. Ortiz, Q. Cui, A. G. Baboul, S. Clifford, J. Cioslowski, B. B. Stefanov, G. Liu, A. Liashenko, P. Piskorz, I. Komaromi, R. L. Martin, D. J. Fox, T. Keith, M. A. Al-Laham, C. Y. Peng, A. Nanayakkara, M. Challacombe, P. M. W. Gill, B. Johnson, W. Chen, M. W. Wong, C. Gonzalez, J. A. Pople, Gaussian, Inc., Wallingford CT, 2004.

(5) A. D. Becke, *J. Chem. Phys.* 1993, **98**, 5648.

(6) C. Lee, W. Yang, R. G. Parr, *Phys. Rev.* 1988, **B37**, 785.

(7) a) T. H. Dunning, Jr., P. J. Hay, In *Modern Theoretical Chemistry*, ed. Schaefer, III, H. F. Plenum, New York, 1976. b) P. J. Hay, W. R. Wadt, *J. Chem. Phys.* 1985, **82**, 270. c) P. J. Hay, W. R. Wadt, *J. Chem. Phys.* 1985, **82**, 299.

(8) a) W. J. Hehre, R. Ditchfield, J. A. Pople, *J. Chem. Phys.*, **1972**, *56*, 2257. b) M. M. Francl, W. J. Petro, W. J. Hehre, J. S. Binkley, M. S. Gordon, D. J. Defrees, J. A. Pople, *J. Chem. Phys.*, **1982**, *77*, 3654.C.

(9) a) C. Amovilli, V. Barone, R. Cammi, E. Cances, M. Cossi, B. Mennucci, C. S. Pomelli, J. Tomasi, *Adv. Quantum Chem.* 1998, **32,** 227. b) M. Cossi, G. Scalmani, N. Rega, V. Barone, *J. Chem. Phys.* 2002, **117**, 43.

(10) a) M. E. Casida, C. Jamorski, K. C. Casida, D. R. Salahub, *J. Chem. Phys.* 1998, **108**, 4439. b) R. E. Statmann, G. E. J. Scuseria, *Chem. Phys.* 1998, **109**, 8218. c) R. Bauernschmitt, R. Ahlrichs, *Chem. Phys. Lett.* 1996, **256**, 454.

(11) a) M. Ardon, G. Stein, *J. Chem. Soc.*, 1956, 104. b) H. J. Maria, J. R. McDonald, S. P. McGlynn, *J. Am. Chem. Soc.*, 1973, **94**, 1050.

(12) S. A. Hayes, P. Yu, T. J. O'Keefe, M. J. O'Keefe, J. O. Stoffer, *J. Electrochem. Soc.*, 2002, **149**, C623.

(13) Lim, D. Bashford, M. Karplus, *J. Phys. Chem.* 1991, **95**, 5610.